UCSF
UC San Francisco Electronic Theses and Dissertations

Title
Brainstem circuits that control appetite

Permalink
https://escholarship.org/uc/item/45g1q48t

ISBN
9798293856046

Author
Ly, Truong

Publication Date
2025-09-19

Peer reviewed|Thesis/dissertation

eScholarship.org Powered by the California Digital Library
University of California

Brainstem circuits that control appetite

by
Truong Ly

DISSERTATION
Submitted in partial satisfaction of the requirements for degree of
DOCTOR OF PHILOSOPHY

in

Neuroscience

in the

GRADUATE DIVISION
of the
UNIVERSITY OF CALIFORNIA, SAN FRANCISCO

Approved:

DocuSigned by:
Kevin Yackle
863799D3911346A...

Kevin Yackle
Chair

DocuSigned by:
Zachary Knight
5F44DA94631A479...

Zachary Knight

DocuSigned by:
Massimo Scanziani
4AF406E430B7472...

Massimo Scanziani

DocuSigned by:
Christian Vaisse
8820D4FC0D5C40C...

Christian Vaisse

Committee Members

Copyright 2025

by

Truong Ly

ACKNOWLEDGEMENTS

I would like to thank my advisor, Zack, for his mentorship, scientific insight and enthusiasm for all the work we have accomplished these past few years. I will not take for granted the opportunity to share a new discovery with someone as excited about the science as I am.

I would like to thank my parents, Tan and Thuy, and family for their endless support of my pursuit of higher education. My parents took a huge risk in immigrating to a foreign country from Vietnam and sacrificed their best years for me to follow my dreams. The work in this dissertation is our collective achievement.

I would like to thank my friends and lab mates for their camaraderie and support. Their presence and humor bring tremendous joy to my life inside and outside of the lab.

Finally, I would like to thank my fiancée Shweta for energizing me to enjoy the small moments in life every day. Her resilience and unwavering zest for life is a constant source of inspiration.

CONTRIBUTIONS

The material in this dissertation is reprinted with permission from the following publications:

Truong Ly, Zachary A. Knight. Interoception: Spinal sensory neurons that innervate the intestines. *Current Biology* 33(18), R945–R947, 2023.

Truong Ly, Jun Y. Oh, Nilla Sivakumar, Sarah Shehata, Naymalis La Santa Medina, Heidi Huang, Zhengya Liu, Wendy Fang, Chris Barnes, Naz Dundar, Brooke C. Jarvie, Anagh Ravi, Olivia K. Barnhill, Chelsea Li, Grace R. Lee, Jaewon Choi, Heeun Jang, Zachary A. Knight. Sequential appetite suppression by oral and visceral feedback to the brainstem. *Nature* 624, 130-137, 2023.

The work in this dissertation was supported by the following funding sources:

UCSF Weill Fellowship, 2020-2023

NIH National Research Service Award Predoctoral Fellowship, 2023-2025

ABSTRACT

Brainstem circuits that control appetite

Truong Ly

Nutrients are essential for sustaining life as we know it. Therefore, organisms, including humans, have evolved complex brain networks to control the decision to seek food, consume it, and when to stop eating. Importantly, the desire to overeat and store excess energy for scarce times must be weighed against the harmful effects of overloading our digestive systems.

The satiation of hunger has traditionally been viewed as a gradual process triggered during a meal by gastrointestinal feedback, which is relayed by sensory nerves to the caudal brainstem to suppress appetite. Therefore, brainstem circuits – namely, the caudal nucleus of the solitary tract - are thought to be activated over tens of minutes to promote satiety. However, this assumption has not been directly tested due to the challenge of studying such a deep brain structure. To address this longstanding question, we developed new methods for recording the activity of distinct cell types in this brain region and determined that they regulate appetite on multiple timescales.

Chapter one of this dissertation reviews our historical understanding of how the caudal brainstem controls hunger satiation. Chapter two explains how new studies have shaped our understanding of spinal sensory neurons and their importance to GI function. Chapter three describes the first in vivo recordings of caudal brainstem circuits during behavior, which revealed that one group of neurons is primarily activated by the taste of food and control the duration of seconds-timescale feeding bursts, while a second distinct group of neurons is activated by mechanical feedback from the gut and promoted satiety that lasted for tens of minutes. These experiments have revealed fundamental principles by which the brain monitors external and visceral sensory signals during a meal to dynamically control ingestive behavior and maintain physiological homeostasis.

TABLE OF CONTENTS

I. Introduction

Background and motivation 2

Overview of the dissertation 4

References 8

II. Interoception: Spinal sensory neurons that innervate the intestines

Summary 11

Main text 11

References 17

III. Sequential appetite suppression by oral and visceral feedback to the brainstem

Abstract 20

Introduction 20

Results 21

Discussion 31

Supplementary Discussion 32

Supplementary Discussion References 37

Methods 65

References 83

LIST OF FIGURES

I. Introduction

Figure 1.1 The brainstem is critical for meal termination 5

Figure 1.2 The cNTS receives direct GI feedback during a meal 6

Figure 1.3 Cells types in the dorsal vagal complex and cNTS..... 7

II. Interoception: Spinal sensory neurons that innervate the intestines

Figure 2.1 Spinal sensory neurons that innervate the intestines 16

III. Sequential appetite suppression by oral and visceral feedback to the brainstem

Figure 3.1 PRLH neurons show different responses to oral ingestion versus IG infusion 41

Figure 3.2 PRLH neurons track the dynamics of ingestion..... 42

Figure 3.3 PRLH neurons are activated by the taste of food 43

Figure 3.4 PRLH neurons pace food ingestion 44

Figure 3.5 GCG neurons track cumulative intake on a timescale of minutes 45

Figure 3.6 GCG neurons activation promotes long-lasting satiety..... 46

Figure 3.7 PRLH and GCG neurons are distinct cNTS cell types that regulate the non-aversive suppression of feeding 47

Figure 3.8 PRLH neurons largely overlap with TH neurons in the cNTS..... 48

Figure 3.9 Regulation of PRLH neurons by ingestive and non-ingestive signals 49

Figure 3.10 PRLH neurons track the moment-to-moment dynamics of ingestion 51

Figure 3.11 PRLH neurons are activated by food tastes 53

Figure 3.12 Individual PRLH neurons are activated by food tastes 55

Figure 3.13 PRLH and GCG neurons are distinct cNTS cell types that regulate the non-aversive suppression of feeding 57

Figure 3.14 Regulation of GCG neurons by oral signals of ingestion 59

Figure 3.15 Regulation of GCG neurons by non-ingestive and GI signals 61

Figure 3.16 GCG neuron activation promotes long-lasting satiety 63

Figure 3.17 Separate circuits for the oral and gastrointestinal control of ingestion 64

I. Introduction

BACKGROUND AND MOTIVATION

All meals come to an end. How do we become full during a meal? What stops us from eating forever in one sitting? The suppression of appetite is thought to be due to GI feedback that progressively accumulates with food consumption. These negative feedback signals are thought to intensify as the meal progresses and activate brain circuits to promote the termination of food consumption.

Our modern understanding that the neural control of meal termination originated with the discovery by Harvey Grill in the 1970s that decerebrate rats missing their forebrain and midbrain could still voluntarily terminate their meals, thereby showing that the brainstem was sufficient for halting food ingestion[1,2] (Figure 1.1a). The brainstem is a large structure – where would one find the neural substrate that controls meal termination? Logically, one would first look at the first site in the brain that receives direct feedback from the GI tract - the caudal nucleus of the solitary tract (cNTS)[3].

During a meal, the vagus nerve, our 10th cranial nerve, relays GI feedback such as nutrients and GI distension via afferent nerves to the cNTS[3,4] (Figure 1.2). The cNTS is located within a larger structure called the dorsal vagal complex, which includes the area postrema (AP) and the dorsal motor vagus (DMV)[3,4]. Bloodborne hormones and nutrients can also directly modulate cNTS neurons due to the weakened blood brain barrier in this region. Indeed, many studies have shown that cNTS neurons located in proximity to vagal afferent terminals express the immediate early gene *Fos* after animals consume a meal[4] (Figure 1.1b). Additionally, neural recordings in anesthetized animals or brain slices have shown that these cells can be activated by meal-related signals[5-11].

The cNTS contains a diversity of genetically distinct cell types and many investigators have independently shown that many of these cell types are critical for hunger satiation (Figure 1.1c and 1.3a-b). Using modern neural circuit techniques like optogenetics and chemogenetics,

investigators showed that activating individual cNTS excitatory neuron cell types in mice can powerfully suppress appetite, and silencing their activity can cause overeating and obesity[12-18]. A longstanding question remains after these important neural circuit manipulation studies: how does the cNTS process different types of ingestive feedback to regulate ingestive behavior during a meal?

Due to the difficulty of accessing such a deep brain structure for neural recording techniques, it is unknown how the cNTS responds to ingestive feedback in an awake, behaving animal. Nor is it known whether the cNTS detects other kinds of ingestive cues that also regulate feeding behavior. One attractive model is that these cell types are tuned to sense different visceral signals, which, in turn, control different aspects of feeding behavior. Surprisingly, anesthetized recordings found that cNTS cell types show little specificity in their responses to various GI stimuli[6]. However, anesthetized preparations lack most of the sensory and motor feedback that arises during natural ingestion, raising the possibility that cNTS neurons may exhibit greater functional specificity in awake behaving animals.

For this dissertation, I developed methods to record the population and single-cell activity of cNTS neurons in mice during a meal. I first investigated PRLH and GCG neurons, which inhibit feeding without inducing nausea or aversion[12-13,17-18]. These neurons are defined by the expression of prolactin-releasing hormone (encoded by the *Prlh* gene) or the expression of glucagon-like peptide 1 (encoded by the *Gcg* gene). These two marker genes are unique in that they label transcriptionally homogeneous cNTS cell types that are intermingled but non-overlapping, directly innervated by vagal afferents, activated by ingestion as measured by *Fos* expression, and functionally validated to inhibit feeding without inducing aversion (Figure 1.3a,c-d). These two group of neurons also overlap with several broader, and more heterogeneous, populations of cNTS neurons that also promote meal termination (Figure 1.3c-d).

OVERVIEW OF THE DISSERTATION

This chapter has reviewed our historical understanding of how the caudal brainstem controls hunger satiation. Chapter two explains how new studies have shaped our understanding of spinal sensory neurons and their importance to GI function. Chapter three describes the first in vivo recordings of caudal brainstem circuits during behavior, which revealed that one group of neurons is primarily activated by the taste of food and control the duration of seconds-timescale feeding bursts, while a second distinct group of neurons is activated by mechanical feedback from the gut and promoted satiety that lasted for tens of minutes. These experiments have revealed fundamental principles by which the brain monitors fast and slow sensory signals during a meal to dynamically control ingestive behavior and maintain physiological homeostasis.

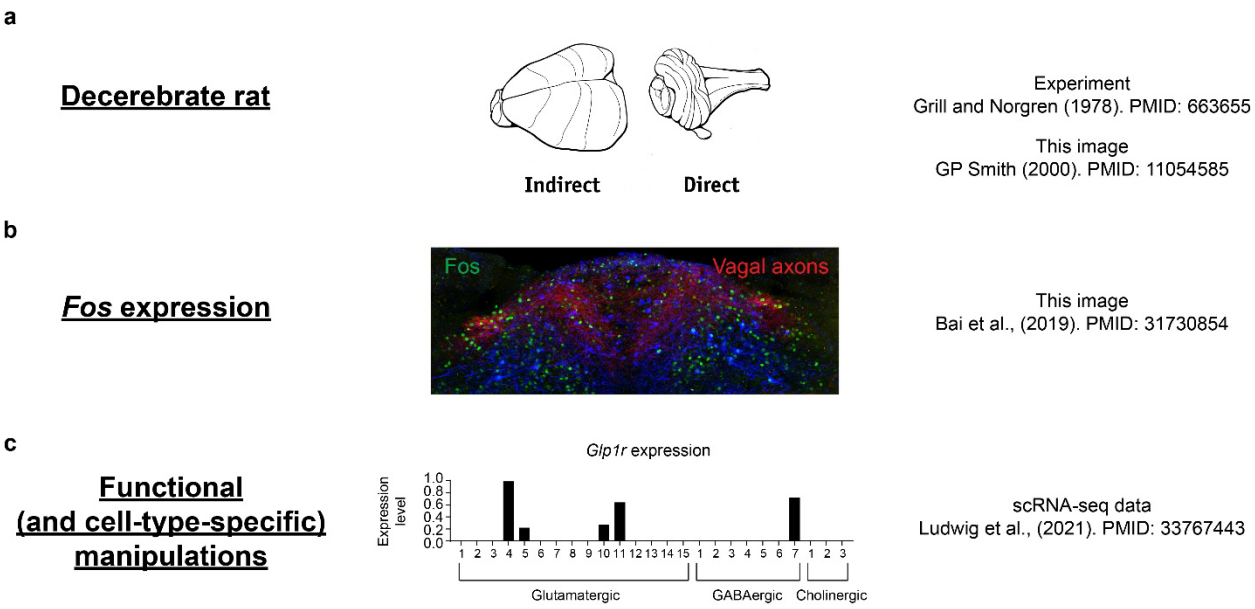


Figure 1.1 | The brainstem is critical for meal termination.
a, Experiments with decerebrate rats showed that the brainstem is sufficient for meal termination. In these experiments, researchers showed that removing the forebrain of rats did not prevent them from regulating their moment-to-moment food ingestion or rejection. **b**, The dorsal vagal complex (DVC) and caudal nucleus of the solitary tract (cNTS) express the immediate early gene *Fos* in proximity to axon terminals from the vagus nerve (10th cranial nerve) when animals are refed after a fast. **c**, Functional and cell-type specific manipulations in the cNTS have shown that many glutamatergic populations are critical for meal termination.

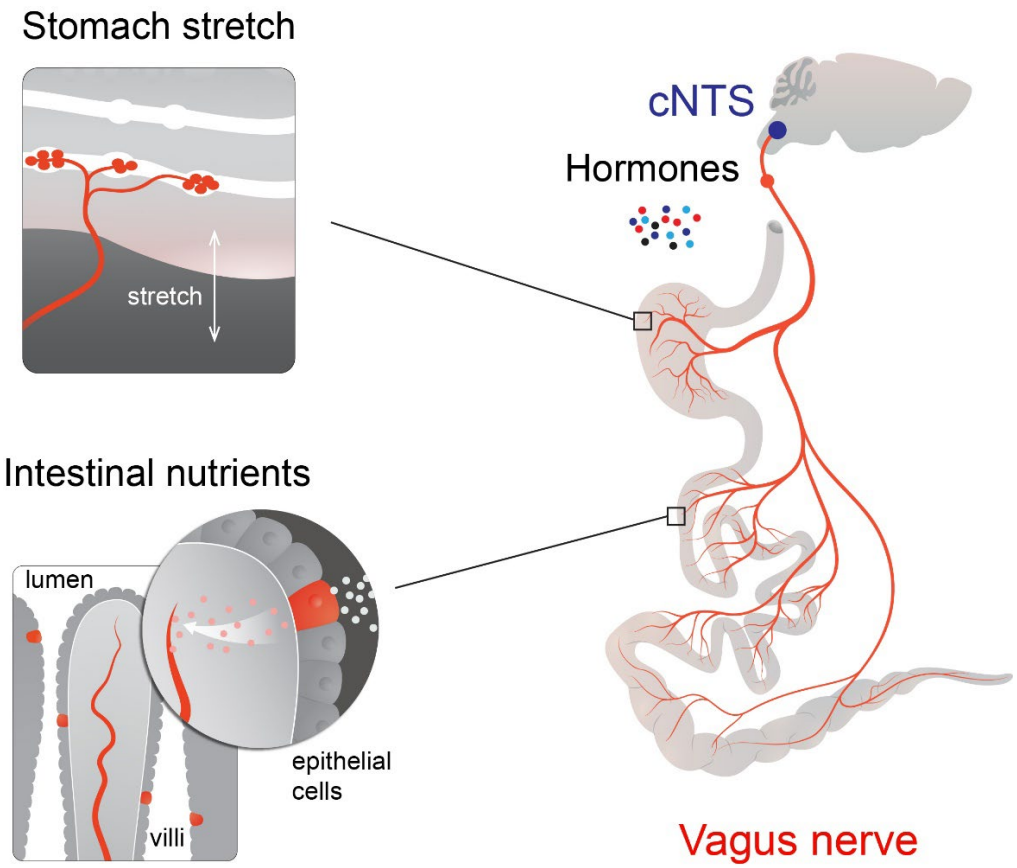


Figure 1.2 | The cNTS receive direct GI feedback during a meal.
The caudal nucleus of the solitary tract (cNTS) is the first site in the brainstem that receives GI feedback during a meal via the vagus nerve (10th cranial nerve). The cNTS is located within a larger structure called the dorsal vagal complex, which includes the area postrema (AP) and the dorsal motor vagus (DMV). The vagus nerve directly relays information such as stomach stretch (top left) and intestinal nutrients (bottom left) to neurons in the cNTS. Bloodborne hormones and nutrients can also directly modulate cNTS neurons due to the weakened blood brain barrier in this region.

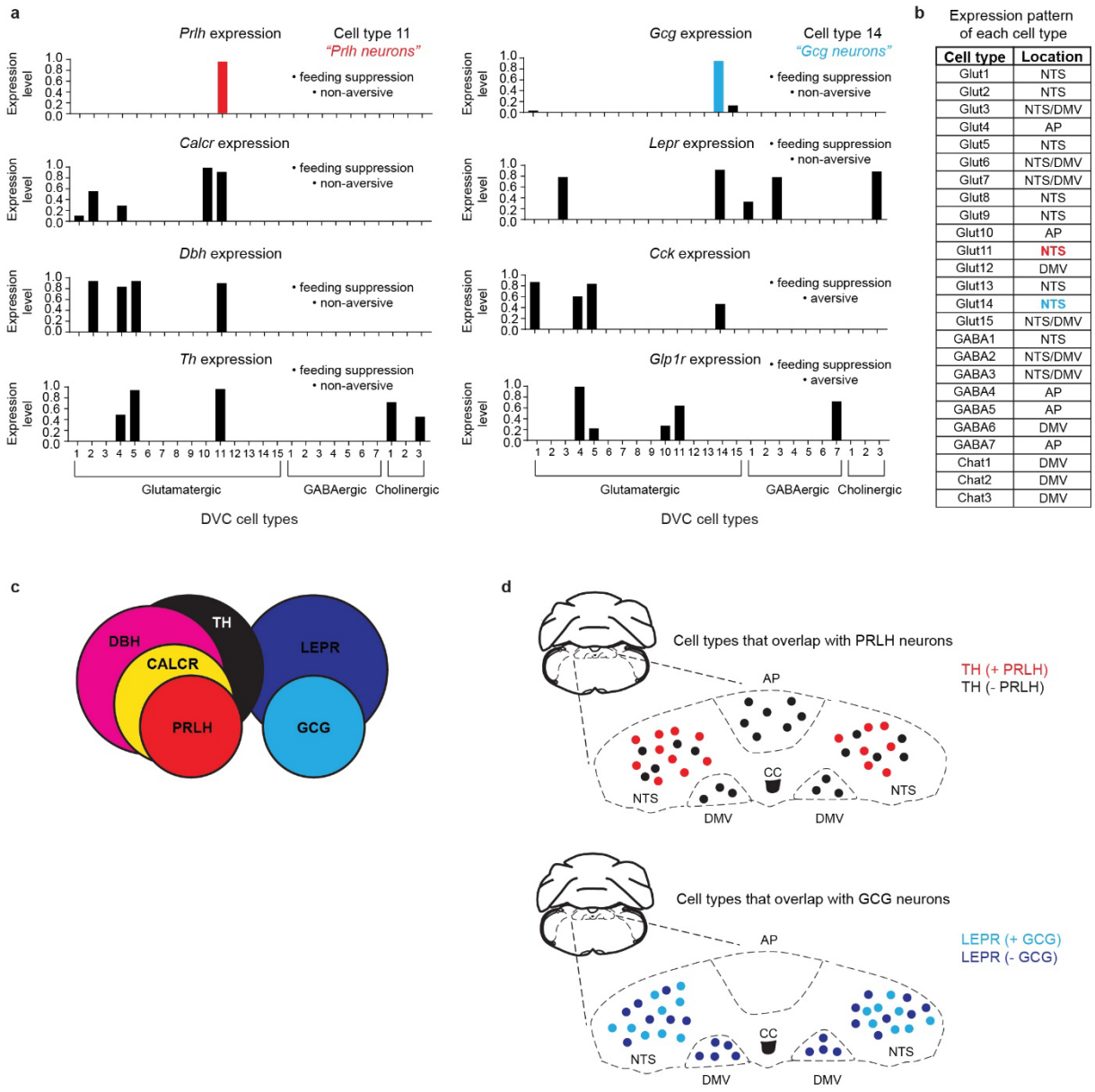


Figure 1.3 | Cell types in the dorsal vagal complex and cNTS.
a, Unique cell types in the dorsal vagal complex (DVC) identified by single-cell RNA sequencing (Data are adapted from Ludwig et al. 2021[21]) that are known to regulate feeding. *Prlh* and *Gcg* expression label distinct cell types that are known to control the non-aversive suppression of feeding. **b**, Table describing where glutamatergic, GABAergic, and cholinergic cell types identified by single-cell sequencing are found in the DVC[21]. AP = area postrema. DMV = dorsal motor vagus. **c**, Schematic showing overlap in RNA expression between cell types that express *Dbh*, *Th*, *Calcr*, *Prlh*, *Lepr*, and *Gcg* based on data from panel a. These cell types have been shown to be activated by natural feeding and/or suppress food intake without inducing conditioned taste aversion (CTA). **d**, Schematic showing the location of cell types – which regulate non-aversive satiety – within the DVC based on data from panel b. Cells expressing *Prlh* ("PRLH neurons") and *Gcg* ("GCG neurons") are specifically located in the cNTS, whereas other cell types show broad expression in the AP and DMV.

REFERENCES

1. Grill, H. J., & Norgren, R. Chronically decerebrate rats demonstrate satiation but not bait shyness. *Science* **201**(4352), 267–269 (1978).
2. Smith G. P. The controls of eating: a shift from nutritional homeostasis to behavioral neuroscience. *Nutrition* **16**(10), 814–820 (2000).
3. Cheng, W. *et al.* Hindbrain circuits in the control of eating behaviour and energy balance. *Nat. Metab.* **4**, 826–835 (2022).
4. Bai, L. *et al.* Genetic Identification of Vagal Sensory Neurons That Control Feeding. *Cell* **179**, 1129-1143.e23 (2019).
5. Vrang, N., Phifer, C. B., Corkern, M. M. & Berthoud, H.-R. Gastric distension induces c-Fos in medullary GLP-1/2-containing neurons. *Am. J. Physiol. Regul. Integr. Comp. Physiol.* **285**, R470-478 (2003).
6. Ran, C., Boettcher, J. C., Kaye, J. A., Gallori, C. E. & Liberles, S. D. A brainstem map for visceral sensations. *Nature* **609**, 320–326 (2022).
7. Zittel, T. T., De Giorgio, R., Sternini, C. & Raybould, H. E. Fos protein expression in the nucleus of the solitary tract in response to intestinal nutrients in awake rats. *Brain Res.* **663**, 266–270 (1994).
8. Roman, C. W., Derkach, V. A. & Palmiter, R. D. Genetically and functionally defined NTS to PBN brain circuits mediating anorexia. Nat. Commun. **7**, 11905 (2016).
9. Schwartz, G. J. & Moran, T. H. Leptin and neuropeptide y have opposing modulatory effects on nucleus of the solitary tract neurophysiological responses to gastric loads: implications for the control of food intake. *Endocrinology* **143**, 3779–3784 (2002).
10. Li, M. *et al.* Gut-Brain Circuits for Fat Preference. *Nature* (2022) doi:10.1038/s41586-022-05266-z.

11. Appleyard, S. M. *et al.* Visceral afferents directly activate catecholamine neurons in the solitary tract nucleus. *J. Neurosci. Off. J. Soc. Neurosci.* **27**, 13292–13302 (2007).

12. Holt, M. K. et al. Preproglucagon Neurons in the Nucleus of the Solitary Tract Are the Main Source of Brain GLP-1, Mediate Stress-Induced Hypophagia, and Limit Unusually Large Intakes of Food. Diabetes **68**, 21–33 (2019).

13. Brierley, D. I. *et al.* Central and peripheral GLP-1 systems independently suppress eating. *Nat. Metab.* **3**, 258–273 (2021).

14. D'Agostino, G. *et al.* Appetite controlled by a cholecystokinin nucleus of the solitary tract to hypothalamus neurocircuit. *eLife* **5**, e12225 (2016).

15. Cheng, W. *et al.* Leptin receptor-expressing nucleus tractus solitarius neurons suppress food intake independently of GLP1 in mice. *JCI Insight* **5**, 134359 (2020).

16. Cheng, W. *et al.* Calcitonin Receptor Neurons in the Mouse Nucleus Tractus Solitarius Control Energy Balance via the Non-aversive Suppression of Feeding. *Cell Metab.* **31**, 301-312.e5 (2020).

17. Cheng, W. *et al.* NTS Prlh overcomes orexigenic stimuli and ameliorates dietary and genetic forms of obesity. *Nat. Commun.* **12**, 5175 (2021).

18. Liu, J. *et al.* Enhanced AMPA Receptor Trafficking Mediates the Anorexigenic Effect of Endogenous Glucagon-like Peptide-1 in the Paraventricular Hypothalamus. *Neuron* **96**, 897-909.e5 (2017).

II. Interoception: Spinal sensory neurons that innervate the intestines

SUMMARY

The gut is innervated by sensory neurons that relay mechanical and chemical signals to the brain. Two new studies characterize the spinal sensory neurons that innervate the intestines and reveal a role for Piezo2 in these cells in sensing colonic distension and regulating gastrointestinal motility.

MAIN TEXT

The gastrointestinal (GI) tract is essential for digesting and absorbing nutrients from food, eliminating waste, and promoting satiety in response to chemical and mechanical signals during a meal[1–4]. Mechanosensation in the gut is mediated by two distinct classes of extrinsic sensory neurons: vagal afferents, which have cell bodies in nodose ganglia and are involved in homeostatic gut-brain signaling[1,3,4], and spinal afferents, which have cell bodies in dorsal root ganglia (DRG)[2,4] and are known for sensing noxious distension, inflammation and other painful visceral stimuli[5–7] (Figure 2.1a). While recent studies have identified molecular markers for the vagal sensory neurons that sense stretch in the upper GI tract[1,3], less is known about the DRG neurons that detect mechanical signals in the gut and how this regulates GI physiology. Two new studies from Wolfson *et al*. and Servin-Vences *et al*. in *Cell* (In Press)[8,9] uncover the functional subtypes of spinal sensory neurons that sense colon distension and reveal that the mechanosensor Piezo2 is involved in controlling gut motility.

A genetic atlas of spinal sensory neurons that innervate the colon

DRG neurons innervate both the skin and internal organs. Previous studies of skin-innervating sensory neurons revealed molecular markers -- such as TrkB, TH, and Bmpr1b -- that label functionally distinct cell types[10]. These cell types are distinguished by the specific cells

and tissue layers that they innervate, the types of sensory endings that their axons form, and how they respond to different kinds of sensory stimuli, ranging from gentle stroking to noxious touch. Viscera-innervating DRG afferents also exhibit distinct innervation patterns and morphologies[11], but how these anatomic properties relate to cell types is not well defined. Wolfson *et al*. therefore used the genetic toolkit of skin-innervating sensory neurons as a starting point to investigate the cell types that innervate the colon[9].

The authors first characterized the anatomy of DRG neurons by performing anterograde tracing using a panel of Cre and Flp drivers that intersectionally label distinct cell types[9]. This revealed that all DRG subtypes densely innervate the myenteric plexus, which is a network of enteric neurons that are responsible for producing the peristaltic activity that propels food through the intestine[12] (Figure 2.1b). Some cell types also innervated the circular muscle layer (TH) or the submucosal plexus (Sstr2+ and Adra2a+) whereas others exclusively innervated the myenteric plexus (TrkB and Bmpr1b). These differences in innervation targets were accompanied by differences in axon terminal morphology. For example, TrkB neurons formed intraganglionic varicose endings that wrapped extensively around myenteric cell bodies, whereas TH neurons innervating the circular muscle layer formed intramuscular arrays. Thus genetically-defined DRG cell types have distinct sensory endings and innervation patterns across layers of the intestine.

The authors next asked how these molecular and anatomical differences correlate with functional responses[9]. Responses to touch stimuli are traditionally classified along several dimensions, including: (1) the force threshold for activation, (2) the response latency, which depends on whether the neurons contains myelinated A-delta fibers or unmyelinated C fibers, and (3) the rate of adaptation to sensory stimuli[10]. The authors therefore measured these properties in response to colonic distension, using a combination of electrophysiological recordings and in vivo imaging. This revealed that DRG subtypes collectively tile force space in the colon, with TrkB neurons having the lowest force threshold for activation and Bmpr1b

neurons the highest. Characterization of response latencies and rates of adaptation revealed that TrkB, TH, Bmpr1b, and SStr2-expressing sensory neurons correspond to four distinct classes of mechanoreceptors: the A-delta low-threshold, C-fiber low-threshold, A-delta high-threshold, and C-fiber high-threshold mechanoreceptors, respectively[10]. Of note, although the individual DRG neurons that responded to colonic distension were distinct from those that responded to pinch of the skin (with the exception of a subset of TrkB neurons), as a class, TrkB, TH, and Bmpr1b-expressing neurons responded to skin touch and colonic distension with similar functional properties. Thus the genetic signature of DRG neurons dictates how they respond to both external and visceral sensory cues.

Piezo2 mediates responses to colon distension

Piezo2 is a mechanosensitive ion channel that is essential for touch and proprioception as well as sensing mechanical signals arising from several internal organs, including changes in blood pressure, lung inflation, and bladder stretch[13,14]. Consistent with this, knocking out the Piezo2 gene resulted in a reduction in the behavioral and autonomic responses to colon distension[8,9] (Figure 2.1c). Moreover, both groups showed that Piezo2-expressing DRG neurons were activated by supraphysiologic distension of the colon, and, using 2-photon imaging, Servin-Vences *et al.* showed that sacral DRG neurons have greatly reduced responses to colon distension in Piezo2 -knockout animals[8]. This reveals that Piezo2 is a major sensor for colonic stretch, adding to the list of important physiologic functions for this protein. However the loss of Piezo2 did not completely eliminate the behavioral responses to supraphysiologic colon distension[9], suggesting that there is another sensor that detects either high-threshold stretch or tissue damage.

What are the key DRG neuron subtypes that use Piezo2 for sensory transduction? Wolfson *et al*. showed that genetic ablation of Piezo2 in Bmpr1b-expressing DRG neurons reduced the behavioral responses to colon distension[9]. They also showed that optogenetic

stimulation of these cells was sufficient to recapitulate the behavioral and autonomic responses to supraphysiologic distension. Responses of colon-innervating DRG afferents are modulated by inflammation[15], and Wolfson and colleagues showed that Bmpr1b neurons were also necessary for behavioral over-reactivity to colon distension after chemically-induced inflammation by the compound dextran sodium sulfate[9]. Thus Bmpr1b cells appear to be a particularly important node for responses to noxious stimuli in the colon.

Loss of Piezo2 impairs GI motility

The discovery that Piezo2 is critical for responses to noxious visceral stimuli raises the question of whether this channel is also involved in normal aspects of GI function. In support of this, Servin-Vences *et al*. found that humans with loss-of-function mutations in Piezo2 report difficulty in sensing their bowel movements, relying instead on sound, smell or vision[8]. Piezo2 deficient humans also reported an increased frequency of both watery stools and constipation, suggesting a potentially complex role for this channel in controlling GI motility.

To determine where Piezo2 acts to control GI motility, Servin-Vences *et al*. ablated the Piezo2 gene from cell classes that could sense mechanical signals from the gut -- vagal afferents, spinal afferents, intestinal epithelial cells, and enteric neurons -- and then measured how this affected the amount of time required for ingested food to be excreted[8]. Surprisingly, only the loss of Piezo2 in DRG neurons had an effect on GI transit, which was accelerated. Piezo2 DRG knockout mice also had watery stools, which mirrors the human phenotype and may be secondary to the more rapid passage of food through the gut, which allows insufficient time for water absorption[8].

The finding that Piezo2 acts in DRG neurons to control GI transit was unexpected, in part because the control of GI motility is traditionally associated with enteric and vagal rather than spinal pathways. As stated above, enteric neurons generate the peristalsis that propels food through the intestine, whereas the vagus nerve controls gastric accommodation and

emptying via vagovagal reflexes[16–18]. Both of these processes involve mechanosensation, and the fact that loss of Piezo2 in vagal and enteric neurons has no effect on GI transit times suggests that other, unidentified mechanosensors operate in these cells to control gut motility. An additional unanswered question regards how mechanosensing by Piezo2 in DRG neurons functions to modulate GI motility – i.e. what is the relevant mechanosensory stimulus and downstream circuitry. Servin-Vences *et al*. showed that loss of Piezo2 independently accelerates GI transit in the stomach, small intestine, and colon, indicating that this effect is not restricted to a single tissue[8]. Interestingly, loss of Piezo2 accelerated GI transit in fed but not fasted animals, suggesting that DRG neurons may sense the presence of food in the gut via Piezo2 and then signal to globally decelerate GI transit. This could occur through a reflex loop involving the activation of sympathetic neurons that innervate the myenteric plexus, which are known to inhibit GI motility, or through a longer loop that passes through the CNS. Given how little is known about the role of spinal afferents in regulating gut motility, elucidation of these pathways is likely to be an active area of future research.

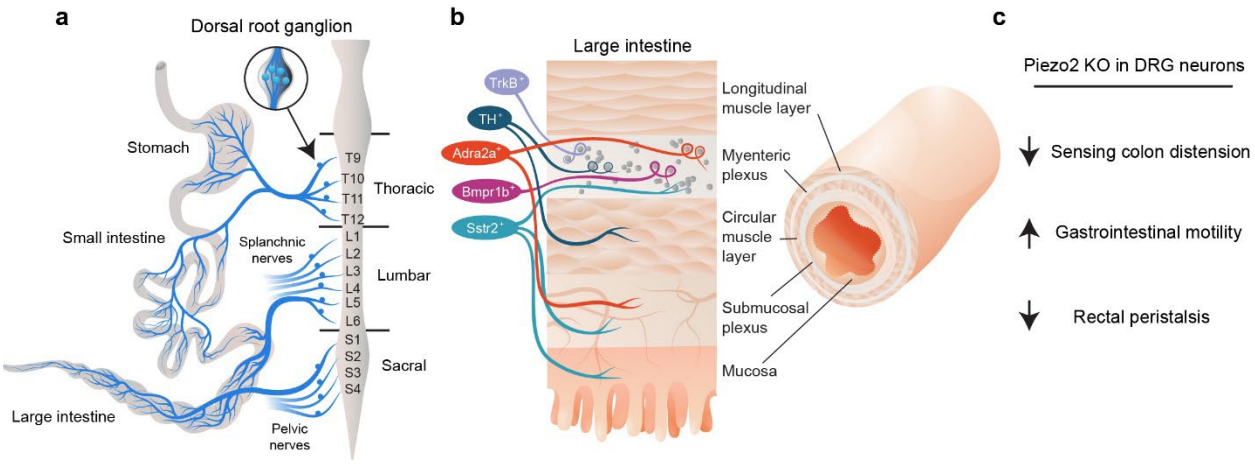


Figure 2.1 | Spinal sensory neurons that innervate the intestines.
a, Spinal sensory neurons in the dorsal root ganglion (DRG) innervate the gastrointestinal tract — from the stomach to the small and large intestines. The sensory neurons that innervate the large intestine (also known as the colon) have cell bodies in the lumbar and sacral segments of the spinal cord. **b**, DRG neurons expressing the genetic markers TrkB, TH, Adra2a, Bmpr1b, or Sstr2 innervate different tissue layers of the large intestine and tile force space. **c**, Loss of the mechanosensitive channel Piezo2 in DRG neurons results in impaired sensing of colon distension, accelerated GI motility, and impaired rectal peristalsis or defecation. (Illustrations by Julia Kuhl.)

REFERENCES

1. Williams, E.K., Chang, R.B., Strochlic, D.E., Umans, B.D., Lowell, B.B., and Liberles, S.D. Sensory Neurons that Detect Stretch and Nutrients in the Digestive System. *Cell* **166**, 209–221 (2016).
2. Mercado-Perez, A., and Beyder, A. Gut feelings: mechanosensing in the gastrointestinal tract. *Nat Rev Gastroenterol Hepatol* **19**, 283–296 (2022).
3. Bai, L., Mesgarzadeh, S., Ramesh, K.S., Huey, E.L., Liu, Y., Gray, L.A., Aitken, T.J., Chen, Y., Beutler, L.R., Ahn, J.S., *et al*. Genetic Identification of Vagal Sensory Neurons That Control Feeding. *Cell* **179**, 1129-1143.e23 (2019).
4. Kim, M., Heo, G., and Kim, S.-Y. Neural signalling of gut mechanosensation in ingestive and digestive processes. *Nat Rev Neurosci* **23**, 135–156 (2022).
5. Gebhart, G.F., and Bielefeldt, K. *Physiology of Visceral Pain. Compr Physiol* **6**, 1609–1633 (2016).
6. Bayrer, J.R., Castro, J., Venkataraman, A., Touhara, K.K., Rossen, N.D., Morrie, R.D., Maddern, J., Hendry, A., Braverman, K.N., Garcia-Caraballo, S., *et al*. Gut enterochromaffin cells drive visceral pain and anxiety. *Nature* **616**, 137–142 (2023).
7. McCoy, E.S., Taylor-Blake, B., and Zylka, M.J. CGRPα-Expressing Sensory Neurons Respond to Stimuli that Evoke Sensations of Pain and Itch. *PLOS ONE* **7**, e36355 (2012).
8. Servin-Vences, M.R., Lam, R.M., Koolen, A., Wang, Y., Saade, D.N., Loud, M., Kacmaz, H., Frausto, S., Zhang, Y., Beyder, A., *et al*. PIEZO2 in somatosensory neurons controls gastrointestinal transit. *Cell* (In Press).
9. Wolfson, R.L., Abdelaziz, A., Rankin, G., Kushner, S., Qi, L., Mazor, O., Seungwon, C., Sharma, N., Ginty, D.D. DRG afferents that mediate physiologic and pathologic mechanosensation from the distal colon. *Cell* (In Press).

10. Handler, A., and Ginty, D.D. The mechanosensory neurons of touch and their mechanisms of activation. *Nat Rev Neurosci* **22**, 521–537 (2021).

11. Spencer, N.J., Kyloh, M., and Duffield, M. Identification of Different Types of Spinal Afferent Nerve Endings That Encode Noxious and Innocuous Stimuli in the Large Intestine Using a Novel Anterograde Tracing Technique. *PLOS ONE* **9**, e112466 (2014).

12. Spencer, N.J., and Hu, H. Enteric nervous system: sensory transduction, neural circuits and gastrointestinal motility. *Nat Rev Gastroenterol Hepatol* **17**, 338–351 (2020).

13. Marshall, K.L., Saade, D., Ghitani, N., Coombs, A.M., Szczot, M., Keller, J., Ogata, T., Daou, I., Stowers, L.T., Bönnemann, C.G., *et al*. PIEZO2 in sensory neurons and urothelial cells coordinates urination. *Nature* **588**, 290–295 (2020).

14. Nonomura, K., Woo, S.-H., Chang, R.B., Gillich, A., Qiu, Z., Francisco, A.G., Ranade, S.S., Liberles, S.D., and Patapoutian, A. Piezo2 senses airway stretch and mediates lung inflation-induced apnoea. *Nature* **541**, 176–181 (2017).

15. Gao, X., Han, S., Huang, Q., He, S.-Q., Ford, N.C., Zheng, Q., Chen, Z., Yu, S., Dong, X., and Guan, Y. Calcium imaging in population of dorsal root ganglion neurons unravels novel mechanisms of visceral pain sensitization and referred somatic hypersensitivity. *Pain* **162**, 1068–1081 (2021).

16. Sanders, K.M., Koh, S.D., Ro, S., and Ward, S.M. Regulation of gastrointestinal motility--insights from smooth muscle biology. *Nat Rev Gastroenterol Hepatol* **9**, 633–645 (2012).

17. Goyal, R.K., Guo, Y., and Mashimo, H. Advances in the physiology of gastric emptying. *Neurogastroenterol Motil* **31**, e13546 (2019).

18. Travagli, R.A., and Anselmi, L. Vagal neurocircuitry and its influence on gastric motility. *Nat Rev Gastroenterol Hepatol* **13**, 389–401 (2016).

III. Sequential appetite suppression by oral and visceral feedback to the brainstem

ABSTRACT

The termination of a meal is controlled by dedicated neural circuits in the caudal brainstem. A key challenge is to understand how these circuits transform the sensory signals generated during feeding into the dynamic control of behavior. The caudal nucleus of the solitary tract (cNTS) is the first site in the brain where many meal-related signals are sensed and integrated[1–4], but how the cNTS processes ingestive feedback during behavior is unknown. Here we describe how PRLH and GCG neurons, two principal cNTS cell types that promote non-aversive satiety, are regulated during ingestion. PRLH neurons showed sustained activation by visceral feedback when nutrients were infused into the stomach, but surprisingly these sustained responses were greatly reduced during oral consumption. Instead, PRLH neurons shifted to a phasic activity pattern that was time-locked to ingestion and linked to the taste of food. Optogenetic manipulations revealed that PRLH neurons control the duration of seconds-timescale feeding bursts, revealing a mechanism by which orosensory signals feedback to restrain the pace of ingestion. In contrast, GCG neurons were activated by mechanical feedback from the gut, tracked the amount of food consumed, and promoted satiety that lasted for tens of minutes. These findings reveal that sequential negative feedback signals from the mouth and gut engage distinct circuits in the caudal brainstem, which in turn control elements of feeding behavior operating on short and long timescales.

INTRODUCTION

The cNTS is the direct target of vagal afferents that innervate the gastrointestinal (GI) tract and detect GI stretch and intestinal nutrients[1–9]. These negative feedback signals are thought to gradually intensify as a meal progresses, thereby activating cNTS circuits that promote the termination of feeding. Consistently, the cNTS contains neurons that are important

for satiation[10–17], and these cells can be activated by meal-related signals, as measured by *Fos* expression[5,8,17] and recordings in anesthetized animals[7,18,19] or brain slices[20].

Nevertheless, the role of the cNTS in feeding behavior has never been tested by recording the activity of these circuits in an awake animal. Thus, it remains unknown how slow feedback from the stomach and intestines – which accumulates over tens of minutes during and after feeding – is utilized by the brain to steer moment-by-moment decisions about behavior. Nor is it known whether the cNTS detects other kinds of ingestive cues that also regulate feeding behavior. Addressing these questions requires defining how the sensory signals generated during a meal are encoded in the circuits that are the direct recipients of visceral feedback.

The cNTS contains a diversity of genetically-distinct cell types[10–17,21], and one attractive model is that these cell types are tuned to sense different visceral signals, which, in turn, control different aspects of feeding behavior. Arguing against this, anesthetized recordings found that cNTS cell types show little specificity in their responses to different GI stimuli[7]. However, anesthetized preparations lack most of the sensory and motor feedback that is generated during natural ingestion, raising the possibility that cNTS neurons may exhibit greater functional specificity in awake animals, as observed in other sensory systems[22]. We therefore investigated the natural dynamics of satiety-promoting cNTS cell types during a meal.

RESULTS

We first investigated prolactin-releasing hormone (PRLH) neurons, a cNTS cell type[21] that is directly innervated by vagal afferents[14,20], expresses *Fos* in response to ingestion[23], and inhibits feeding without inducing conditioned taste avoidance[15], and for this reason is thought to be critical for non-aversive satiety[3] (Figure 3.7). We generated and validated *Prlh*^{Cre} knock-in mice (616 ± 84 cNTS neurons per mouse; Figure 3.8a-g)[17,23] and showed that optogenetic

stimulation of PRLH neurons inhibited food but not water intake (Figure 3.9a-c), confirming that these cells specifically regulate feeding.

We next prepared mice for fiber photometry recordings of PRLH neurons in awake animals (Figure 3.1a). Because PRLH neurons can be activated by GI feedback[23], we also equipped mice with intragastric (IG) catheters and first measured responses to direct infusion of nutrients into the stomach (Figure 3.1a). Infusion of the liquid diet Ensure (1.5 mL) resulted in a ramping activation (latency: 3.5 ± 0.6 min) that correlated with the amount infused, peaked several minutes after the infusion ended (16 ± 4 min), and then remained elevated for the duration of the session (Figure 3.1b, Figure 3.9d). Similar ramping activation was observed in response to infusions of glucose, fat (Intralipid), or MDG (an agonist of the intestinal glucose sensor SGLT1[24]) but not saline (Figure 3.1b; time to peak: 21 ± 2 min for glucose; 22 ± 4 min for Intralipid). Thus, PRLH neurons are progressively activated over tens of minutes following IG nutrient infusions in a manner consistent with intestinal feedback[25].

Oral intake renders GI cues dispensable

We next fasted mice overnight and measured responses to self-paced feeding (30 min; Figure 3.1c). In contrast to IG infusion of the same substances, PRLH neurons were activated within seconds by oral consumption of nutritive solutions (3.5 ± 0.6 z during Ensure consumption, $p < 0.0001$; Figure 3.1c, Figure 3.9e-g). A similar rapid activation was observed during consumption of chow and high-fat diet (HFD) but not water or saline (Figure 3.9k-q). Interestingly, PRLH neuron activation during oral ingestion did not further increase as the trial progressed, and, as a result, PRLH neuron activity during natural feeding did not track cumulative food intake (in contrast to the response to IG infusions; Figure 3.1d-f and Figure 3.9o). This discrepancy between oral and IG responses persisted when we precisely matched the amount and duration of nutrient delivery to the mouth and stomach (Figure 3.9h-j).

To test the necessity of GI signals during oral ingestion, we designed an experiment in which GI feedback could be blocked while mice consumed food by mouth. We did this by taking advantage of the fact that many gut-brain signals of fat ingestion are mediated by cholecystokinin (CCK)[19,24,26,27]. First, we confirmed that intraperitoneal (IP) injection of CCK activated PRLH neurons, consistent with *Fos* studies[28,29] (Figure 3.9r). Next, we showed that the PRLH neuron activation following IG infusion of Intralipid was abolished by prior injection of the CCKAR antagonist devazepide[19,26,27,30], indicating that CCK is required for the response to IG fat (Figure 3.1g). Finally, we repeated this experiment, but this time allowed the mice to consume Intralipid by mouth (Figure 3.1h). Remarkably, the activation of PRLH neurons by oral Intralipid was unaffected by devazepide pretreatment, even though this abolished the response to IG Intralipid in the same animals (Figure 3.1g-h and Figure 3.9s). This reveals that, although all food consumed by mouth reaches the stomach, some feedback mechanisms that activate PRLH neurons following IG infusion become dispensable during a normal meal.

PRLH neurons track ingestion dynamics

PRLH neuron activity was most strongly correlated with intake in the preceding 10 s, indicating that these cells are regulated by oral contact with food or its close correlate (PCC = 0.60 ± 0.01, $p < 0.0001$ compared to shuffled controls; Figure 3.2a-b). Consistently, their activation during ingestion of liquid diets was time-locked to licking (Figure 3.2a). For example, during Ensure consumption, PRLH neuron activity rapidly increased after the first lick in each bout (τ = 3.7 ± 0.4 s; Figure 3.2c) and then declined to baseline after licking stopped (λ = 7.5 ± 0.5 s; Figure 3.2d) in a manner that did not vary with satiety state or trial progression (Figure 3.10a-c). Glucose and Intralipid consumption induced similar time-locked activation of PRLH neurons (Figure 3.2e-g and Figure 3.10d), indicating that this rapid response is not linked to a single macronutrient, whereas these responses were much smaller when mice drank water or saline (indicating that fluid consumption is insufficient); when they performed dry licks at an

empty sipper (indicating that motor signals are insufficient); or following insertion of an oral gavage needle into the esophagus (indicating a limited role for esophageal distension; Figure 3.2e-f and Figure 3.10e-i). We also observed little response to social or stressful stimuli or sickness-inducing agents (Figure 3.9t-v). Thus, PRLH neurons are specifically and rapidly activated by oral contact with food.

The stronger activation of PRLH neurons by food relative to water could be a direct consequence of its sensory properties (e.g. taste or nutrient content) or secondary to differences in behavior (e.g. faster ingestion of nutritive solutions). There was a small increase in the neural response per bout for larger bouts of water consumption (Figure 3.2h), indicating that ingestion rate influences PRLH neuron activity independent of nutrients. However, consumption of glucose and Intralipid resulted in larger PRLH neuron responses at all bout sizes (Figure 3.2h-i and Figure 3.10j). To further characterize the contribution of these variables, we built a generalized linear model of PRLH neuron dynamics during consumption of multiple tastants (Figure 3.2j-l). The model that explained the most variance incorporated a constant variable indicating whether the tastant had calories, cumulative intake in the preceding 10 s, and the instantaneous lick rate (Figure 3.2j-k and Figure 3.10k). Thus PRLH neurons are activated by a signal linked to the chemical properties of food, which then interacts with the ingestion rate.

PRLH neurons are activated by food tastes

The preferential activation of PRLH neurons by caloric foods could be due to their nutrient content or their taste. Consumption of the non-caloric sweetener sucralose caused strong, time-locked activation during licking that was similar to glucose in dynamics and magnitude, whereas IG infusions of sucralose did not activate PRLH neurons (Figure 3.11a-h). Thus, sweet taste alone is sufficient to activate PRLH neurons during normal ingestion.

To test whether taste is required for the lick-triggered activation of PRLH neurons, we crossed *Prlh*^{Cre} mice into the background of “taste-blind” *Trpm5* knockout mice (*Prlh*^{Cre} *Trpm5*$^{-/-}$)

to perform photometry recordings of PRLH neurons in mice that have greatly reduced ability to taste (Figure 3.3a and Figure 3.11i). CCK injection activated PRLH neurons to a similar extent in both taste-blind mice and wild type controls (Figure 3.3b), but responses to glucose ingestion were greatly reduced in taste-blind animals (3.8 ± 0.6 z vs. 0.6 ± 0.3 z for WT vs. taste-blind mice, p = 0.0004; Figure 3.3c and Figure 3.11j-l,w). These differences persisted after accounting for the number of licks in each bout (Figure 3.11k) and were not fully rescued by long-term exposure to glucose (Figure 3.11m-o). We observed a similar loss of neural responses to sucralose, but not fat ingestion, in taste-blind mice (Figure 3.3d and Figure 3.11p-w). Thus the activation of PRLH neurons by sweet substances requires taste signaling, whereas fat may be detected by *Trpm5* – independent pathways[31].

Fiber photometry reports population responses but cannot reveal the activity of individual neurons. Previous efforts to perform single-cell imaging in the cNTS of awake animals were hindered by large motion artifacts[7]. However we found that combining head-fixation with lower body restraint was sufficient to enable stable single-cell recordings of PRLH neurons while mice consumed liquid diets (Figure 3.3e and Figure 3.12a). Mice were food deprived overnight, acclimated to the restraint, and then given brief access to different tastants. Ensure consumption rapidly activated most PRLH neurons (70% of cells) in a manner that was triggered by contact with food, reached a peak near the end of the bout (τ = 5.8 ± 0.4 s), and then gradually decayed when the sipper was removed (Figure 3.3f-g and Figure 3.12b-e). Intralipid or sucralose consumption produced similar responses, whereas fewer cells were activated by water consumption and the magnitude of their activation was smaller (Figure 3.3h-k and Figure 3.12f-r). Thus individual PRLH neurons are activated by tastes associated with food but only weakly by ingestion per se.

The high percentage of cells activated by consumption of sweet solutions (sucralose: 74% of all neurons) and fatty solutions (Intralipid: 80% of all neurons) implies that most PRLH neurons are not specialized to respond to a single taste. To ask whether gustatory and post-

ingestive signals activate the same neurons, we allowed mice to briefly lick sucralose and then injected them with CCK. We observed strong, sustained activation of many PRLH neurons in response to CCK (Figure 3.3l and Figure 3.12s), but the overlap between these CCK-activated cells and those that responded to sucralose was not different from chance ($p = 0.784$ from Fisher's exact test), and the magnitude of the individual cell responses to these two stimuli was not correlated (Figure 3.3m). Thus gustatory and visceral signals each activate a large and partially overlapping subset of PRLH neurons.

PRLH neurons pace food ingestion

PRLH neuron stimulation inhibits food intake (Figure 3.9a-b), but this tonic activation does not match the natural, ingestion-triggered activity of these cells. We therefore selectively manipulated PRLH neuron activity during licking using closed-loop optogenetics (Figure 3.4a). Stimulation during licking (Lick-ON) decreased Ensure consumption via a reduction in bout size (111 ± 11 licks vs. 23 ± 8 licks, no laser vs. laser trials, $p<0.0001$) with no effect on bout number (Figure 3.4b and Figure 3.13a-b). In contrast, stimulation of PRLH neurons only when mice were not licking (Lick-OFF) had no effect on ingestion, even though mice received ten times more laser pulses compared to the Lick-ON test (Figure 3.13c-d). Thus PRLH neuron stimulation only inhibits food intake when mice are actively licking.

To test whether the natural bursts in PRLH neuron activity during licking are required for feeding regulation, we targeted the optogenetic silencer GtACR1 to PRLH neurons and performed closed-loop inhibition (Figure 3.4c-d and Figure 3.13e-g). Silencing PRLH neurons during licking increased bout size for Ensure and Intralipid consumption, both as measured by the number of licks and duration of licking (Figure 3.4c-d and Figure 3.13f-h). Thus, PRLH neurons influence feeding primarily by regulating the size of ingestion bursts.

We next investigated the mechanism by which PRLH neurons restrain the size of individual bouts. Several observations suggest that PRLH neurons do not control motor circuits

directly (Figure 3.13i-l and Supplementary Discussion). On the other hand, the size or duration of a lick bout is correlated with the palatability of an ingested solution and can reflect hedonic motivation or "liking"[32]. This suggests that PRLH neurons may modulate feeding bursts by rapidly altering the valence of ingestion. To test this, we asked whether PRLH neuron stimulation or silencing could bias an animal's real-time preference for one of two sippers containing identical solutions (Figure 3.4e). Pairing the preferred sipper with PRLH neuron stimulation caused a near complete switch in sipper preference, such that animals drank only from the bottle that lacked stimulation (0.8 ± 0.1 vs. 0.02 ± 0.004 preference ratio on day 1 vs. day 2, $p<0.0001$; Figure 3.4f-g and Figure 3.13m). Switching the sipper that was paired with optogenetic stimulation again reversed the sipper preference to the other side (Figure 3.4f-g and Figure 3.13m). These changes in sipper preference occurred without any changes in total intake (Figure 3.4g and Figure 3.13n-o), indicating that activation of these cells does not produce lasting satiety or aversion.

Pairing one sipper with closed-loop silencing of PRLH neurons gave the opposite result, in which the animals preferentially drank out of the sipper coupled to silencing without any change in total consumption (Figure 3.4h and Figure 3.13p-r). We observed a similar response to closed-loop silencing during sucralose ingestion, whereas silencing during water consumption had no effect (consistent with the activation of PRLH neurons by sucralose but not water ingestion; Figure 3.13s-t). Taken together, these data support a model in which PRLH neurons are activated by food tastes and, in turn, rapidly modulate food palatability, thereby restraining the pace of ingestion. This negative feedback function would operate in parallel with, and partially counteract, the well-known effect of appetitive tastes to promote food consumption.

GCG neurons track visceral feedback

The fact that PRLH neurons control ingestion on a seconds timescale in response to gustatory cues raises the question of which cNTS cells regulate ingestion in response to GI

feedback, which is the traditional function ascribed to this structure[1–4]. To address this, we examined GCG neurons, a distinct cell type that has been extensively studied alongside PRLH neurons for its role in non-aversive satiety[10,11,13,33]. GCG neurons express the anorexigenic peptide GLP-1[13], are activated by ingestion as measured by *Fos* staining[10,34], and inhibit food intake when stimulated without inducing conditioned taste avoidance[13,33].

GCG neurons were spatially intermingled with PRLH neurons in the cNTS but non-overlapping (290 ± 74 cells per mouse; Figure 3.14a). We prepared mice for photometry recordings of GCG neurons and measured neural responses to Ensure consumption (Figure 3.5a-b and Figure 3.14a-b). In contrast to PRLH neurons, which were activated coincident with the first lick, GCG neurons responded after a delay of several seconds (Figure 3.5a and Figure 3.14d) with ramping activation (T_{50} = 2.4 ± 0.9 min) that then remained above baseline for the duration of the session (6.3 ± 1 z across the 30 min trial, $p < 0.0001$; Figure 3.5b). A similar sustained activation was observed following consumption of glucose, Intralipid, chow or HFD, but not in response to non-food or aversive stimuli (Figure 3.5b and Figure 3.14b-d, 3.14o-r, 3.15a-c). Thus, GCG neurons are strongly and specifically activated by consumption of food.

Several lines of evidence indicated that, in contrast to PRLH neurons, GCG neuron activity is not driven primarily by gustatory or other pre-gastric cues. First, the time-locked activation of GCG neurons during each lick bout was much weaker than for PRLH neurons for all liquid diets tested (Figure 3.14e-g). Second, GCG neurons were not activated by ingestion of sucralose and their activation by glucose was not impaired in taste-blind mice (Figure 3.5b and Figure 3.14h-j, l-n), indicating that taste is neither necessary nor sufficient. Indeed, we found that GCG neuron activity was most strongly correlated with Ensure consumption over longer timescales (4-10 min; Figure 3.14k), suggesting that these cells are regulated by feedback from the stomach and intestines.

We performed two experiments to test the hypothesis that GCG neurons track cumulative food intake on a minutes timescale. First, we controlled the rate at which mice were

allowed to ingest Ensure and then measured the neural response to different ingestion volumes (Figure 3.5c-d). Consumption of Ensure for 5 s every 60 s (repeated 10 times) failed to activate GCG neurons (Figure 3.5c), in contrast to the strong activation of PRLH neurons in similar brief-access taste tests (Figure 3.3). However, increasing the access duration to 60 s resulted in a clear ramping activation of GCG neurons that correlated with the amount consumed ($R^2 = 0.42$, $p < 0.0001$; Figure 3.5d and Figure 3.15e), suggesting that they are progressively activated by GI fill. Second, to characterize how post-prandial GCG neuron activity relates to the amount of food consumed, we gave fasted mice access to either chow or HFD for 10 min, then removed the food and measured GCG neuron responses over the following 20 min (Figure 3.5e). We found that the post-ingestive activity of GCG neurons scaled linearly with the amount of food consumed during the preceding 10 min access, confirming that these cells track cumulative food intake ($R^2 = 0.85$, $p < 0.0001$; Figure 3.5e and Figure 3.15f-g). In contrast, there was no correlation between the post-ingestive activity of PRLH neurons and the amount consumed, consistent with the fact that PRLH neurons track short-term orosensory cues (Figure 3.5f and Figure 3.15h-i).

To demonstrate the sufficiency of GI signals, we performed IG infusions of nutritive solutions, which triggered a strong, ramping activation of GCG neurons that correlated with the amount infused (Figure 3.15j-m). Of note, we observed strong responses in GCG neurons to infusions of only 1.0 mL, whereas PRLH neuron responses at this volume were weak (Figure 3.15j-l,p), indicating that GCG neurons are inherently more sensitive to GI feedback. Furthermore, GCG neuron responses to nutrient infusion into the stomach closely resembled GCG neuron responses to the same nutrient consumed by mouth (Figure 3.15n-o), whereas PRLH neurons showed dramatic differences depending on the route of ingestion (Figure 3.1). Thus, GI feedback is sufficient to explain the activation of GCG neurons during natural ingestion.

The activation of GCG neurons by post-ingestive feedback could be due to signals of GI stretch, nutrient sensing, or both[5,24]. To test the sufficiency of GI stretch, we infused into the stomach the non-nutritive sugar mannitol, which is not absorbed and therefore induces significant intestinal distension[35]. Mannitol infusion strongly activated GCG neurons (5.0 ± 1.7 z, p = 0.0002), but not PRLH neurons (0.6 ± 0.6 z, p = 0.71; Figure 3.15j-l). IG infusions of air (1.0 mL), a pure mechanosensory signal, also activated GCG neurons but not PRLH neurons (Figure 3.15q). In contrast to these robust responses to distension, GCG neurons were broadly insensitive to gut peptides released in response to intestinal nutrients, including CCK (Figure 3.15d,r-t). These data indicate that GCG neurons respond preferentially to GI stretch, although a modulatory role for nutritive signals is possible.

GCG neurons promote long-lasting satiety

Continuous optogenetic stimulation of GCG neurons inhibited consumption of solid and liquid food but not water (Figure 3.6a-c and Figure 3.16a-d), confirming that these neurons are involved in regulating feeding but not drinking. The fact that GCG neuron activity was not strongly time-locked to bouts of ingestion suggests that, unlike PRLH neurons, these cells do not specifically control the moment-by-moment dynamics of feeding. Indeed, closed-loop stimulation of GCG neurons during licking not only inhibited ongoing consumption but also reduced the initiation of later bouts (Figure 3.16e).

This long-lasting effect, combined with the observation that GCG neurons remain activated throughout feeding (Figure 3.5), led us to hypothesize that GCG neuron activity may be integrated over time to influence the duration of post-prandial satiety. To test this, we used a pre-stimulation protocol[36,37] (Figure 3.6d) in which we stimulated GCG neurons in the absence of food (thereby mimicking the activation that would occur during and immediately after a meal), then turned the laser off and made food available. Pre-stimulation of GCG neurons (1 h) caused a strong reduction subsequent food intake that persisted long after the offset of laser stimulation

(2.5 ± 0.1 vs. 0.8 ± 0.2 mL, no pre-stim vs. pre-stim trials, p=0.0008; Figure 3.6e-f and Figure 3.16f). This long-lasting effect was due to a reduction in the initiation of feeding bouts (Figure 3.6f and Figure 3.16f), with no effect on bout size. This was observed with both solid and liquid food and, importantly, was dose-dependent, with longer pre-stimulation causing greater inhibition of subsequent feeding (Figure 3.6g and Figure 3.16g). In contrast, pre-stimulation of PRLH neurons had no effect in any feeding assay (Figure 3.6h-i and Figure 3.16h-i), confirming that PRLH neurons control behavior on shorter timescales.

DISCUSSION

The cNTS is the first site in the brain where many meal-related signals are sensed and integrated, including almost all GI signals transmitted by the vagus nerve. Thus it is critical to establish how ingestive feedback is represented in the cNTS and used to control behavior. Here we have focused on PRLH and GCG neurons, which are the two principal cell types in the cNTS that have been implicated in the non-aversive suppression of feeding[10–17] (Figure 3.7). We found that PRLH neuron activity was synchronized to bouts of ingestion and controlled the duration of seconds-timescale feeding bursts, whereas GCG neurons were activated by slower post-ingestive feedback and promoted satiety that lasts for tens of minutes. These findings reveal that negative feedback signals from the mouth and gut engage genetically-distinct circuits in the caudal brainstem, which in turn control feeding behavior operating on short and long timescales (Figure 3.17).

PRLH neurons receive abundant feedback from the vagus nerve[14,20] and remain activated for tens of minutes after nutrient infusion into the stomach, but this sustained activation by visceral feedback is greatly reduced during normal feeding. Instead, PRLH neuron activity is dominated by time-locked responses to orosensory cues, including taste. Because the cNTS does not receive direct gustatory feedback[1], these orosensory signals are likely relayed

by forebrain structures or premotor areas that innervate the cNTS[15]. Consistent with their primary regulation by orosensory rather than visceral cues, we found that PRLH neurons function to limit the size of ingestion bursts, with little effect on total intake, thereby restraining the pace of ingestion. This may be important for preventing the GI distress that occurs when food is consumed too quickly[38].

In contrast to PRLH neurons, GCG neurons responded strongly to mechanosensory feedback from the gut, consistent with results from *Fos* studies[5] and rabies tracing[11]. The fact that optogenetic pre-stimulation of GCG neurons caused a dose-dependent, long-lasting satiety suggests that release of GLP-1 can be integrated over time in downstream circuits to produce sustained reductions in appetite. A similar long-lasting effect may be important for the clinical efficacy of GLP-1 receptor agonists in reducing food intake[39].

SUPPLEMENTARY DISCUSSION

PRLH and GCG neurons are distinct cell types in the cNTS that regulate the non-aversive suppression of feeding

In this study, we focused on investigating the two principal cNTS cell types that have been implicated in “non-aversive satiety”, i.e. the suppression of feeding in the absence of nausea or sickness[1–10]. One of these cell types is defined by the expression of prolactin-releasing hormone (encoded by the *Prlh* gene) and the other by the expression of glucagon-like peptide 1 (encoded by the *Gcg* gene). These two marker genes are unique in that they label transcriptionally homogeneous cNTS cell types[11] that are intermingled but non-overlapping[11,12], directly innervated by vagal afferents[2,5,13,14], activated by ingestion as measured by *Fos* expression[1,4,15], and functionally validated to inhibit feeding without inducing aversion[2,6,10,16] (Figure 3.7). These two genes also overlap with several broader, and more heterogeneous,

populations of cNTS neurons that have been independently implicated in the control of feeding (described in Figure 3.7 and refs.[4,6,11,17]).

Post-Ingestive learning does not rescue the response of PRLH neurons to sweet taste

To test whether post-ingestive learning can rescue the rapid activation of PRLH neurons by sweet taste, we gave *Prlh*^{Cre} *Trpm5*$^{-/-}$ mice access to a glucose solution (24%) overnight twice, with a day of separation in between (Methods). Long-term exposure to glucose increased glucose consumption in a subset of taste-blind mice, consistent with previous reports that these animals acquire preferences for nutritive solutions via post-ingestive feedback[18–21] (Figure 3.11m). This increase in ingestion rate partially restored the rapid response of PRLH neurons to glucose ingestion (Figure 3.11n) but did not rescue the neural response per lick, indicating that this requires taste (0.03 ± 0.01 z for learned animals compared to 0.02 ± 0.01 z for naïve animals, p = 0.5476; Figure 3.11o). Thus, the activation of PRLH neurons by sweet substances requires canonical taste signaling.

PRLH neurons receive orosensory feedback

The rapid activation of PRLH neurons during feeding was driven by an interaction between the taste of food and the rate of ingestion. This was unexpected in part because gustatory signals are relayed primarily to the rostral NTS (rNTS)[22], whereas the cNTS is associated with visceral feedback transmitted by the vagus nerve. However, PRLH neurons receive descending input from several forebrain structures that could contain information about taste and ingestion dynamics, including the central amygdala, paraventricular hypothalamus, and lateral hypothalamus[23]. In addition, PRLH neurons receive a direct projection from the intermediate reticular formation, a structure that contains premotor neurons for licking[6,24]. The function of these centrifugal projections to the cNTS has received limited attention and dissecting these pathways will be an important area for future investigation.

PRLH neurons do not appear to control sensory-specific satiety

The control of feeding behavior by PRLH neurons appears be unrelated to sensory-specific satiety[25], the process by which repeated exposure to a taste within a meal reduces further consumption of that taste, but does not affect consumption of different tastes. This is because PRLH neuron responses do not increase as the meal progresses (Figure 3.1-2) and because blocking PRLH neuron activation does not increase total consumption (Figure 3.4).

PRLH neuron activation is gated by behavioral state

PRLH neurons receive abundant feedback from the vagus nerve[5,13] and remain activated for tens of minutes after nutrient infusion into the stomach (Figure 3.1c). Thus, the fact that PRLH neurons track orosensory cues during normal ingestion (Figure 3.2) implies that their activation by visceral feedback is in some way suppressed during normal feeding. Indeed, we found that the sustained activation of PRLH neurons observed after IG infusion was absent during normal feeding, even when the amount and duration of food consumption/infusion were matched (Figure 3.1 and Figure 3.9g-i). Consistently, the hormone CCK was required for PRLH neuron activation during IG infusion of fat (CCK) but became dispensable during oral ingestion of the same nutrient (Figure 3.1i-k). How this hierarchy of sensory responses is established is unknown but could involve the filtering of predicted visceral inputs by cNTS interneurons[26,27] to shift learned neural responses forward in time, as is observed in motivational circuits[28,29]. In this regard, the sensory signals generated during a meal occur in a specific sequence (from mouth to stomach to intestines), and they may be interpreted correctly by the brain only when this natural progression is respected[30]. Alternatively, there may be a signal from the mouth-to-gut that suppresses certain GI signals during normal ingestion. The ability to monitor cNTS dynamics during behavior will enable investigation of these basic questions about how signals from the mouth and gut interact during a meal.

Microendoscopic imaging of cNTS neurons in awake behaving mice

In this study, we developed a preparation for recording the single-cell activity of PRLH neurons during ingestion. We implanted an angled GRIN lens above the cNTS (Figure 3.3e) and first attempted to perform imaging in freely moving animals, which was associated with severe brainstem motion (Figure 3.3e). This motion was reduced by head-fixing, but not to the extent that it was feasible to track the dynamics of single cells (Figure 3.3e). This is consistent with previous reports of unsuccessful attempts to perform cNTS imaging in awake animals[26]. However, we noticed that the largest motion artifacts were correlated with lower body movements of the mouse, which could be eliminated by further restraining the torso of the head-fixed animals (Figure 3.3e). This head-fixed, restrained preparation enabled stable calcium recordings while awake mice consumed liquid diets.

PRLH neurons do not control motor circuits directly

In Figure 3.4, we investigated the mechanism by which PRLH neuron activity decreases the size of individual lick bouts. It seemed unlikely that PRLH neurons control motor circuits directly, because manipulating PRLH neuron activity did not change the inter-lick interval (ILI) during a bout (Figure 3.13i-l), a parameter which is determined by central motor pattern generators[31–33] and is invariant during normal behavior. In addition, we failed to observe fictive feeding behaviors (e.g. orofacial movements) in response to PRLH neuron stimulation or silencing in the absence of food, as has been observed for circuits that directly control motor outputs[34].

Disentangling the effects of nutrients from GI distension

In Figure 3.5, the activation of GCG neurons by post-ingestive feedback could be due to signals of GI stretch, nutrient sensing, or both[35–37]. Of note, because calories and food volume are highly correlated[38], and because calories can increase gastric distension by delaying gastric

emptying[39], the feeding experiments described in Figure 3.5 cannot distinguish between these two mechanisms. To test the sufficiency of GI stretch, we infused into the stomach the non-nutritive sugar mannitol, which is not absorbed from the intestines, and therefore induces significant intestinal distension[38]. Mannitol infusion strongly activated of GCG neurons (5.0 ± 1.7 z, p = 0.0002 compared to baseline; Figure 3.15j), but not PRLH neurons (0.6 ± 0.6 z, p = 0.7082 compared to baseline; Figure 3.15k), and the magnitude of this activation was at least as large as that caused by equi-osmotic and equi-volemic infusions of glucose and Ensure (3.2 ± 0.6 z for Ensure infusion, p = 0.6282 compared to mannitol infusion; Figure 3.15j). To present a pure mechanosensory signal to the stomach, we also performed IG infusions of air (1.0 mL), which activated GCG neurons (2.0 ± 0.3 z, p <0.0001 compared to baseline) but not PRLH neurons (-0.1 ± 0.2 z, p = 0.8353 compared to baseline; Figure 3.15p). Together, these data indicate that GI stretch is sufficient to activate GCG neurons but has little effect on PRLH neurons.

GCG neuron stimulation triggers long-lasting satiety

In Figure 6, we found that GCG neuron pre-stimulation in the absence of food caused a striking, long-lasting suppression of the initiation of new feeding bouts (Figure 3.6f). The fact that this response was dose-dependent (Figure 3.6g and Figure 3.16g) suggests that GCG neuron activity can be integrated over time in downstream circuits, likely via release of GLP-1[7], to produce satiety that lasts much longer. Of note, this provides a mechanism to link the amount of food consumed to the time interval before initiation of the next meal. A similar signal integration mechanism has been proposed for hunger-promoting AgRP neurons[40], which promote long-lasting hunger via changes in downstream circuits caused by neuropeptide release[41]. It is likely that competition between these and other neuropeptides, which are released in proportion to the duration of food deprivation or ingestion, is an important part of the mechanism that controls the long-lasting transitions between hunger and satiety.

SUPPLEMENTARY DISCUSSION REFERENCES

1. Holt, M. K. *et al.* Preproglucagon Neurons in the Nucleus of the Solitary Tract Are the Main Source of Brain GLP-1, Mediate Stress-Induced Hypophagia, and Limit Unusually Large Intakes of Food. *Diabetes* **68**, 21–33 (2019).
2. Brierley, D. I. *et al.* Central and peripheral GLP-1 systems independently suppress eating. *Nat. Metab.* **3**, 258–273 (2021).
3. D'Agostino, G. *et al.* Appetite controlled by a cholecystokinin nucleus of the solitary tract to hypothalamus neurocircuit. *eLife* **5**, e12225 (2016).
4. Cheng, W. *et al.* Leptin receptor-expressing nucleus tractus solitarius neurons suppress food intake independently of GLP1 in mice. *JCI Insight* **5**, 134359 (2020).
5. Cheng, W. *et al.* Calcitonin Receptor Neurons in the Mouse Nucleus Tractus Solitarius Control Energy Balance via the Non-aversive Suppression of Feeding. *Cell Metab.* **31**, 301-312.e5 (2020).
6. Cheng, W. *et al.* NTS Prlh overcomes orexigenic stimuli and ameliorates dietary and genetic forms of obesity. *Nat. Commun.* **12**, 5175 (2021).
7. Liu, J. *et al.* Enhanced AMPA Receptor Trafficking Mediates the Anorexigenic Effect of Endogenous Glucagon-like Peptide-1 in the Paraventricular Hypothalamus. *Neuron* **96**, 897-909.e5 (2017).
8. Roman, C. W., Derkach, V. A. & Palmiter, R. D. Genetically and functionally defined NTS to PBN brain circuits mediating anorexia. *Nat. Commun.* **7**, 11905 (2016).
9. Roman, C. W., Sloat, S. R. & Palmiter, R. D. A tale of two circuits: CCKNTS neuron stimulation controls appetite and induces opposing motivational states by projections to distinct brain regions. *Neuroscience* **358**, 316–324 (2017).

10. Qui, W. *et al.* Multiple NTS Neuron Populations Synergistically Suppress Physiologic Food Intake but are Dispensable for the Response to VSG. 2022.12.23.521804 Preprint at https://doi.org/10.1101/2022.12.23.521804 (2022).

11. Ludwig, M. Q. *et al.* A genetic map of the mouse dorsal vagal complex and its role in obesity. *Nat. Metab.* **3**, 530–545 (2021).

12. Maniscalco, J. W., Kreisler, A. D. & Rinaman, L. Satiation and stress-induced hypophagia: examining the role of hindbrain neurons expressing prolactin-releasing Peptide or glucagon-like Peptide 1. *Front. Neurosci.* **6**, 199 (2012).

13. Appleyard, S. M. *et al.* Visceral afferents directly activate catecholamine neurons in the solitary tract nucleus. *J. Neurosci. Off. J. Soc. Neurosci.* **27**, 13292–13302 (2007).

14. Holt, M. K. *et al.* Synaptic Inputs to the Mouse Dorsal Vagal Complex and Its Resident Preproglucagon Neurons. *J. Neurosci. Off. J. Soc. Neurosci.* **39**, 9767–9781 (2019).

15. Cheng, W. *et al.* NTS Prlh overcomes orexigenic stimuli and ameliorates dietary and genetic forms of obesity. *Nat. Commun.* **12**, 5175 (2021).

16. Gaykema, R. P. *et al.* Activation of murine pre-proglucagon-producing neurons reduces food intake and body weight. *J. Clin. Invest.* **127**, 1031–1045 (2017).

17. Rinaman, L. Hindbrain noradrenergic A2 neurons: diverse roles in autonomic, endocrine, cognitive, and behavioral functions. *Am. J. Physiol. Regul. Integr. Comp. Physiol.* **300**, R222-235 (2011).

18. Zukerman, S., Ackroff, K. & Sclafani, A. Post-oral appetite stimulation by sugars and nonmetabolizable sugar analogs. *Am. J. Physiol. Regul. Integr. Comp. Physiol.* **305**, R840-853 (2013).

19. Sclafani, A., Zukerman, S., Glendinning, J. I. & Margolskee, R. F. Fat and carbohydrate preferences in mice: the contribution of alpha-gustducin and Trpm5 taste-signaling proteins. *Am. J. Physiol. Regul. Integr. Comp. Physiol.* **293**, R1504-1513 (2007).

20. Sclafani, A. & Ackroff, K. Flavor preference conditioning by different sugars in sweet ageusic Trpm5 knockout mice. *Physiol. Behav.* **140**, 156–163 (2015).

21. de Araujo, I. E. *et al.* Food reward in the absence of taste receptor signaling. *Neuron* **57**, 930–941 (2008).

22. Hamilton, R. B. & Norgren, R. Central projections of gustatory nerves in the rat. *J. Comp. Neurol.* **222**, 560–577 (1984).

23. Gasparini, S., Howland, J. M., Thatcher, A. J. & Geerling, J. C. Central afferents to the nucleus of the solitary tract in rats and mice. *J. Comp. Neurol.* **528**, 2708–2728 (2020).

24. Dempsey, B. *et al.* A medullary centre for lapping in mice. *Nat. Commun.* **12**, 6307 (2021).

25. Rolls, B. J., Rolls, E. T., Rowe, E. A. & Sweeney, K. Sensory specific satiety in man. *Physiol. Behav.* **27**, 137–142 (1981).

26. Ran, C., Boettcher, J. C., Kaye, J. A., Gallori, C. E. & Liberles, S. D. A brainstem map for visceral sensations. *Nature* **609**, 320–326 (2022).

27. Bailey, T. W., Appleyard, S. M., Jin, Y.-H. & Andresen, M. C. Organization and properties of GABAergic neurons in solitary tract nucleus (NTS). *J. Neurophysiol.* **99**, 1712–1722 (2008).

28. Ljungberg, T., Apicella, P. & Schultz, W. Responses of monkey dopamine neurons during learning of behavioral reactions. *J. Neurophysiol.* **67**, 145–163 (1992).

29. Cohen, J. Y., Haesler, S., Vong, L., Lowell, B. B. & Uchida, N. Neuron-type-specific signals for reward and punishment in the ventral tegmental area. *Nature* **482**, 85–88 (2012).

30. Antin, J., Gibbs, J. & Smith, G. P. Intestinal satiety requires pregastric food stimulation. *Physiol. Behav.* **18**, 421–425 (1977).

31. Boughter Jr, J. D., Baird, J.-P., Bryant, J., St. John, S. J. & Heck, D. C57BL/6J and DBA/2J mice vary in lick rate and ingestive microstructure. *Genes Brain Behav.* **6**, 619–627 (2007).

32. Travers, J. B., Dinardo, L. A. & Karimnamazi, H. Motor and premotor mechanisms of licking. *Neurosci. Biobehav. Rev.* **21**, 631–647 (1997).

33. Nakamura, Y. & Katakura, N. Generation of masticatory rhythm in the brainstem. *Neurosci. Res.* **23**, 1–19 (1995).

34. Han, W. *et al.* Integrated Control of Predatory Hunting by the Central Nucleus of the Amygdala. *Cell* **168**, 311-324.e18 (2017).

35. Vrang, N., Phifer, C. B., Corkern, M. M. & Berthoud, H.-R. Gastric distension induces c-Fos in medullary GLP-1/2-containing neurons. *Am. J. Physiol. Regul. Integr. Comp. Physiol.* **285**, R470-478 (2003).

36. Tsang, A. H., Nuzzaci, D., Darwish, T., Samudrala, H. & Blouet, C. Nutrient sensing in the nucleus of the solitary tract mediates non-aversive suppression of feeding via inhibition of AgRP neurons. *Mol. Metab.* **42**, 101070 (2020).

37. Tolhurst, G., Reimann, F. & Gribble, F. M. Intestinal sensing of nutrients. *Handb. Exp. Pharmacol.* 309–335 (2012) doi:10.1007/978-3-642-24716-3_14.

38. Bai, L. *et al.* Genetic Identification of Vagal Sensory Neurons That Control Feeding. *Cell* **179**, 1129-1143.e23 (2019).

39. Calbet, J. A. & MacLean, D. A. Role of caloric content on gastric emptying in humans. *J. Physiol.* **498** (Pt 2), 553–559 (1997).

40. Chen, Y., Lin, Y.-C., Zimmerman, C. A., Essner, R. A. & Knight, Z. A. Hunger neurons drive feeding through a sustained, positive reinforcement signal. *eLife* **5**, e18640 (2016).

41. Chen, Y. *et al.* Sustained NPY signaling enables AgRP neurons to drive feeding. *eLife* **8**, e46348 (2019).

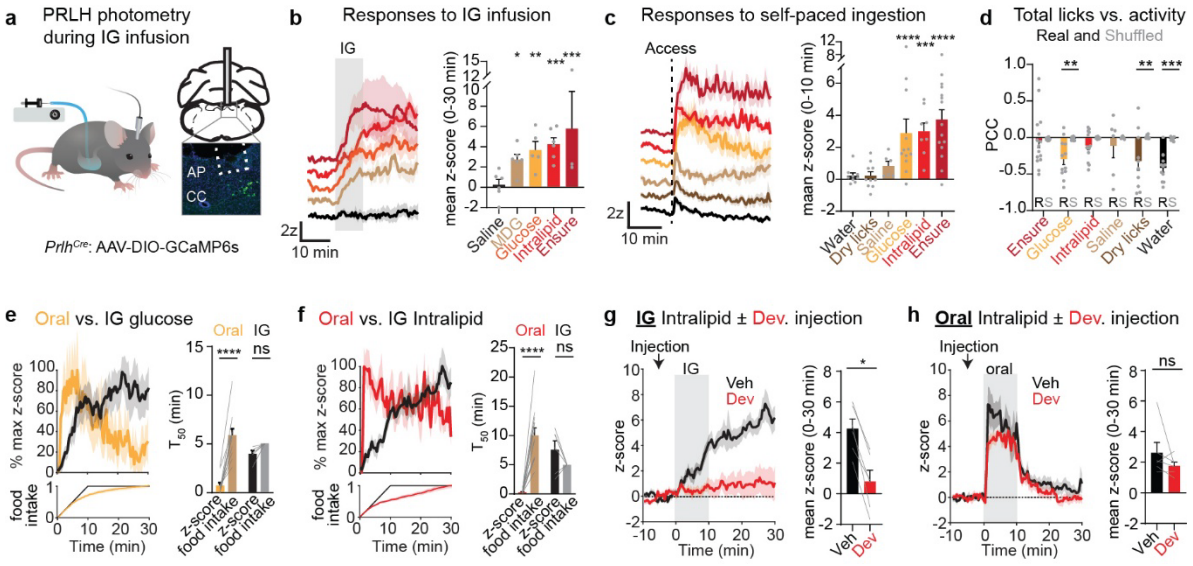


Figure 3.1 | PRLH neurons show different responses to oral ingestion versus IG infusion. **a**, Left, fiber photometry during IG infusions. Right, fiber placement and GCaMP6s expression in PRLH neurons. **b**, Left, Peri-stimulus time histograms (PSTH) of PRLH neuron responses for IG infusions (0-30 min; 1.5 mL) of indicated solutions. Right, z-scores (0-30 min). **c**, Left, PSTH aligned to lickometer access for self-paced consumption. Right, z-scores (0-10 min). **d**, PCC for the cumulative licks performed for each tastant vs. the z-scored change in activity across the 30 min trial. Real data (color) is compared vs. shuffled controls (gray). **e**, Left, PTSH of the percentage of max z-score during oral ingestion (orange) or IG infusion (black) of glucose (1.5 mL). The percentage of total intake is shown on the bottom panel. Right, time to reach 50% of the max z-score ("z-score") versus time to consume 50% of total glucose ("food intake"). **f**, As in panel e, except that data are for oral (red) versus IG Intralipid. **g**, Left, PSTH of PRLH neuron responses to Intralipid IG infusion (0-10 min; 1.5 mL) after an IP injection of devazepide or vehicle. Right, z-scores (0-30 min). **h**, Left, PSTH of PRLH neuron responses for Intralipid oral consumption after an IP injection of devazepide or vehicle. Right, z-scores (0-30 min). NS, *P<0.05, **P<0.01, ***P<0.001, ****P<0.0001. Data are mean ± sem.

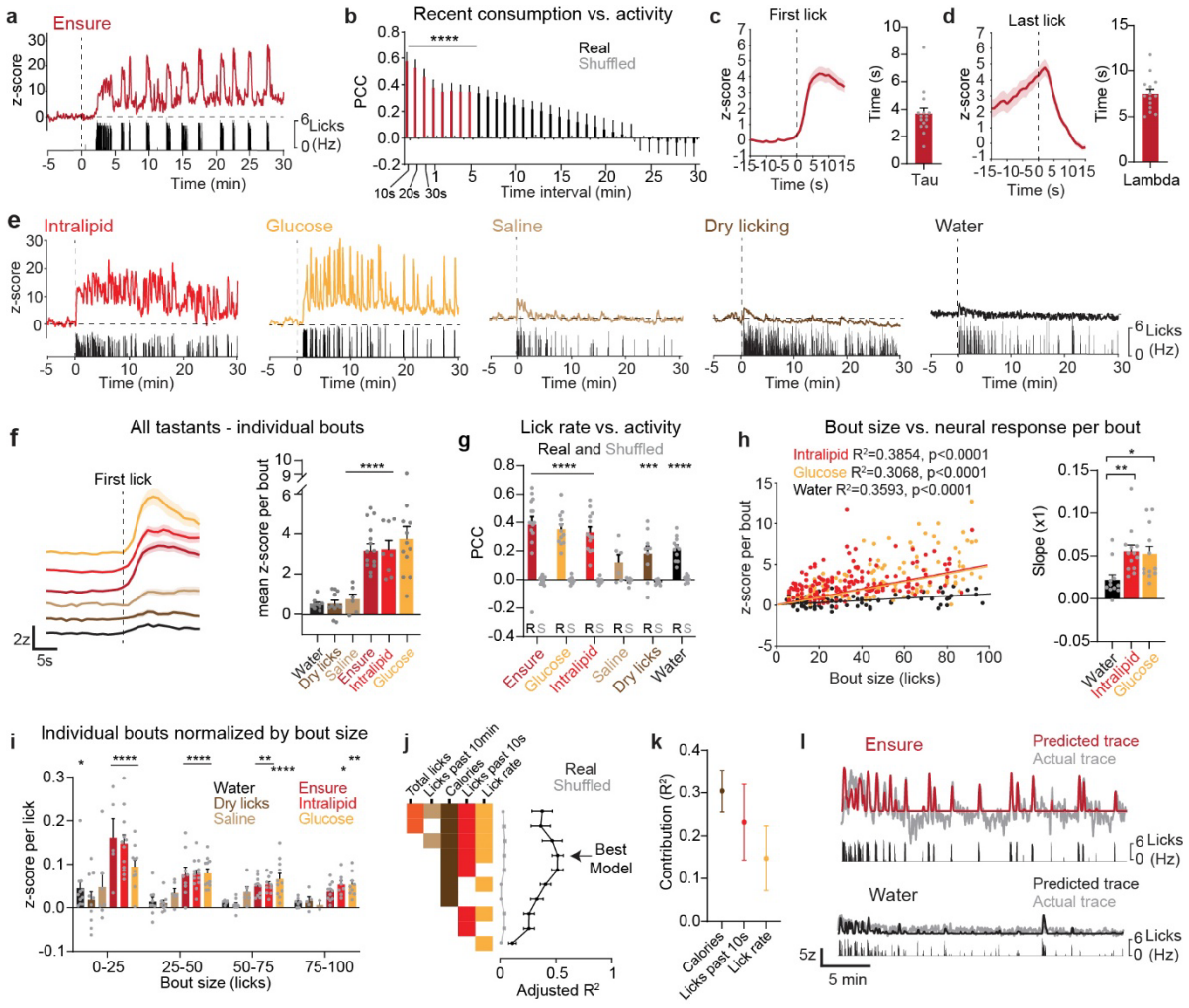


Figure 3.2 | PRLH neurons track the dynamics of ingestion.
a, Example calcium dynamics of PRLH neurons during self-paced Ensure consumption. The lick rate is shown below. **b**, PCC for the relationship between the cumulative licks performed in the preceding time interval and the z-scored change in activity during Ensure consumption. **b**, Left, PSTH aligned to the first lick of the bout for Ensure consumption. Right, time constant (tau) when 63.8% of the z-scored activity change is reached. **d**, Left, PSTH aligned to the last lick of the bout for Ensure consumption. Right, time constant (lambda) when the z-score has decayed to 37% of its value during the last lick of the bout. **e**, Example traces of calcium dynamics during consumption of indicated solutions or dry licking at an empty sipper. Dashed line indicates sipper access. **f**, PSTH of PRLH neuron activity aligned to the first lick for all tastants. Right, response (0-10 s) after first lick. **g**, PCC for the relationship between the instantaneous lick rate during consumption and the z-scored change in activity. **h**, Left, scatterplot for bout size vs. z-score for all bouts during Intralipid, glucose, or water consumption. Right, slope for Intralipid, glucose, and water consumption. **i**, z-score per lick stratified by bout size for each animal. **j**, A GLM was constructed for each animal using subsets of variables (n = 10 mice). See Methods. Adjusted R2 (black line) is plotted against the shuffled controls (gray line). **k**, Contribution of individual variables to the variance explained (R2) by the best model. **l**, Examples of a predicted z-score trace using the GLM model vs. the actual z-score trace during Ensure or water consumption. NS, *P<0.05, **P<0.01, ***P<0.001, ****P<0.0001. Data are mean ± sem.

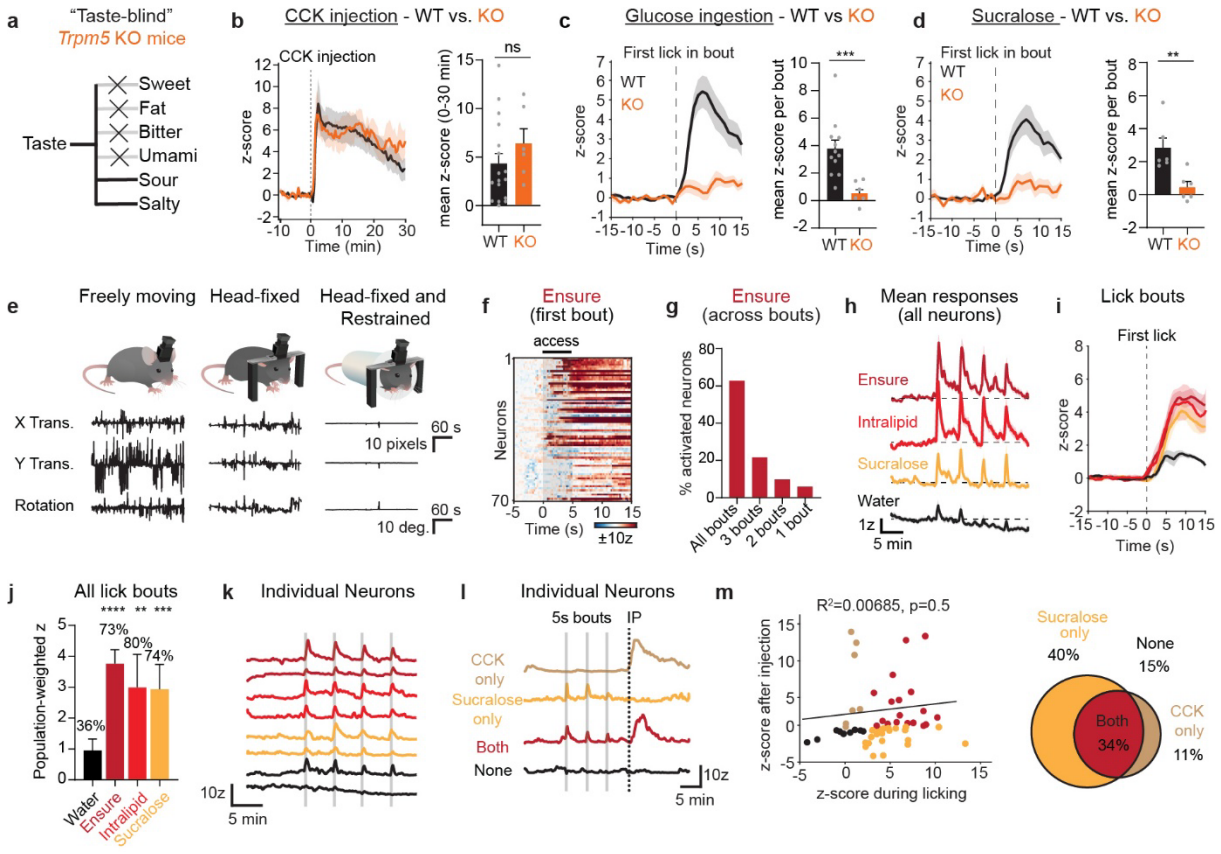


Figure 3.3 | PRLH neurons are activated by the taste of food.
a, Taste impairments in taste-blind *Trpm5*$^{-/-}$ mice. **b**, Left, PSTH of PRLH neuron responses aligned to IP injection of CCK in *Trpm5*$^{-/-}$ mice and WT controls. Right, z-scores (0-30 min). **c**, Left, PSTH of PRLH neuron responses across all glucose lick bouts in WT and *Trpm5*$^{-/-}$ mice. Right, z-scores (0-10 s). **d**, Left, PSTH of PRLH neuron responses across all sucralose lick bouts in WT and *Trpm5*$^{-/-}$ mice. Right, z-scores (0-10 s). **e**, Top, microendoscopic imaging of PRLH neurons in a freely moving, head-fixed, or head-fixed and restrained mouse. Bottom, example trace of movement artifacts detected by Mosaic analysis software in each configuration during imaging. **f**, Heatmap of individual neuron responses to the first bout of brief access (5s) Ensure consumption. **g**, Percentage of neurons activated by all four bouts, only three bouts, only two bouts, or only lick bout during Ensure consumption. **h**, PTSH aligned to brief access consumption of Intralipid, sucralose, and water (averaged across all neurons). **i**, PSTH aligned to the first lick of all lick bouts (averaged across all lick bouts and neurons). **j**, Population-weighted z-score (calculated as the fraction of neurons activated multiplied by their z-scored activity change) for consumption of indicated solutions. The percentage of neurons activated are listed above each bar graph. **k**, Example traces of calcium dynamics in representative neurons during consumption of indicated solutions. **l**, Example traces of calcium dynamics in representative neurons responding to sucralose consumption, a CCK injection, both stimuli, or neither. **m**, Left, scatterplot of z-score during brief access sucralose consumption (averaged across all lick bouts) vs. z-score after CCK injection. Right, Venn diagram showing percentage of cells activated by these stimuli. NS, *P<0.05, **P<0.01, ***P<0.001, ****P<0.0001. Data are mean ± sem.

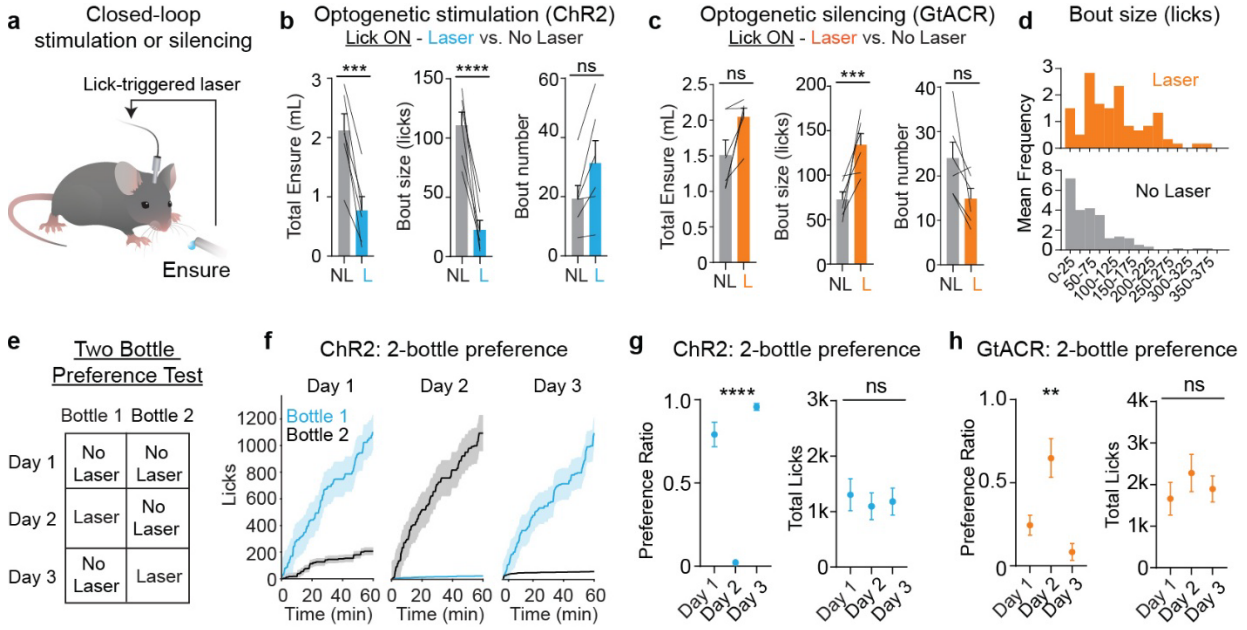


Figure 3.4 | PRLH neurons pace food ingestion.
a, Closed-loop optogenetic stimulation or silencing of PRLH neurons expressing ChR2 or GtACR1. **b**, Left, Ensure consumption during closed-loop stimulation (60 min trial) of PRLH neurons or no laser trials. Middle, bout size (licks). Right, bout number. NL-no laser. L-laser. **c**, Left, Ensure consumption during closed-loop silencing (60 min) of PRLH neurons expressing GtACR1 or no laser trials. Middle, bout size. Right, bout number. **d**, Distribution of bout sizes (bins are 25 lick increments) for trials in which PRLH neurons received closed-loop silencing (top) or no laser trials (bottom). **e**, Schematic for two-bottle preference test in which animals are presented with two identical bottles containing Ensure. Day 1 establishes initial preference. On day 2, the preferred or less preferred bottle is paired with optogenetic stimulation or silencing, respectively. The pairing is switched on day 3. **f**, Cumulative licks of Ensure for preferred (bottle 1) vs non-preferred (bottle 2) bottle on days 1-3. **g**, Preference ratio for bottle 1 (licks from bottle 1/total licks) and total Ensure consumption (licks from bottle 1 + licks from bottle 2) from day 1-3 of closed-loop stimulation paradigm. **h**, Preference ratio for bottle 1 and total Ensure consumption from day 1-3 of closed-loop silencing paradigm. NS, *P<0.05, **P<0.01, ***P<0.001, ****P<0.0001. Data are mean ± sem.

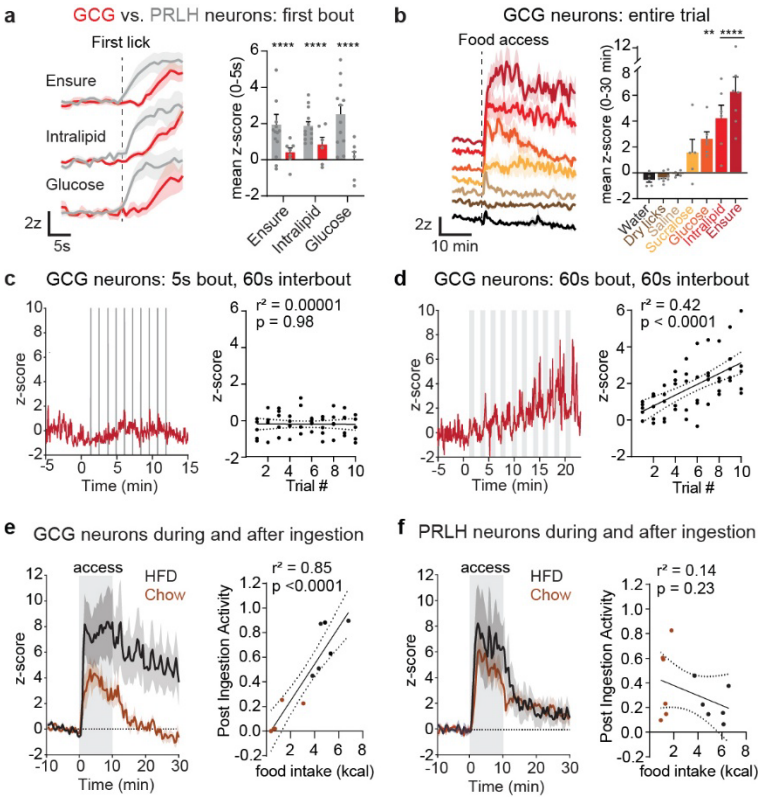


Figure 3.5 | GCG neurons track cumulative intake on a minutes timescale.
a, Left, PSTH of PRLH and GCG neuron responses during the first lick bout. Right, z-scores (0-5 s after first lick in first bout). **b**, Left, PSTH of GCG neuron activity aligned to lickometer access for all tastants. Right, z-scores (0-30 min). **c**, Mice were given access to Ensure at defined time intervals. Left, example trace of calcium dynamics from GCG neurons during 5s access to Ensure every 60s (10 trials). Right, z-score during each brief access (0-5 s) vs. number of trials. **d**, Left, example trace of calcium dynamics from GCG neurons during 60s brief access to Ensure every 2 min (10 trials). Same animal from panel c. Right, z-score during each brief access (0-60 s) vs. number of trials. **e**, Left, PSTH of GCG neuron responses in mice given access to chow or HFD from 0-10 min (gray). Right, correlation between total food intake during 10 min access (kcal) and post-ingestive activity. Post-ingestive activity = mean z-score after food removal (10-30 min) / mean z-score during food access (0-10 min). **f**, Left, PSTH of PRLH neuron responses in mice given access to chow or HFD (0-10 min). Right, correlation between total food intake during 10 min access (kcal) and post-ingestive activity. NS, *P<0.05, **P<0.01, ***P<0.001, ****P<0.0001. Data are mean ± sem.

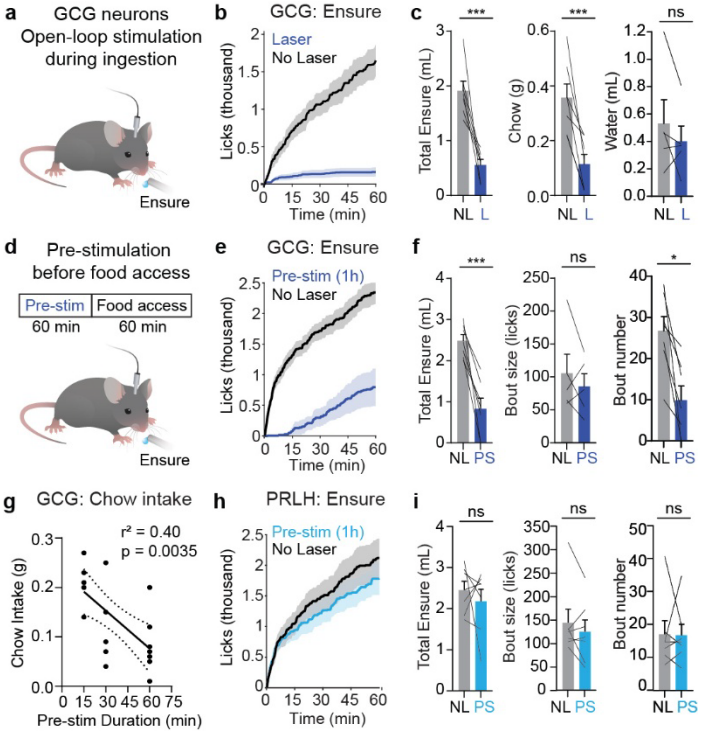


Figure 3.6 | GCG neuron activation promotes long-lasting satiety.
a, Mice received continuous stimulation of GCG neurons expressing ChR2. **b**, Cumulative licks of Ensure during open-loop stimulation (60 min) of GCG neurons. **c**, Left, Ensure consumption in b. middle, chow consumption during open-loop stimulation (30 min; food-deprived mice). Right, water consumption during open-loop stimulation (30 min; water-deprived mice). NL-no laser. L-laser. **d**, Mice are pre-stimulated in the absence of food (60 min) and then given access to Ensure (60 min). **e**, Cumulative licks of Ensure after pre-stimulation (60 min) of GCG neurons. **f**, Left, Ensure consumption in e. Middle, bout size (two animals consumed zero bouts after pre-stimulation). Right, bout number. **g**, Negative correlation between total chow intake after pre-stimulation and the pre-stimulation duration. **h**, Cumulative licks of Ensure after pre-stimulation (60 min) of PRLH neurons. **i**, Left, Ensure consumption in h. Middle, bout size. Right, bout number. NS, *P<0.05, **P<0.01, ***P<0.001, ****P<0.0001. Data are mean ± sem.

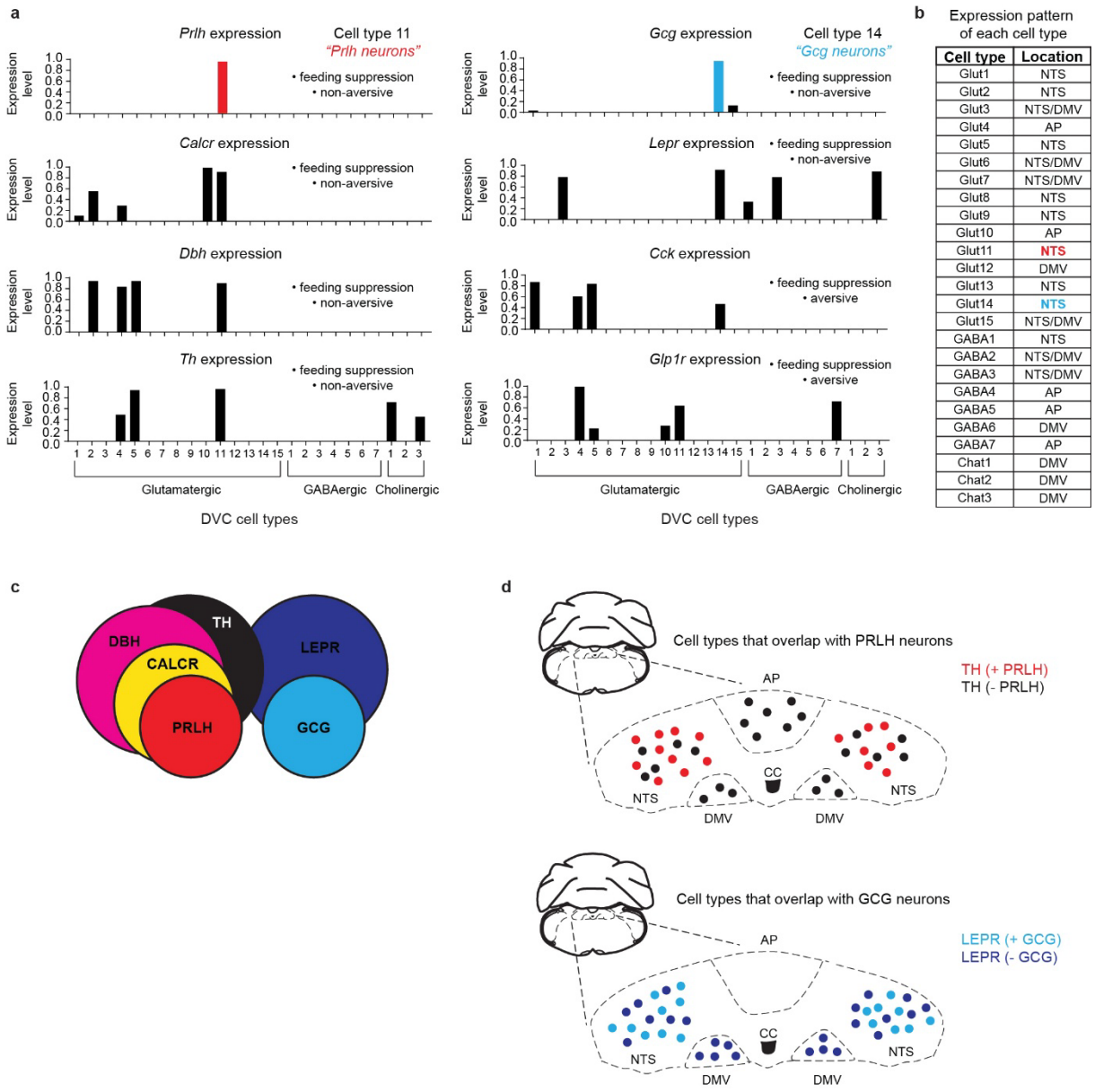


Figure 3.7 | PRLH and GCG neurons are distinct cNTS cell types that regulate the non-aversive suppression of feeding.
a, Unique cell types in the dorsal vagal complex (DVC) identified by single-cell RNA sequencing (Data are adapted from Ludwig et al. 2021[21]) that are known to regulate feeding. *Prlh* and *Gcg* expression label distinct cell types that are known to control the non-aversive suppression of feeding. **b**, Table describing where glutamatergic, GABAergic, and cholinergic cell types identified by single-cell sequencing are found in the DVC[21]. AP = area postrema. DMV = dorsal motor vagus. **c**, Schematic showing overlap in RNA expression between cell types that express *Dbh*, *Th*, *Calcr*, *Prlh*, *Lepr*, and *Gcg* based on data from panel a. These cell types have been shown to be activated by natural feeding and/or suppress food intake without inducing conditioned taste aversion (CTA). **d**, Schematic showing the location of cell types – which regulate non-aversive satiety – within the DVC based on data from panel b. Cells expressing *Prlh* ("PRLH neurons") and *Gcg* ("GCG neurons") are specifically located in the NTS, whereas other cell types show broad expression in the AP and DMV.

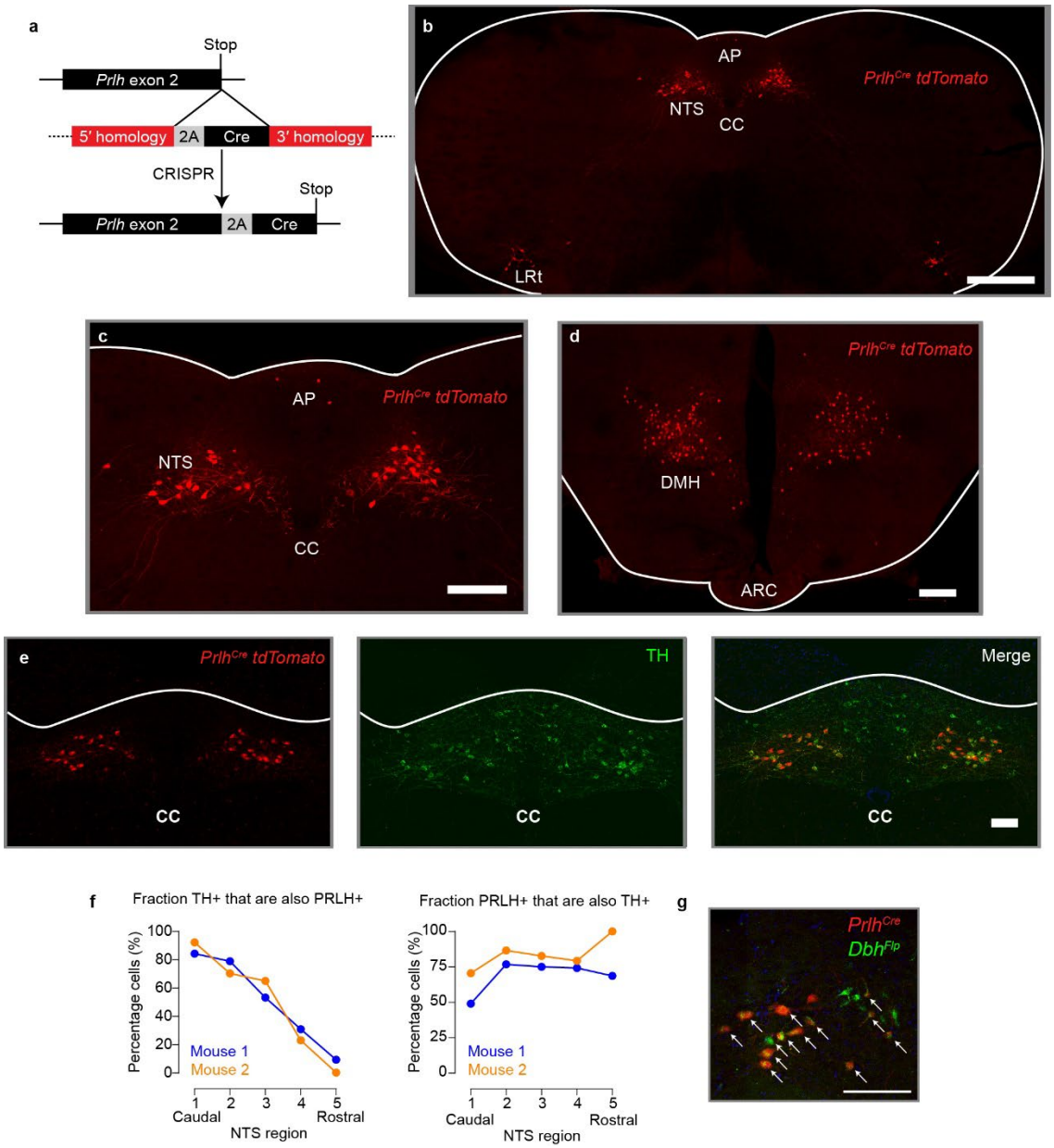


Figure 3.8 | PRLH neurons largely overlap with TH neurons in the cNTS.
a, Schematic for generating *Prlh*^{Cre} knock-in mice. **b**, Coronal slice at the level of the area postrema (AP) showing *Prlh*^{Cre} recombination. The AP, central canal (CC), NTS, and the lateral reticular formation (LRt) are labelled. The recombination pattern here and in the next panel (DMH) closely matches published reports of PRLH expression[15]. Scale bar = 500 µm. **c**, Zoom-in of AP/NTS. Scale bar = 200 µm. **d**, Recombination in the dorsomedial hypothalamus (DMH). The arcuate nucleus (ARC) is labelled for reference. Scale bar = 200 µm. **e**, *Prlh*^{Cre} recombination (red) and immunohistochemistry for tyrosine hydroxylase (TH) in the NTS at the level of the AP. This shows extensive co-localization, consistent with reports that PRLH and A2 neurons are overlapping in the cNTS. Scale bar = 100 µm. **f**, Co-localization between PRLH and TH across the rostrocaudal axis of the cNTS. Each region corresponds to 200 µm between -6.5 mm to -7.5 mm relative to bregma. **g**, *Prlh* and *Dbh* are co-localized in the cNTS. *Prlh*^{Cre} and *Dbh*^{Flp} mice were crossed to reporter mice to co-label neurons (Methods). Scale bar = 50 µm.

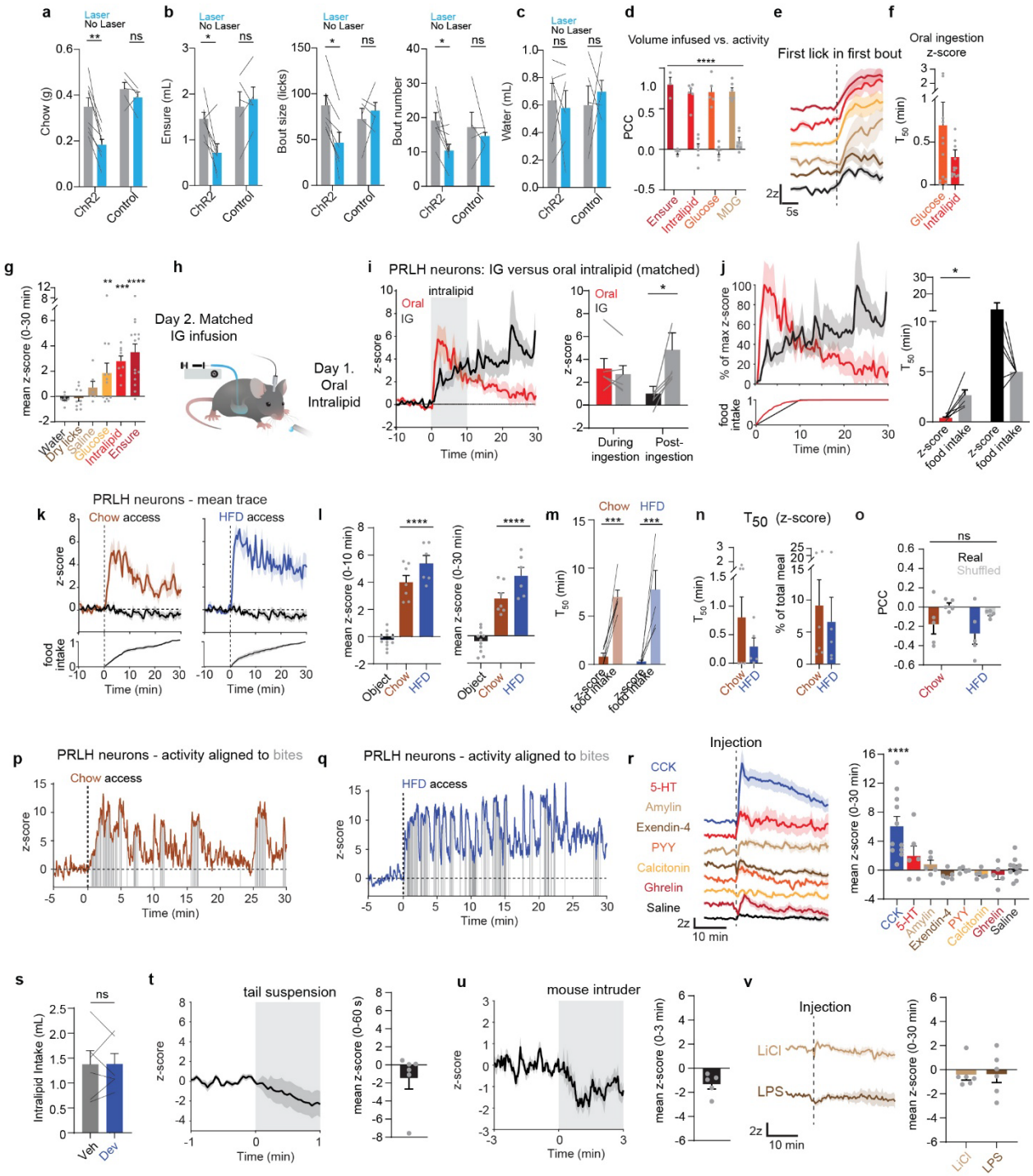


Figure 3.9 | Regulation of PRLH neurons by ingestive and non-ingestive signals.
a, Mean chow consumption (g) after open-loop stimulation (30 min; food-deprived mice) of PRLH neurons or no laser trials for ChR2-expressing mice or control mice. **b**, Left, mean Ensure consumption (mL) after open-loop stimulation (60 min; dark phase) of PRLH neurons or no laser trials. Middle, mean bout size (licks) after open-loop stimulation. Right, mean bout number after open-loop stimulation. (Figure caption continued on the next page.)

(Figure caption continued from the previous page.) **c**, Mean water consumption (mL) after open-loop stimulation (30 min; water-deprived) of PRLH neurons or no laser trials. **d**, Mean Pearson Correlation Coefficient (PCC) for the cumulative infusion volume vs. the z-scored change in activity during infusions. Real data (color) is compared vs. shuffled controls (gray). **e**, PSTH of PRLH neuron responses during just the first lick bout of the trial for the indicated solutions. **f**, Mean time to 50% of maximum z-score (T50) over the entire 30 min trial during oral ingestion of glucose or Intralipid. **g**, Mean z-scores (0-30 min) after lickometer access to tastants. **h**, Mice were fasted overnight before given access to Intralipid for 10 min of self-paced consumption (day 1). Two days later (day 2), fasted mice were given an IG infusion of Intralipid based on the amount consumed on day 1. **i**, Left, PSTH of PRLH neuron responses to volume-matched oral ingestion or IG infusion of Intralipid. Right, mean z-scores during oral ingestion or IG infusion (0-10 min) or post-ingestion (10-30 min). **j**, Left, PTSH of the percentage of max z-score during oral ingestion (red) or IG infusion (black) of Intralipid (volume-matched), with the percentage of total intake on the bottom panel. Right, mean time to reach 50% of the max z-score (”z-score”) versus mean time to consume 50% of total Intralipid (”food intake”) for oral ingestion (red) and IG infusion (black). **k**, Top, PSTH of PRLH neuron responses during self-paced chow or HFD consumption, or presentation of a non-food object (black), aligned to moment of food presentation. Bottom, cumulative fraction of total bites during the trial. **l**, Left, mean z-scores (0-10 min) after food/object access. Right, mean z-scores (0-30 min) after food/.object access. **m**, Mean time to reach 50% of the max z-score (”z-score”) versus mean time to consume 50% of total bites (”food intake”) for chow (brown) and HFD (blue). **n**, Left, mean time to 50% of maximum z-score (T50) over the entire 30 min trial during oral ingestion of chow or HFD. Right, mean percentage of total bites (“meal”) performed at the earliest time point with >50% of the max z-score (T50). **o**, Mean PCC for the relationship between the cumulative bites of chow or HFD and the z-scored change in activity across the entire 30 min trial. **p**, Example trace of calcium dynamics from PRLH neurons during chow consumption (individual bites are shown in gray). **q**, Example trace of calcium dynamics from PRLH neurons during HFD consumption (individual bites are shown in gray). **r**, Left, PSTH of PRLH neuron responses to IP injection of 5-HT, CCK, amylin, Exendin-4, PYY, calcitonin, ghrelin, and saline. Right, mean z-scores (0-30 min) after IP injection of each gut peptide. **s**, Devazepide pretreatment does not change total Intralipid consumption in $Prlh^{Cre}$ mice (from Fig. 1l). **t**, Left, PSTH of PRLH neuron responses to tail suspension. Right, mean z-scores (0-60 s) during tail suspension. **u**, Left, PSTH of PRLH neuron responses to presentation of a same-sex mouse intruder. Right, mean z-scores (0-3 min) during intruder presentation. **v**, Left, PSTH of PRLH neuron responses to IP injection of LiCl (84 mg/kg) or LPS (100 ug/kg). Right, mean z-scores (0-30 min) after IP injection of LiCl or LPS. NS, *P<0.05, **P<0.01, ***P<0.001, ****P<0.0001. Data are mean ± sem.

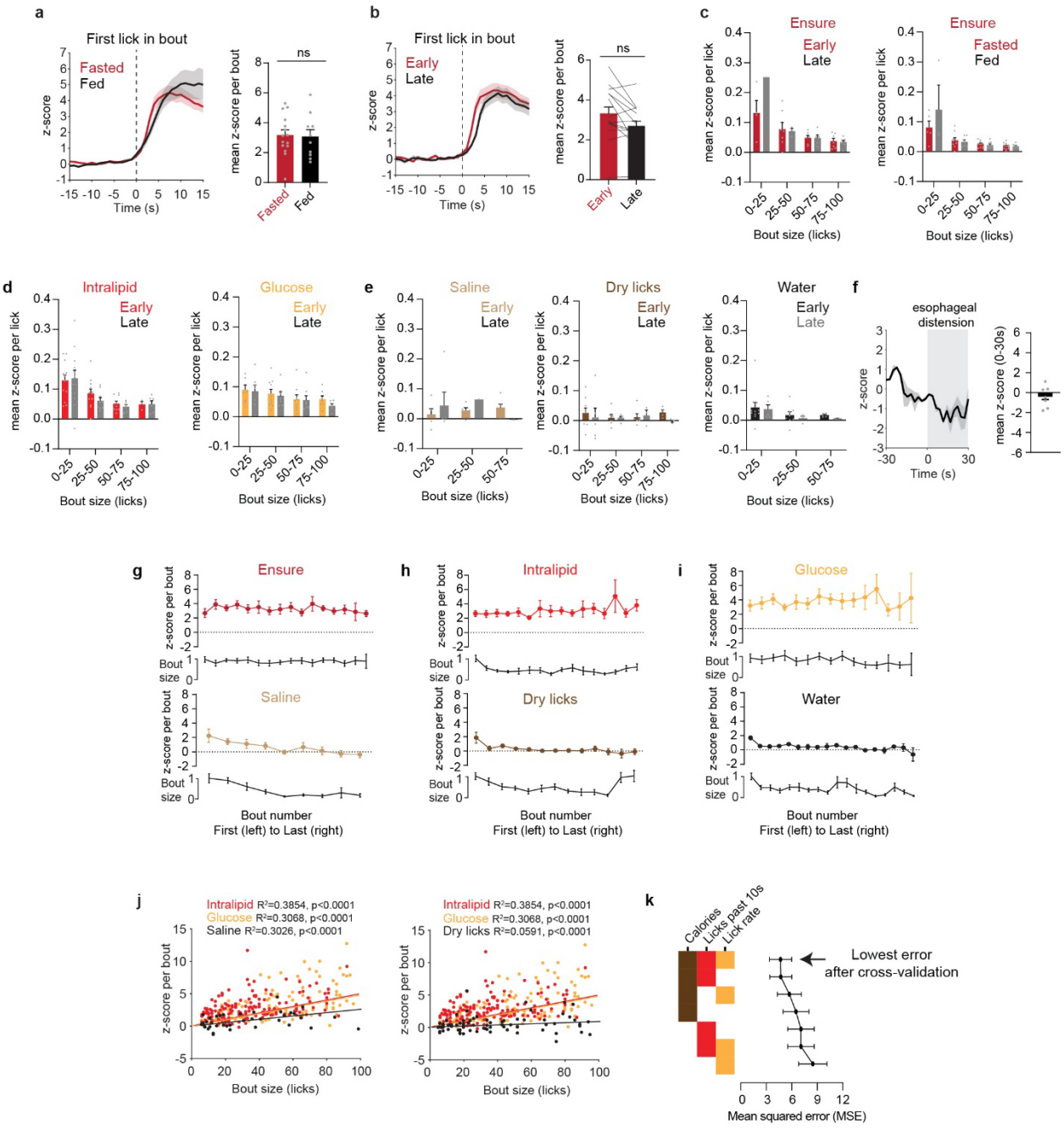


Figure 3.10 | PRLH neurons track the moment-to-moment dynamics of ingestion.
a, Left, PSTH of PRLH neuron activity aligned to the first lick of all lick bouts from overnight fasted mice ("fasted") or ad libitum fed mice ("fed") during a 30 min Ensure consumption test. Right, mean z-scores (0-10 s after first lick in bout) from fasted and fed mice. **b**, Left, PSTH of PRLH neuron activity aligned to the first lick of all lick bouts in the first 15 min of the trial ("early") or the last 15 min of the trial ("late") during a 30 min Ensure consumption test. Right, mean z-scores (0-10 s after first lick in bout) from early and late time intervals. **c**, Left, mean z-score per lick from Ensure consumption during early (first 15 min) vs. late (last 15 min) periods of a 30 min trial. Right, mean z-score per lick during Ensure consumption from overnight fasted ("fasted") or ad libitum fed animals. (Figure caption continued on the next page.)

(Figure caption continued from the previous page.) **d**, Left, mean z-score per lick from Intralipid consumption during early (first 15 min) vs. late (last 15 min) periods of a 30 min trial. Right, mean z-score per lick from glucose consumption during early (first 15 min) vs. late (last 15 min) periods of a 30 min trial. **e**, Left, mean z-score per lick from saline consumption during early (first 15 min) vs. late (last 15 min) periods of a 30 min trial. Middle, mean z-score per lick from dry licking during early (first 15 min) vs. late (last 15 min) periods of a 30 min trial. Right, mean z-score per lick from water consumption during early (first 15 min) vs. late (last 15 min) periods of a 30 min trial. **f**, Left, PSTH of PRLH neuron responses during feeding tube insertion into the esophagus (0-30s). Right, mean z-scores (0-30 s) during feeding tube insertion. **g**, Top, mean z-score for each bout of Ensure consumption (0-10 s) from the first bout (left) to the last bout (right), with the percentage of the max bout size (licks) shown below. Bottom, mean z-score for each bout of saline consumption (0-10 s) from the first bout to the last bout. **h**, Top, mean z-score for each bout of Intralipid consumption (0-10 s) from the first bout to the last bout. Bottom, mean z-score for each bout of dry licking (0-10 s) from the first bout to the last bout. **i**, Top, mean z-score for each bout of glucose consumption (0-10 s) from the first bout to the last bout. Bottom, mean z-score for each bout of water consumption (0-10 s) from the first bout to the last bout. **j**, Left, scatterplot showing the relationship between bout size (# of licks in the first 10 s of each bout) and mean z-score (0-10 s of each bout) for all bouts during Intralipid, glucose, or saline consumption. Each dot represents a single lick bout. Right, scatterplot showing the relationship between bout size and mean z-score for all bouts during Intralipid or glucose consumption, or dry licking at an empty bottle. **k**, The mean squared error (MSE) is plotted for each model after performing cross-validation. To perform cross-validation, 80% of the data was used to train the GLM coefficients and calculate the MSE from the remaining 20% of the data. This was performed for 100 iterations to obtain an average MSE value for each animal. NS, *P<0.05, **P<0.01, ***P<0.001, ****P<0.0001. Data are mean ± sem.

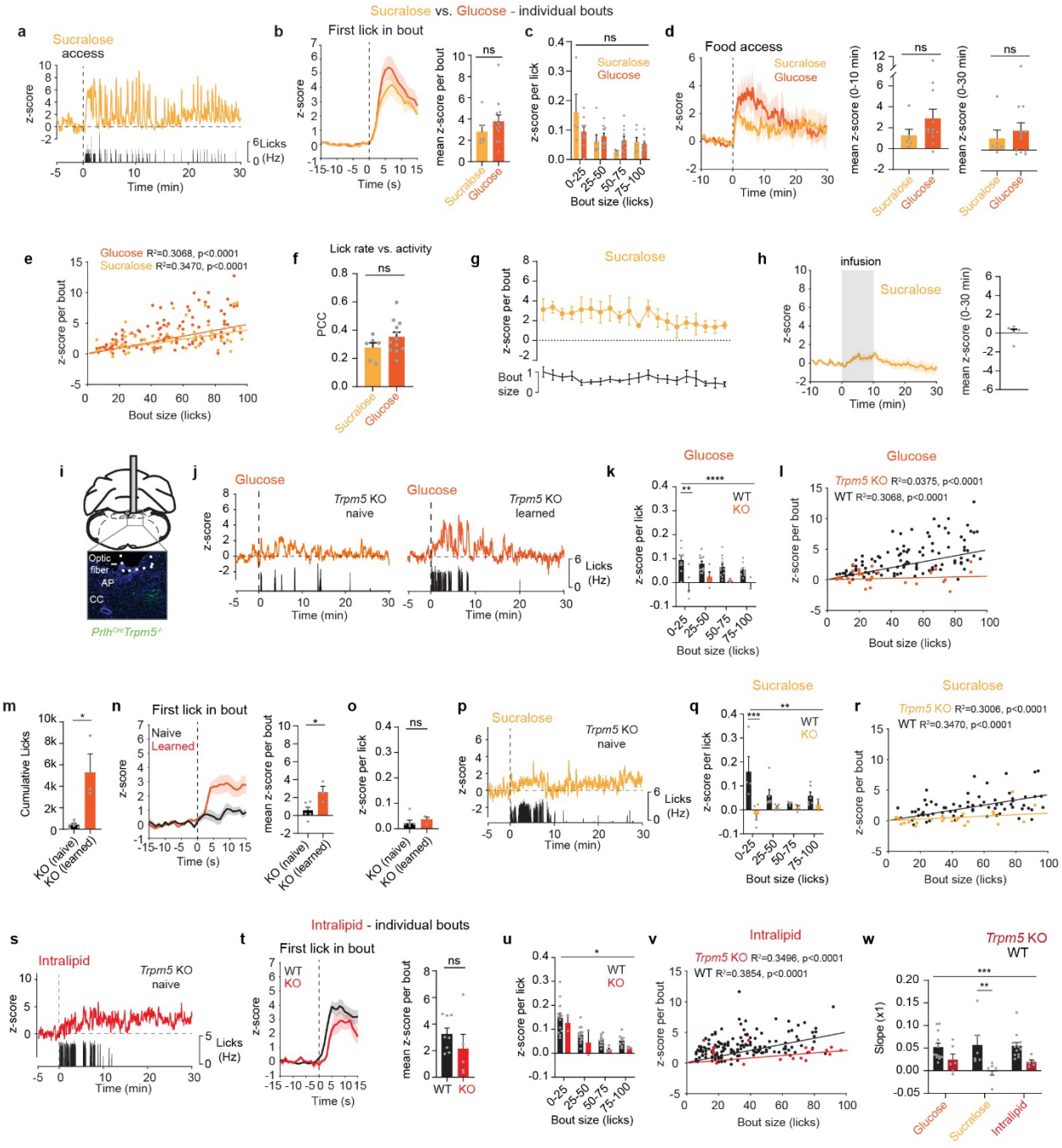


Figure 3.11 | PRLH neurons are activated by food tastes.
a, Example trace of calcium dynamics from PRLH neurons during sucralose consumption. **b**, Left, PSTH of PRLH neuron activity aligned to the first lick of all lick bouts during sucralose or glucose consumption. Right, mean response (0-10 s after first lick) averaged across all lick bouts for sucralose and glucose consumption. **c**, Mean z-score per lick stratified by bout size for sucralose and glucose consumption. **d**, Left, PSTH of PRLH neuron responses to sucralose or glucose consumption. Middle, mean z-scores (0-10 min) during sucralose or glucose consumption. Right, mean z-scores (0-30 min) during sucralose or glucose consumption.
(Figure caption continued on the next page.)

(Figure caption continued from the previous page.) **e**, Scatterplot showing the relationship between bout size (# of licks in the first 10 s of each bout) and mean z-score (0-10 s of each bout) for all bouts during sucralose or glucose consumption. **f**, Mean PCC for the relationship between the instantaneous lick rate each second during consumption of sucralose or glucose and the z-scored change in activity across the entire 30 min trial. **g**, Mean z-score for each bout of sucralose consumption (0-10 s) from the first bout (left) to the last bout (right), with the percentage of the max bout size (licks) shown below. **h**, Left, PSTH of PRLH neuron responses to IG infusion of sucralose (1.5 mL). Right, mean z-scores (0-30 min) during IG infusion of sucralose. **i**, Fiber placement and GCaMP6s expression in PRLH neurons of a *Trpm5*$^{-/-}$ mouse. **j**, Left, example trace of calcium dynamics from PRLH neurons during glucose consumption from a naïve *Trpm5*$^{-/-}$ mouse. Right, Left, example trace from a learned *Trpm5*$^{-/-}$ mouse. **k**, Mean z-score per lick stratified by bout size for glucose consumption in WT and *Trpm5*$^{-/-}$ mice. **l**, Scatterplot showing the relationship between bout size (# of licks in the first 10 s of each bout) and mean z-score (0-10 s of each bout) for all bouts during glucose consumption from WT and *Trpm5*$^{-/-}$ mice. **m**, Mean cumulative licks performed during a glucose consumption test by naive and learned *Trpm5*$^{-/-}$ mice. Animals were defined as “learned” if they performed at least 1000 licks during the second test (Methods). **n**, PSTH of PRLH neuron responses across all glucose lick bouts in naive and learned *Trpm5*$^{-/-}$ mice. **o**, Mean z-score per lick for glucose consumption in naive and learned *Trpm5*$^{-/-}$ mice. **p**, Example trace of calcium dynamics from PRLH neurons during sucralose consumption from a *Trpm5*$^{-/-}$ mouse. **q**, Mean z-score per lick stratified by bout size for sucralose consumption in WT and *Trpm5*$^{-/-}$ mice. **r**, Scatterplot showing the relationship between bout size and mean z-score for all bouts during sucralose consumption from WT and *Trpm5*$^{-/-}$ mice. **s**, Example trace of calcium dynamics from PRLH neurons during Intralipid consumption from a *Trpm5*$^{-/-}$ mouse. **t**, Left, PSTH of PRLH neuron responses across all Intralipid lick bouts in WT and *Trpm5*$^{-/-}$ mice. Right, mean z-scores (0-10 s) for all lick bouts during Intralipid consumption. **u**, Mean z-score per lick stratified by bout size for Intralipid consumption in WT and *Trpm5*$^{-/-}$ mice. **v**, Left, scatterplot showing the relationship between bout size and mean z-score for all bouts during Intralipid consumption from WT and *Trpm5*$^{-/-}$ mice. **w**, mean slope (coefficient x1) for glucose, sucralose, and Intralipid consumption from WT and *Trpm5*$^{-/-}$ mice. NS, *P<0.05, **P<0.01, ***P<0.001, ****P<0.0001. Data are mean ± sem.

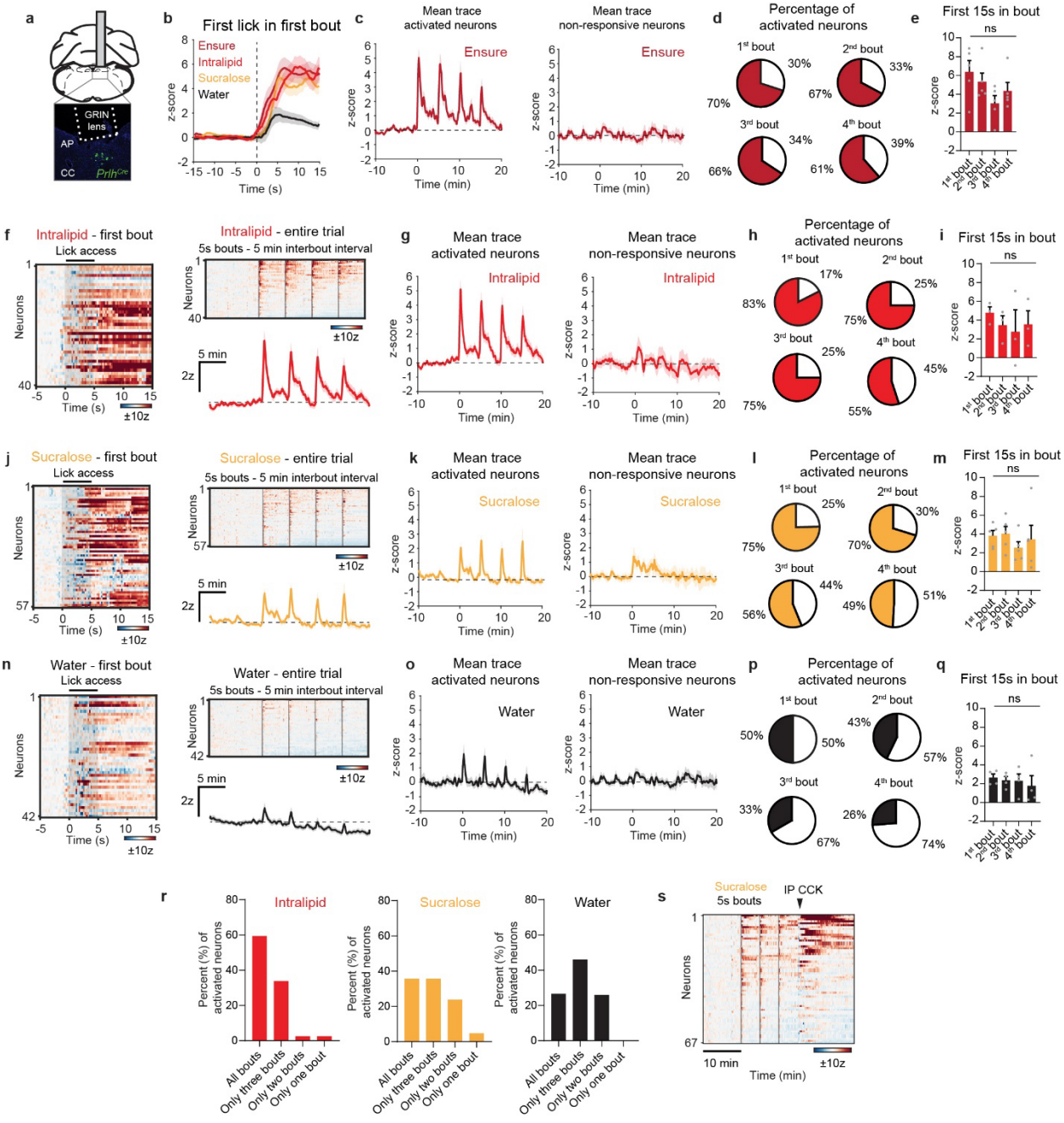


Figure 3.12 | Individual PRLH neurons are activated by food tastes.
a, GRIN lens placement and GcaMP6s expression in PRLH neurons. **b**, PSTH of PRLH neuron responses during the first lick bout of the trial for the indicated solutions. **c**, Left, PTSH of activated PRLH neurons (mean z-score > 1 across all 5s bouts) during Ensure consumption from Fig. 3. Right, PTSH of non-responsive PRLH neurons (mean z-score < 1 across all 5s bouts). **d**, Percentage of activated and non-responsive neurons during each Ensure lick bout. **e**, Mean z-score for each 5s bout during Ensure consumption. Each data point is the averaged value from a single animal. (Figure caption continued on the next page.)

(Figure caption continued from the previous page.) **f**, Left, heatmap of individual neuron responses to the first bout of Intralipid consumption. Right, heatmap of individual neuron responses to brief access (5s) Intralipid consumption at 5 min intervals over 20 min. Bottom, PTSH aligned to brief access Intralipid consumption (averaged across all neurons). **g**, Left, PTSH of activated PRLH neurons (mean z-score > 1 across all 5s bouts) during Intralipid consumption from Fig. 3. Right, PTSH of non-responsive PRLH neurons (mean z-score < 1 across all 5s bouts). **h**, Percentage of activated and non-responsive neurons during each Intralipid lick bout. **i**, Mean z-score for each 5s bout during Intralipid consumption. **j**, Left, heatmap of individual neuron responses to the first bout of sucralose consumption. Right, heatmap of individual neuron responses to brief access (5s) sucralose consumption. Bottom, PTSH aligned to brief access sucralose consumption (averaged across all neurons). **k**, Left, PTSH of activated PRLH neurons (mean z-score > 1 across all 5s bouts) during sucralose consumption from Fig. 3. Right, PTSH of non-responsive PRLH neurons (mean z-score < 1 across all 5s bouts). **l**, Percentage of activated and non-responsive neurons during each sucralose lick bout. **m**, Mean z-score for each 5s bout during sucralose consumption. **n**, Left, heatmap of individual neuron responses to the first bout of water consumption. Right, heatmap of individual neuron responses to brief access (5s) water consumption. Bottom, PTSH aligned to brief access water consumption (averaged across all neurons). **o**, Left, PTSH of activated PRLH neurons (mean z-score > 1 across all 5s bouts) during water consumption from Fig. 3. Right, PTSH of non-responsive PRLH neurons (mean z-score < 1 across all 5s bouts). **p**, Percentage of activated and non-responsive neurons during each water lick bout. **q**, Mean z-score for each 5s bout during water consumption. **r**, Left, percentage of neurons activated by all four bouts, three bouts, two bouts, or only one lick bout for Ensure consumption. Right, percentage of neurons activated by all four bouts, three bouts, two bouts, or only one lick bout for Intralipid consumption. **s**, Heatmap of individual neuron responses to brief access sucralose consumption before an IP injection of CCK. NS, *P<0.05, **P<0.01, ***P<0.001, ****P<0.0001. Data are mean ± sem.

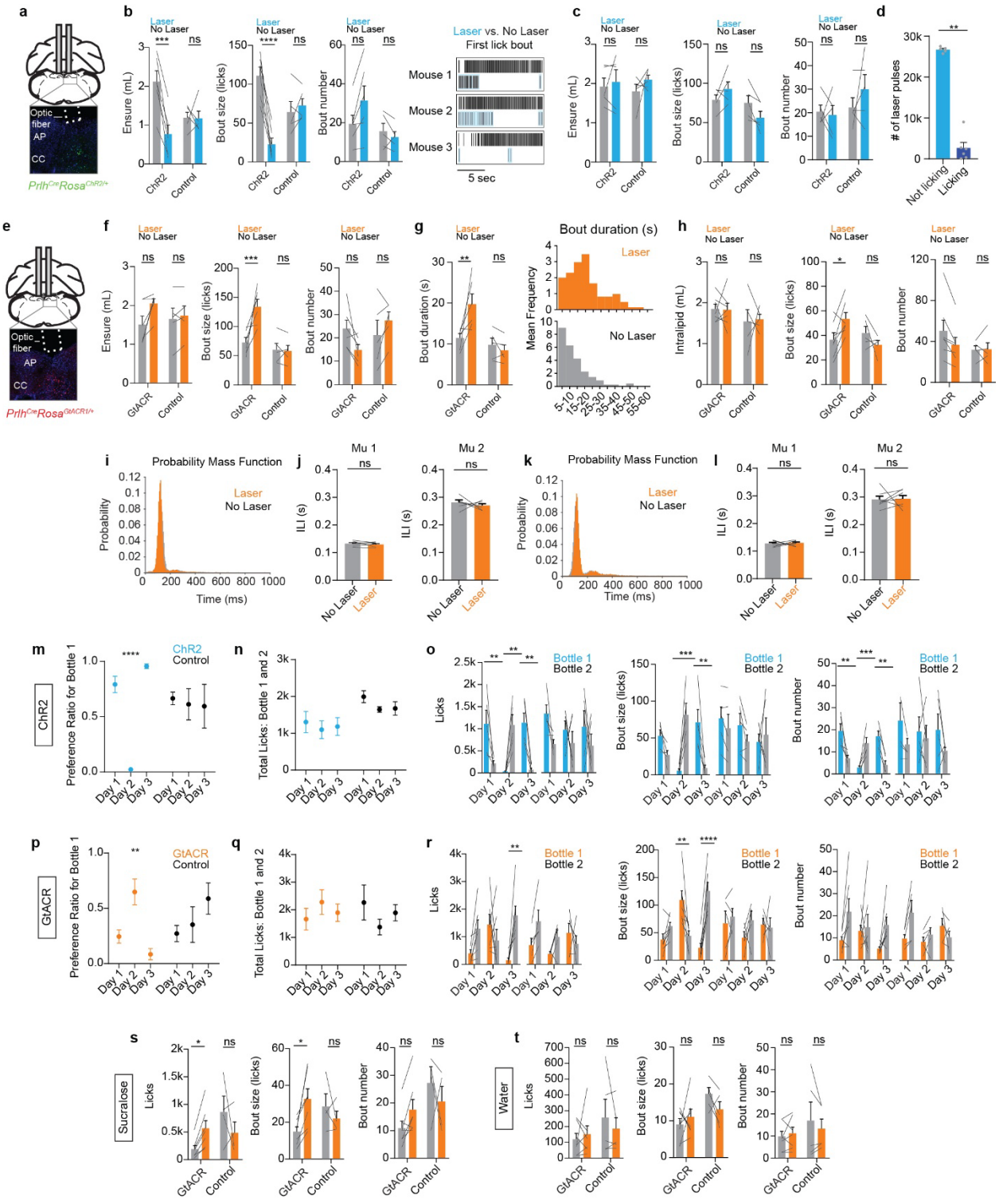


Figure 3.13 | PRLH neurons pace food ingestion by modulating valence associated with food tastes.

a, Fiber placement and ChR2-GFP expression in PRLH neurons of the cNTS. **b**, Left, mean Ensure consumption (mL) after closed-loop stimulation (60 min; dark phase) of PRLH neurons (when animals are licking) or sham trials. (Figure caption continued on the next page.)

(Figure caption continued from the previous page.) Middle, mean bout size (licks) after closed-loop stimulation. Right, mean bout number after closed-loop stimulation. Example raster plots from three animals showing individual licks of Ensure. **c**, Left, mean Ensure consumption (mL) during closed-loop stimulation (60 min; dark phase feeding) of PRLH neurons (when animals are not licking) or no laser trials. Middle, mean bout size (licks) during closed-loop stimulation. Right, mean bout number during closed-loop stimulation. **d**, Mean number of laser pulses received by individual animals receiving closed-loop stimulation during licking or when not actively licking. **e**, Fiber placement and GtACR1-FusionRed expression in PRLH neurons of the cNTS. **f**, Left, mean Ensure consumption (mL) during closed-loop silencing (60 min; dark phase feeding) of PRLH neurons or no laser trials. Middle, mean bout size (licks) during closed-loop silencing. Right, mean bout number during closed-loop silencing for Ensure consumption. **g**, Left, mean bout duration (s) during closed-loop silencing. Left, distribution of bout durations (bins are 5 s) for trials in which PRLH neurons received closed-loop silencing (top) or no laser trials (bottom). **h**, Left, mean Intralipid consumption (mL) during closed-loop silencing (60 min; dark phase feeding) of PRLH neurons or no laser trials. Middle, mean bout size (licks) during closed-loop silencing. Right, mean bout number during closed-loop silencing. **i**, Probability mass function (PMF) for interlick interval (ILI) between 0-1 s during closed-loop silencing of PRLH neurons or no laser trials (Ensure consumption). **j**, Left, mean values for mu1 constant (left peak on PMF). Right, mean values for mu2 constant (right peak on PMF). **k**, Probability mass function (PMF) for interlick interval (ILI) between 0-1 s during closed-loop silencing of PRLH neurons or no laser trials (Intralipid consumption). **l**, Left, mean values for mu1 constant (left peak on PMF). Right, mean values for mu2 constant (right peak on PMF). **m**, Preference ratio for bottle 1 (licks from bottle 1/licks from bottle 1 + licks from bottle 2) from day 1-3 of closed-loop stimulation paradigm (when animals are licking). **n**, Total Ensure consumption (licks from bottle 1 + licks from bottle 2) from day 1-3 of closed-loop stimulation paradigm. **o**, Left, mean number of licks for bottle 1 and bottle 2 from day 1-3 of closed-loop stimulation paradigm (Ensure consumption). Middle, mean bout size (licks) for bottle 1 and 2 from day 1-3. Right, mean bout number for bottle 1 and 2 from day 1-3. **p**, Preference ratio for bottle 1 from day 1-3 of closed-loop silencing paradigm. **q**, Total Ensure consumption from day 1-3 of closed-loop silencing paradigm. **r**, Left, mean number of licks for bottle 1 and 2 from day 1-3 of closed-loop silencing paradigm (Ensure consumption). Middle, mean bout size (licks) for bottle 1 and 2 from day 1-3. Right, mean bout number for bottle 1 and 2 from day 1-3. **s**, Left, mean number of licks for bottle 1 and 2 from closed-loop silencing paradigm (sucralose consumption). Middle, mean bout size (licks) for bottle 1 and 2. Right, mean bout number for bottle 1 and 2. **t**, Left, mean number of licks for bottle 1 and 2 from closed-loop silencing paradigm (water consumption). Middle, mean bout size (licks) for bottle 1 and 2. Right, mean bout number for bottle 1 and 2. NS, *P<0.05, **P<0.01, ***P<0.001, ****P<0.0001. Data are mean ± sem.

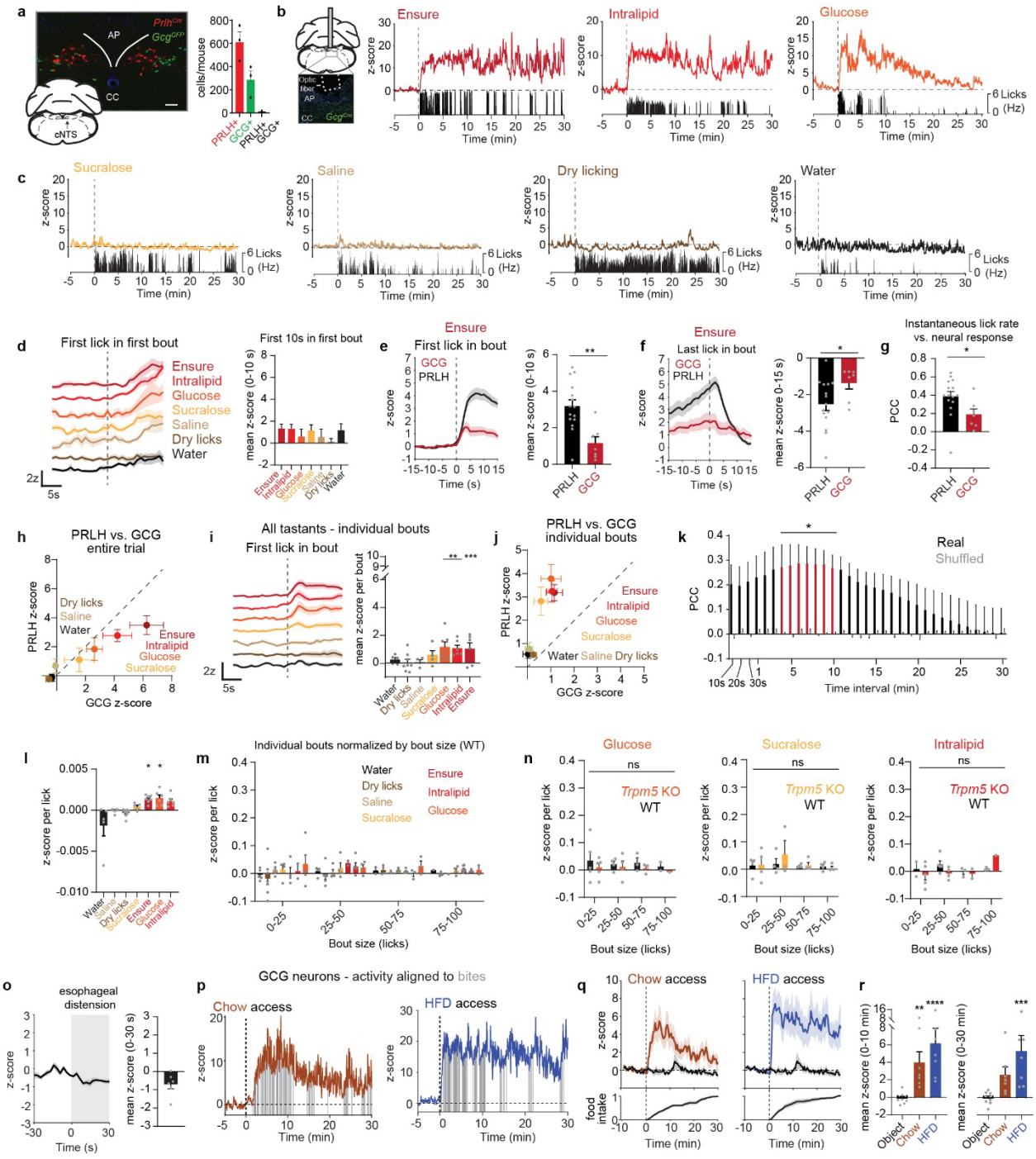


Figure 3.14 | Regulation of GCG neurons by oral signals of ingestion.
a, Left, PRLH (*Prlh*^{Cre}*Rosa*^{Tom}, red) and GCG (*Gcg*^{GFP}, green) neurons are intermingled but non-overlapping in the cNTS. Scale bar = 100 µm. Right. Quantification of overlap for *Prlh*^{Cre}*Rosa*^{Tom} (red) and *Gcg*^{GFP} (green) cells in the cNTS (n=3 mice). **b**, Left, fiber placement and GcaMP6s expression in GCG neurons. Right, example traces of calcium dynamics from GCG neurons during self-paced Ensure, Intralipid, or glucose consumption. **c**, Example traces of calcium dynamics from GCG neurons during self-paced sucralose, saline, or water consumption, or dry licking at an empty sipper. (Figure caption continued on the next page.)

(Figure caption continued from the previous page.) **d**, Left, PSTH of GCG neuron responses during just the first lick bout of the trial, aligned to the first lick of the trial, for the indicated solutions. Right, mean z-scores (0-10 s) during the first lick bout. **e**, Left, PSTH aligned to the first lick of the bout (averaged across all lick bouts) during Ensure consumption for GCG and PRLH neurons. Right, mean z-scores (0-10 s) during Ensure consumption for GCG and PRLH neurons. **f**, Left, PSTH aligned to the last lick of the bout (averaged across all lick bouts) during Ensure consumption for GCG and PRLH neurons. Right, mean decrease in z-score (0-15 s after last lick of each bout) during Ensure consumption for GCG and PRLH neurons. **g**, Mean Pearson Correlation Coefficient (PCC) for the relationship between the instantaneous lick rate each second during Ensure consumption and the z-scored change in activity across the entire 30 min trial for GCG and PRLH neurons. **h**, Comparison of the mean z-scores (0-30 min after lickometer access) for PRLH neurons (from Figure 1) and GCG neurons (from Figure 5). **i**, Left, PSTH of GCG neuron activity aligned to the first lick (averaged across all lick bouts). Right, mean response (0-10 s after first lick) averaged across all licking bouts. **j**, Comparison of the mean z-scores (0-10 s after first lick in bout) for PRLH neurons (from Figure 2) and GCG neurons (from Figure 5). **k**, Mean PCC for the relationship between the cumulative licks performed in the preceding time intervals and the z-scored change in activity across the entire 30 min trial of self-paced Ensure consumption. **l**, Mean z-score per lick (mean z-score over 30 min trial/total number of licks) for each tastant. **m**, Mean z-score per lick (mean z-score 0-10 s of each bout divided by the number of licks in the same time frame) stratified by bout size for all tastants from GCG neurons. Each data point is an averaged value from a single animal. **n**, Left, mean z-score per lick by bout size for glucose consumption in WT and *Trpm5*$^{-/-}$ mice (GCG neurons). Middle, mean z-score per lick by bout size for sucralose consumption in WT and *Trpm5*$^{-/-}$ mice. Right, mean z-score per lick by bout size for Intralipid consumption in WT and *Trpm5*$^{-/-}$ mice. **o**, Left, PSTH of GCG neuron responses during feeding tube insertion into the esophagus (0-30s). Right, mean z-scores (0-30 s) during feeding tube insertion. **p**, Left, example trace of calcium dynamics from GCG neurons during self-paced chow consumption. Right, example trace of calcium dynamics from GCG neurons during self-paced HFD consumption. **q**, Top, PSTH of PRLH neuron responses during self-paced chow or HFD consumption, or presentation of a non-food object (black), aligned to moment of food presentation. Bottom, cumulative fraction of total bites during the trial. **r**, Left, mean z-scores (0-10 min) after food/object access. Right, mean z-scores (0-30 min) after food/object access. NS, *P<0.05, **P<0.01, ***P<0.001, ****P<0.0001. Data are mean ± sem.

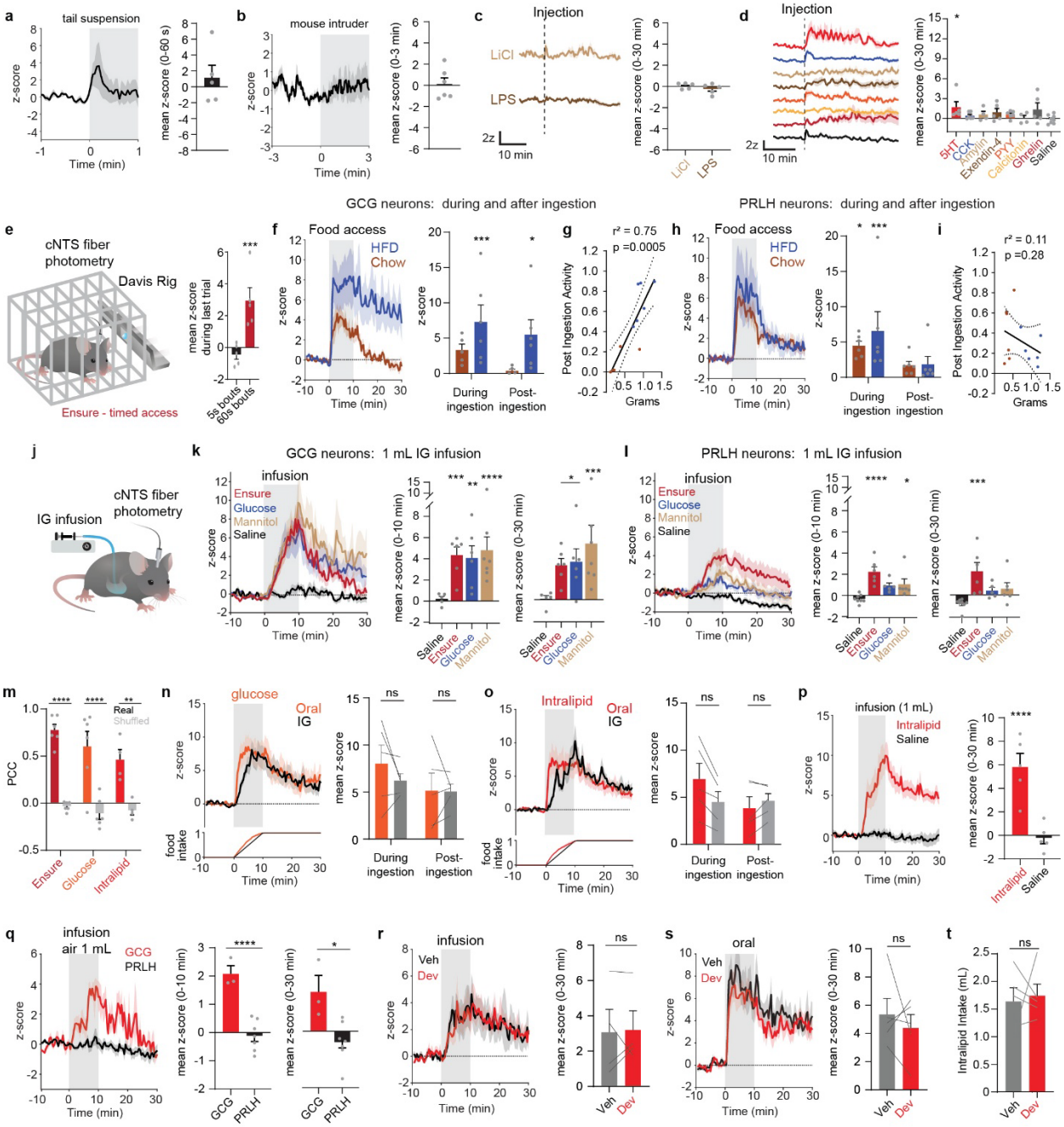


Figure 3.15 | Regulation of GCG neurons by non-ingestive and GI signals.
a, Left, PSTH of GCG neuron responses to tail suspension. Right, mean z-scores (0-60 s) during tail suspension. **b**, Left, PSTH of GCG neuron responses to presentation of a same-sex mouse intruder. Right, mean z-scores (0-3 min) during intruder presentation. **c**, Left, PSTH of GCG neuron responses to IP injection of LiCl (84 mg/kg) or LPS (100 ug/kg). Right, mean z-scores (0-30 min) after IP injection of LiCl or LPS. **d**, Left, PSTH of GCG neuron responses to IP injection of 5HT, CCK, amylin, Exendin-4, PYY, calcitonin, ghrelin, and saline. Right, mean z-scores (0-30 min) after IP injection of each gut peptide. **e**, A Davis Rig gustometer was used to give mice access to Ensure at defined time intervals. Right, mean z-score during the last trial of 5s or 60s brief access Davis rig experiments. (Figure caption continued on the next page.)

(Figure caption continued from the previous page.) **f**, Left, PSTH of GCG neuron responses in mice given access to chow or HFD from 0-10 min (gray shaded). Right, mean z-scores during 0-10 min food access ("during ingestion") or 10-30 min ("post ingestion"). **g**, There is a positive correlation between total food intake during 10 min access (grams) and post-ingestive activity of GCG neurons. Post-ingestive activity was calculated as the average z-score after food removal (10-30 min) divided by the average z-score during food access (0-10 min). Colored dots indicate chow (brown) or HFD (blue). **h**, Left, PSTH of PRLH neuron responses in mice given access to chow or HFD from 0-10 min (gray shaded). Right, mean z-scores during 0-10 min food access ("during ingestion") or 10-30 min ("post ingestion"). **i**, There is no correlation between total food intake during 10 min access (grams) and post-ingestive activity of PRLH neurons. **j**, cNTS photometry recordings were performed while mice received intragastric (IG) infusions of various solutions. **k**, Left, PSTH of GCG neuron responses during and after IG infusions (infusion 0-10 min; 1 mL) of Ensure, glucose, mannitol, or saline. Middle, mean z-scores during IG infusions (0-10 min). Right, mean z-scores during and after IG infusions (0-30 min). **l**, Left, PSTH of PRLH neuron responses during after IG infusions (0-10 min; 1 mL) of Ensure, glucose, mannitol, or saline. Middle, mean z-scores during IG infusions (0-10 min). Right, mean z-scores during and after IG infusions (0-30 min). **m**, Mean PCC for the relationship between the volume infused (1 mL) over time and the z-scored change in activity during the 10 min IG infusion of Ensure, glucose, or Intralipid. **n**, Left, PSTH of GCG neuron responses to volume-matched oral ingestion or IG infusion of glucose. Bottom panel shows mean trace for percentage of total food consumption. Right, mean z-scores during oral ingestion or IG infusion (0-10 min), or post-ingestion (10-30 min). **o**, Left, PSTH of GCG neuron responses to volume-matched oral ingestion or IG infusion of Intralipid. Right, mean z-scores during oral ingestion or IG infusion (0-10 min), or post-ingestion (10-30 min). **p**, Left, PTSH of GCG neuron responses to IG infusion of Intralipid or saline (1 mL) in *Trpm5*$^{-/-}$ mice. Right, mean z-scores (0-30 min) after infusion of Intralipid or saline. **q**, Left, PTSH of PRLH and GCG neuron responses to IG infusion of air (1 mL) from 0-10 min. Right, mean z-scores during IG infusion of air (0-10 min) or during the entire trial (0-30 min). **r**, Left, PSTH of GCG neuron responses during and after IG infusions of Intralipid (0-10 min; 1.5 mL) in mice that received prior IP injection of devazepide or vehicle. Right, mean z-scores during and after IG infusions (0-30 min). **s**, Left, PSTH of GCG neurons during and after oral consumption of Intralipid, following injection of either devazepide or vehicle. Right, mean z-scores (0-30 min) during Intralipid consumption. **t**, Devazepide pretreatment does not change total Intralipid consumption in GcgiCre mice (from panel r). NS, *P<0.05, **P<0.01, ***P<0.001, ****P<0.0001. Data are mean ± sem.

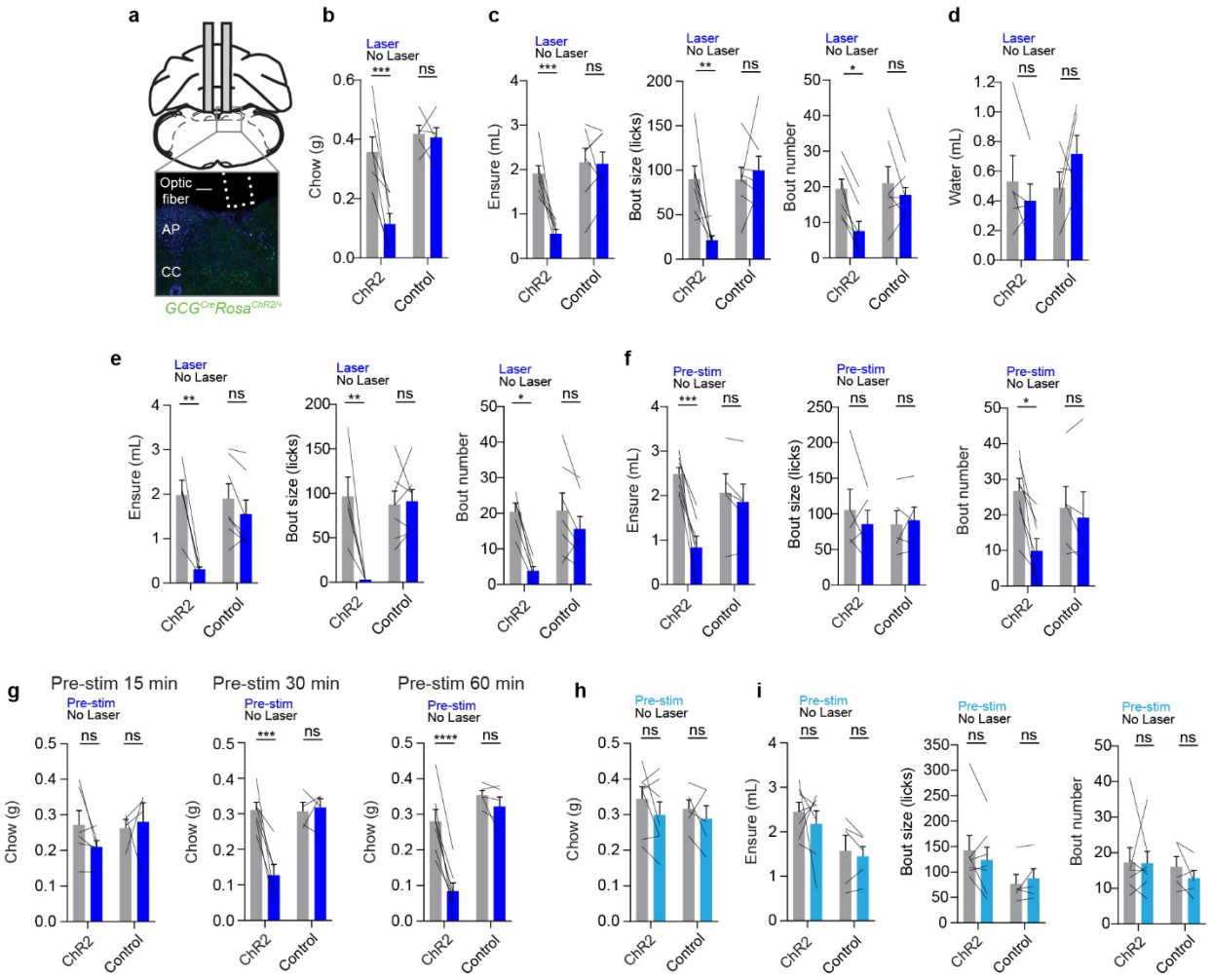


Figure 3.16 | GCG neuron activation promotes long-lasting satiety.
a, Fiber placement and ChR2-GFP expression in GCG neurons of the cNTS. **b**, Mean chow consumption (g) after open-loop stimulation (30 min; food-deprived mice) of GCG neurons or no laser trials for ChR2-expressing mice or control mice. **c**, Left, mean Ensure consumption (mL) after open-loop stimulation (60 min; dark phase) of GCG neurons or no laser trials. Middle, mean bout size (licks) after open-loop stimulation. Right, mean bout number after open-loop stimulation. **d**, Mean water consumption (mL) after open-loop stimulation (30 min; water-deprived) of GCG neurons or no laser trials. **e**, Left, mean Ensure consumption (mL) after closed-loop stimulation (60 min; dark phase) of GCG neurons (when animals are licking) or sham trials. Middle, mean bout size (licks) after closed-loop stimulation. Right, mean bout number after closed-loop stimulation. **f**, Left, mean Ensure consumption (mL) after pre-stimulation (60 min) of GCG neurons or no laser trials. Middle, mean bout size (licks) after pre-stimulation. Right, mean bout number after pre-stimulation. **g**, Mean chow consumption (g) after pre-stimulation of GCG neurons for 15 min (left), 30 min (middle), or 60 min (right). **h**, Mean chow consumption (g) after pre-stimulation of PRLH neurons for 60 min. **i**, Left, mean Ensure consumption (mL) after pre-stimulation (60 min) of PRLH neurons or no laser trials. Middle, mean bout size (licks) after pre-stimulation. Right, mean bout number after pre-stimulation. NS, *P<0.05, **P<0.01, ***P<0.001, ****P<0.0001. Data are mean ± sem.

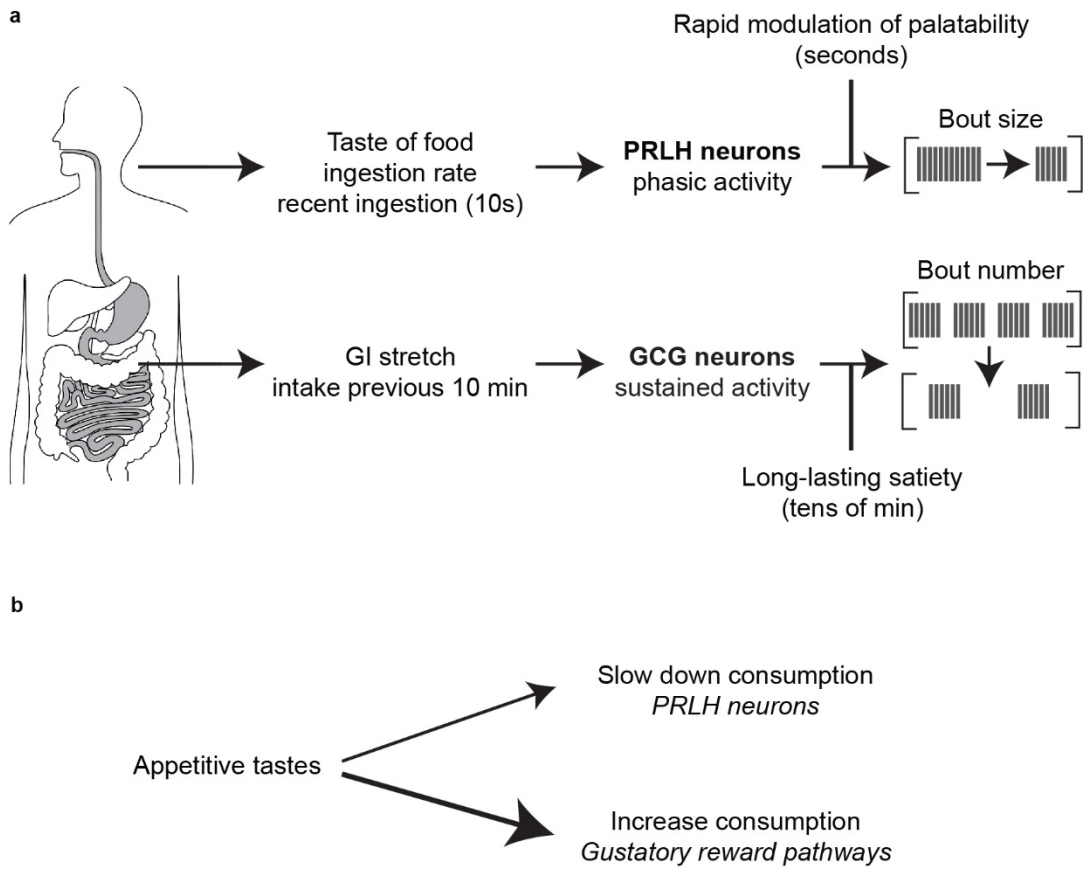


Figure 3.17 | Separate circuits for the oral and gastrointestinal control of ingestion. **a**, Food intake generates both fast orosensory and slower GI signals that feed back to the cNTS to modulate appetite. Orosensory signals, including taste, preferentially target PRLH neurons, which are phasically activated during bouts of ingestion and function to acutely restrain bout size, thereby slowing down the pace of ingestion. Mechanosensory signals from the GI tract preferentially target GCG neurons, which show sustained activity during feeding and transmit a long-lasting satiety signal that delays reinitiation of feeding. **b**, Our data suggest that appetitive tastes, such as sweet and fat, are used by different brain systems for opposing purposes. Activation of well-known gustatory reward pathways by palatable tastes functions to increase food consumption. In parallel, activation of PRLH neurons by palatable tastes feeds back to slow down the rate of ingestion by limiting bout size. Although it may seem counterintuitive that palatable tastes would be used by some brain systems to inhibit ingestion, the existence of this mechanism is supported by several lines of evidence. This evidence includes the results of sham feeding studies in rats[42,43], which showed that a pre-gastric signal (likely involving taste) slows down ingestion.

METHODS

Experimental protocols were approved by the University of California, San Francisco IACUC following the National Institutes of Health guidelines for the Care and Use of Laboratory Animals.

Mouse strains

Experimental animals (>6 weeks old, both sexes) were maintained in temperature- and humidity-controlled facilities with 12 h light-dark cycle and ad libitum access to water and standard chow (PicoLab 5053). We obtained wild-type (C57BL/6J, Jackson cat.no.000664), *Gcg*^{iCre} (B6;129S-Gcg$^{tm1.1(iCre)Gkg/J}$, Jackson cat.no.030663), Ai14 (B6.CgGt(ROSA)26 Sor$^{tm14(CAGtdTomato)\ Hze}$/J, Jackson cat.no.007914), Ai213 (B6; 129S6-Igs7$^{tm213(CAG-EGFP,CAG-mOrange2,CAGmKate2)\ Hze}$/J, Jackson cat.no.034113), *Trpm5*$^{-/-}$ (B6.129P2-Trpm5$^{tm1Dgen/J}$, Jackson cat.no.005848), Ai32 (B6.Cg-Gt(ROSA)26Sor$^{tm32(CAG-COP4*H134R/EYFP)Hze}$/J, Jackson cat.no.024109), and R26-LNL-GtACR1-Fred-Kv2.1 (B6;129S6-Gt(ROSA)26Sor$^{tm3Ksvo/J}$, Jackson cat.no.033089) mice from Jackson Labs. We obtained GCG-GFP mice as a gift from Hayashi Yoshitaka[40]. Nano-L10 mice have been described previously[41]. We obtained *Dbh*$^{2A-FlpO}$ (B6.129S7(FVB) Dbh$^{em2.1(flpo)Rray/}$Mmucd) mice from MMRRC (041575-UCD). *Prlh*^{Cre} knock-in mice were crossed to Ai14, GCG-GFP, and Nano-L10 mice to generate quadruple mutants (Figure 3.14a). *Prlh*^{Cre} knock-in mice were crossed with *Dbh*$^{2A-FlpO}$ and Ai213 mice to generate triple mutants (Figure 3.8g). *Prlh*^{Cre} knock-in mice or *Gcg*^{iCre} mice were crossed with *Trpm5*$^{-/-}$ mice to generate triple mutants (*Prlh*^{Cre}*Trpm5*$^{-/-}$ and *Gcg*^{iCre}*Trpm5*$^{-/-}$ mice). *Prlh*^{Cre} knock-in mice were crossed with R26-LNL-GtACR1-Fred-Kv2.1 mice to generate double mutants (*Prlh*$^{Cre/+}$*Rosa*$^{GtACR1/+}$ mice). *Prlh*^{Cre} knock-in mice or *Gcg*^{iCre} mice were crossed with Ai32 mice to generate double mutants (*Prlh*$^{Cre/+}$ *Rosa*$^{ChR2/+}$ and *Gcg*$^{iCre/+}$*Rosa*$^{ChR2/+}$ mice). All transgenic or

knock-in mice used in these studies were on a pure C57BL/6J background, except for *Prlh*^{Cre} mice that were partially backcrossed to C57BL/6J (from FVB).

Generation of *Prlh*^{Cre} mice

Prlh^{Cre} mice were generated by homologous recombination at the endogenous *Prlh* locus, aided by targeted CRISPR endonuclease activity. The targeting vector was constructed containing a T2A-Cre cassette inserted immediately upstream of the endogenous stop codon, a 1 kb upstream homology arm, and a 2kb downstream homology arm. An sgRNA was selected (CAGCACTTTTATTAGATCAG) to introduce CRISPR double strand breaks near the stop codon, and the corresponding PAM sequence was mutated in the targeting vector (AGG to AGC) to prevent vector cleavage. Super-ovulated female FVB/N mice were mated to FVB/N stud males, and fertilized zygotes were collected from oviducts. Cas9 protein (100 ng/uL), sgRNA (250 ng/uL), and targeting vector DNA (100 ng/mL) were mixed and injected into the pronucleus of fertilized zygotes. Zygotes were implanted into oviducts of pseudopregnant CD1 female mice. Screening of the pups by qPCR identified five independent founder lines that contained insertion of Cre but not sequences from the targeting vector (i.e. knock-ins). These founders were crossed to Ai14 reporter mice, and all five lines showed a brain-wide recombination pattern that was identical to previous reports of *Prlh* expression (i.e. restricted to the NTS, LRt, and DMH) (Figure 3.8a-d). One *Prlh*^{Cre} line was selected to maintain and further characterized by showing that recombination in the cNTS was highly overlapping with TH and DBH but not GCG, as previously reported (Figure 3.8e-g and Figure 3.14a).

Intracranial surgery

General procedures: Animals were anesthetized with 2% isoflurane and placed in a stereotaxic head frame on a heating pad. Ophthalmic ointment was applied to the eyes and subcutaneous injections of meloxicam (5 mg/kg) and sustained-release buprenorphine (1.5

mg/kg) were given to each mouse prior to surgery. The scalp was shaved, scrubbed (betadine and alcohol three times), local anesthetic applied (Bupivacaine 0.25%), and then incised through the midline. A craniotomy was made using a dental drill (0.5 mm). Virus was injected at a rate of 150 nL/min using glass pipette connected with 10 uL Hamilton syringe (WPI, Sarasota, FL), controlled by a Micro4 microsyringe pump controller (WPI, Sarasota, FL). The needle was kept at the injection site for 2 min before withdrawal. Fiber optic cannulas or GRIN lens were implanted after virus injection in the same surgery, and were secured to the skull using Metabond (Patterson Dental Supply INC: 07-5533559, 07-5533500; Henry Schein INC: 1864477) and Flow-It (Patterson Dental Supply INC: 07-6472542).

Fiber photometry recordings in the cNTS: $Prlh^{Cre}$ (n = 31), $Prlh^{Cre}Trpm5^{-/-}$ (n = 6), Gcg^{iCre} (n = 12), and $Gcg^{iCre}Trpm5^{-/-}$ (n = 5) mice were prepared for photometry recordings by injecting AAV1-CAG-Flex-GCaMP6s-WPRE-SV40 (400 nL; 1.7 x 10^{13} viral genome copies (vg) mL^{-1}; Addgene) or AAV8-Syn-DIO-GCaMP6s (300 nL; 4.7 x 10^{13} viral genome copies (vg) mL^{-1}; Janelia Vector Core) into the cNTS (1.3 mm AP; ±0.3 mm ML; -4.3 mm DV relative to the occipital crest with 20° in the AP direction). In the same surgery, an optical fiber (Doric Lenses, MFC_400/430- 0.48_6.5mm_MF2.5_FLT) and sleeve (Doric Lenses, SLEEVE_BR_2.5) were installed 0.1-0.15 mm above the injection site. Mice were allowed to recover for a minimum of three weeks before the first photometry experiment. In subsequent surgeries, mice were equipped with an intragastric catheter.

Microendoscopy in the cNTS: $Prlh^{Cre}$ mice (n = 6) were prepared for imaging by injecting AAV1-CAG-Flex-GCaMP6s-WPRE-SV40 (200 nL; 1.5 x 10^{12} viral genome copies (vg) mL^{-1}; Addgene) into the cNTS (1.3 mm AP; ±0.3 mm ML; -4.3 mm DV relative to the occipital crest with 20° in the AP direction) and installing a GRIN lens (8 x 0.5 mm length; Inscopix 1050-004611) 0.15 mm above the injection site in the same surgery. After at least two weeks of recovery from the lens implantation surgery, mice were anesthetized, and head bars were affixed to the skull with metabond. A baseplate (Inscopix 100-000279) was placed above the

lens and affixed with Metabond. When mice were not being used for imaging experiments, a baseplate cover (Inscopix 100-000241) was attached to prevent damage to the GRIN lens.

Optogenetics in cNTS: *Prlh*$^{Cre/+}$, *Prlh*$^{Cre/+}$*Rosa*$^{ChR2/+}$, *Gcg*$^{iCre/+}$, *Gcg*$^{iCre/+}$*Rosa*$^{ChR2/+}$, *Rosa*$^{ChR2/+}$, and *Prlh*$^{Cre/+}$*Rosa*$^{GtACR1/+}$ mice were prepared for optogenetic experiments by installing a dual fiber optic cannula (Doric, DFC_200/245-0.37_6.5mm_DF0.8_FLT) above the cNTS (1.3 mm AP; 0 mm ML; -3.95 mm DV relative to the occipital crest with 20° in the AP direction). Mice were allowed to recover for a minimum of one week before optogenetic experiments.

Intragastric catheter surgery

Mice were anesthetized deeply with 2% isoflurane and surgical sites were shaved and cleaned with betadine and ethanol. Subcutaneous injections of meloxicam (5 mg/kg) and sustained-release buprenorphine (1.5 mg/kg) were given to each mouse prior to surgery. A midline abdominal skin incision was made, extending from the xyphoid process about 1.5 cm caudally, and a secondary incision of 1 cm was made between the scapulae for externalization of the catheter. The skin was separated from the subcutaneous tissue using blunt dissection, such that a subcutaneous tunnel was formed between the two incisions along the left flank to facilitate catheter placement. A small incision was made in the abdominal wall and the catheter (Instech, C30PU-RGA1439) was pulled through the intrascapular skin incision and into the abdominal cavity using a pair of curved hemostats. The stomach was externalized using atraumatic forceps and a purse string stitch was made in the middle of the forestomach using 7-0 non-absorbable Ethilon suture. A puncture was then made in the center of the purse string and the end of the catheter was inserted and secured by the purse string suture. For the gastric implant, 2-5 mm of catheter end was fixed within the stomach.

At the end of the surgery, the abdominal cavity was irrigated with 1mL of sterile saline and the stomach was replaced. The abdominal incision was closed in two layers, and the

catheter was sutured to the muscle layer at the interscapular site. The interscapular incision was then closed and the external portion of the catheter capped using a 22-gauge PinPort (Instech, PNP3F22). Mice received Baytril (5 mg/kg) and warm saline at the end of surgery and were allowed to recover for one week prior to photometry experiments.

Fiber photometry

Photometry setup: Mice were tethered to a patch cable (Doric Lenses, MFP_400/460/900-0.48_2m_FCM-MF2.5). Continuous 6 mW blue LED (470 nm) and UV LED (405 nm) served as excitation light sources. These LEDs were driven by a multichannel hub (Thorlabs), modulated at 305 hz and 505 hz respectively, and delivered to a filtered minicube (Doric Lenses, FMC6_AE(400-410)_E1(450-490)_F1(500-540)_E2(550-580)_ F2(600-680)_S) before connecting through optic fibers (Doric Lenses, MFP_400/460/900-0.48_2m_FCM-MF2.5). GCaMP calcium GFP signals and UV isosbestic signals were collected through the same fibers back to the dichroic ports of the minicube into a femtowatt silicon photoreceiver (Newport, 2151). Digital signals sampled at 1.0173 kHz were then demodulated, lock-in amplified, and collected through a processor (RZ5P, Tucker-Davis Technologies). Data was then collected through the software Synapse (TDT), exported via Browser (TDT), and downsampled to 4 Hz in MATLAB before analysis.

Behavior: For all recordings, mice were placed in sound-isolated behavioral chambers (Coulbourn, Habitest Modular System; Med Associates, Davis Rig) without water or food access unless otherwise specified. Chambers were cleaned between experiments to remove olfactory cues from previous experiments. Mice were habituated for one night in the chambers before experiments. On a subsequent day, mice were attached to photometry] patch cords and habituated to the chambers for a second session. Before each recording, photometry implants on individual mice were cleaned with 70% ethanol using connector cleaning sticks (MCC-S25) and connected to a photometry patch cable immediately afterward. For all photometry

experiments, mice were acclimated to the behavior chamber for 20 min with recording before presentation of a stimulus.

For intragastric infusion experiments, mice were food-deprived overnight prior to the experiment. Solutions - saline (0.9%), glucose (24%), Intralipid (20%), Ensure (21%), MDG (16%), sucralose (6.25mM) - were delivered using a syringe pump (Harvard Apparatus 70-2001) over 10 min. The infusion rate was 100 μL min^{-1} and 150 μL min^{-1} for a total infusion volume of 1 or 1.5 mL, respectively. Before mice were placed into the Coulbourn behavioral chambers for habituation, the intragastric catheter was attached to the syringe pump using plastic tubing and adapters (AAD04119, Tygon; LS20, Instech).

For lick response experiments, mice were food-deprived overnight prior to the experiments before receiving access to a lickometer containing the appropriate solution for the entire 30 min session. Solutions were prepared using deionized water at the following concentrations: 0.24 g/mL glucose (1.33 M, 24%), 0.009 g/mL saline (0.15 M, 0.9%), 0.21 g/mL Ensure original vanilla nutrition powder (21%), and 0.8 mg/mL sucralose (in saline). Intralipid 20% (Sigma, I141-100ML; Medline, BHL2B6064H) was used without dilution. To measure lick responses to Ensure in fed mice, ad libitum fed mice were given access to Ensure (21%) for 30 min in the dark phase (after 5 pm). All mice were habituated initially to the lickometer and photometry setup by receiving access to a bottle containing Ensure for one hour with the photometry patch cord attached.

For chow and high-fat diet (HFD) experiments, mice were food-deprived overnight prior to the experiment. Mice were then given access to a non-food object (metal cage), standard chow (PicoLab 5053), or HFD (Research Diets, D12492) for the entire 30 min session, or for 10 min in restricted access experiments for chow and HFD. Bites – defined as individual time points when the mouse lowers its head to make contact with the food pellet – were manually scored by an experimenter blinded to the experimental conditions. Behavioral annotation was

performed using BORIS (Behavioral Observation Research Interactive Software, http://www.boris.unito.it/).

For IP injection experiments, mice were injected with compounds at concentrations based on previously published reports: CCK octapeptide 30 μg/kg (Bachem), devazepide 1 mg/kg (R&D Systems), serotonin hydrochloride 2 mg/kg (Sigma-Aldrich), PYY 0.1 mg/kg (R&D Systems), exendin-4 150 μg/kg (Bachem), salmon calcitonin 150 μg/kg (Bachem), amylin 10 μg/kg (Tocris), ghrelin 2 mg/kg (R&D Systems), LiCl (84 mg/kg), and LPS (100 μg/kg). All of these compounds were dissolved in saline (0.9%) while devazepide was dissolved in 5% DMSO, 5% Tween-80 in saline (vehicle solution for devazepide). All compounds were injected at the volume of 10 μL/gram of mouse body weight.

For Intralipid and devazepide experiments, mice were food-deprived prior to the experiment. For the IG infusion experiment, after receiving an IP injection of vehicle or devazepide, mice were given an IG infusion of Intralipid (20%) over 10 min. The infusion rate was 150 μL min^{-1} for a total infusion volume of 1.5 mL, respectively. For the oral ingestion experiment, mice received an IP injection of vehicle or devazepide before receiving access to a lickometer containing Intralipid (20%) for 10 min (same time frame as IG infusion experiment).

For volume-matched glucose or Intralipid experiments, mice were food-deprived prior to the experiment. On day 1, mice were given access to a lickometer containing glucose or Intralipid for 10 min before removal and an additional 20 min of photometry recording. Two days later (day 2 of experiment), overnight fasted mice were given an IG infusion of glucose or Intralipid over 10 min at the same volume that each animal individually consumed on day 1. In summary, mice received the same volume of glucose or Intralipid solution with the same timing on day 1 and 2, through oral ingestion or IG delivery.

For esophageal distension experiments, mice were food-deprived overnight prior to the experiment. Mice were scruffed and restrained for 30 s before a 24-gauge reusable feeding tube (FST, 18061-24) was inserted and held in the esophagus for 30 s.

For lick response experiments comparing *Prlh*^{Cre} and *Prlh*^{Cre} *Trpm5*$^{-/-}$ mice or *Gcg*^{iCre} and *Gcg*^{iCre}*Trpm5*$^{-/-}$ mice, mice were food-deprived overnight before getting access to a lickometer containing glucose (24%), sucralose (6.25 mM), or Intralipid (20%). All solutions were prepared using deionized water except for Intralipid, which was not diluted. *Prlh*^{Cre} *Trpm5*$^{-/-}$ mice were initially habituated to the lickometer and photometry setup for three sessions across multiple days, in which they were given ad libitum access to water after being water-deprived overnight. This was performed in order to train the taste-blind mice to perform licks with the lickometer in subsequent experiments, since they perform fewer licks than WT mice at baseline. After this initial habituation procedure, taste-blind mice were still naïve to glucose, sucralose, and Intralipid. For post-ingestive training of taste-blind mice with glucose, we gave the animals ab libitum access to a bottle containing glucose (24%) overnight twice, with a day of separation between these two exposure periods. We defined taste-blind mice as “learned” if they performed more than 1,000 licks during a second 30 min test with glucose. Naïve WT mice perform at least 1,000 licks in a 30 min test with glucose while all naïve taste-blind mice perform less than that value when all are food-deprived.

For brief access taste tests using the Davis Rig (MED-DAV-160M, Med Associates), mice were food-deprived overnight. Mice were given 5 and 60 s lick access to a bottle of Ensure for ten total trials. In all experiments, the end of a trial and the beginning of the next trial were separated by 1 min. Prior to photometry experiments, mice were initially habituated to the Davis Rig and photometry setup for three sessions across multiple days, where they were given ad libitum access to Ensure after being food-derived overnight.

Analysis: GCaMP6s calcium responses at 470 nm excitation were normalized to the 405/415 nm “isosbestic” signal using a linear regression model of both signals during the baseline period to generate $F_{normalized}$ (the fluorescence predicted using the signal obtained with 405/415 nm excitation). Data were analyzed using the function $z = (F_{normalized} - \mu)/\sigma$, where $F_{normalized}$ is the normalized photometry signal, μ is the mean $F_{normalized}$ during the baseline period

before stimulus presentation and σ is the standard deviation of $F_{normalized}$ during the same baseline period. For example traces from individual mice, the z-score trace and lick rate were smoothed using a moving average filter with spans of 20 and 5 data points. For data presentation only, plotted mean traces (30 min) were additionally downsampled by a factor of 100 (this was done to decrease the size of each graph).

For most experiments, the baseline period was the 10 min prior to stimulus presentation, a period in which the mouse was left undisturbed in the behavior chamber. The photometry data from this period was used to calculate the baseline activity, which was then compared to the average z-score during the selected epoch after stimulus presentation.

To determine T_{50} values, we determined the earliest time point where 50% of the maximum z-score over the entire 30 min trial is attained, or the time point where animals have consumed at least 50% of the total food during the 30 min period. For IG infusions, the T_{50} value is always 5 min, since infusions are performed from 0-10 min. T_{50} values were used to define the time point for “full activation” of PRLH or GCG neurons.

To calculate the Pearson Correlation Coefficient (PCC) for relationships between two variables, we used the “coorcoef” function in MATLAB with the instantaneous lick rate (Hz), cumulative intake from 0-10 min (IG infusion) or the entire 30 min trial, or the cumulative licks over preceding time intervals (from 10 s to 30 min) as an input vector. The “movsum” function in MATLAB was used to calculate the total licks in different preceding time windows. The z-scored change in activity (compared to the 10 min baseline period) over 0-10 min (IG infusion) or 0-30 min (all other comparisons) was used as the other input vector. A PCC value was calculated for each animal. To calculate the PCC for the shuffled controls, the input vector for food intake was scrambled for each animal.

For analysis of photometry responses time-locked to licking, the 15 s prior to the start of each lick bout was used to calculate the baseline activity. A lick bout was defined as any set of licks that (1) last four or more seconds and (2) are separated from the previous lick bout by at

least 20 s. Z-score per bout was calculated as the average z-score in the first 10 s of each individual licking bout. Z-score per lick was calculated by dividing the z-score per bout (defined above) by the number of licks in the first 10 s of that particular licking bout. To calculate the z-score per lick for individual animals at different bout size bins, z-score per lick values falling into each bin of 5-25 licks, 26-50 licks, 51-75 licks, or 76-100 licks were averaged. For example, all values from bouts containing 26-50 licks from a single animal would be averaged into a single value and used for statistical analyses.

To determine the Tau time constant across all Ensure lick bouts, we determined the earliest time point where 63.8% of the maximum z-score within a bout (averaged across all bouts) is reached. To determine the Lambda decay constant across all Ensure lick bouts, we determined the earliest time point where the z-score is 37% of the value during the last lick of the bout (averaged across all bouts).

For comparing licking responses in the early or late portion of the 30 min trial, photometry data in the first 15 min (early) or last 15 min (late) were separated for subsequent analyses. The 15 s prior to the start of each lick bout was always used to calculate the baseline activity.

To calculate the mean z-score per bout for the first bout to the last bout (Figure 3.10g-i), the neural response during that bout number was averaged across all mice. The max bout size (in licks) was always the first lick bout. The percentage of this maximum bout size, from 0 = 0% to 1 = 100%, was plotted for each bout below the corresponding bout. Bouts that had only one animal were not included.

To calculate the slope (x1 coefficient), we used the “fitlm” function in MATLAB to assess the relationship between bout size (licks) and the z-score in a bout for the first 10 s in a bout. The x1 value is equal to the change in z-score per bout for each additional lick, and this was obtained for each individual animal (Figure 3.2h).

To train coefficients for generalized linear models (GLM), we use the “fitglm” function in MATLAB with caloric density (kcal/mL; vector containing constant value), licks in the past 10 s (at each second of a 30 min trial), and instantaneous lick rate (at each second of a 30 min trial) as the predictor variables. Caloric densities were 2 kcal/mL for Intralipid, 0.923 kcal/mL for Ensure, 0.96 kcal/mL for glucose, and zero for saline, dry licks, or water. The response variable was the z-scored change in activity (relative to 10 min baseline prior to lick access) at each second of a 30 min trial. A GLM model was built for each animal using all photometry data from 30 min trials of Ensure, glucose, Intralipid, saline, and water consumption, and dry licking at an empty bottle. The adjusted R^2 value from the GLM model for each animal was used to determine the average fraction of the variance in the z-score (t) explained by models with different subsets of variables. To calculate each variable’s contribution, the R^2 value of each model without that variable was subtracted from the R^2 value of the full model and then averaged (i.e. to calculate the contribution of caloric density. To perform cross validation, we used 80% of the photometry data to train the GLM coefficients and calculate the mean squared error (MSE) from the remaining 20% of the data. This was performed for 100 iterations to obtain an average MSE value for each animal.

For esophageal distension experiments, photometry data collected in the 60 s before feeding tube insertion were used to calculate the baseline activity.

To calculate the average drop in z-score at the end of a lick bout (Figure 3.14f), we determined the difference between the peak z-score within the 15 s before the last lick and the mean z-score after the last lick: ((*mean z-score 0-15 s*) – (*peak z-score -15-0 s*)).

For brief access Davis rig experiments with Ensure (Figure 3.5), lick responses were calculated as the average z-scored change of activity in the 5 or 60 s following the first lick of a trial. Photometry data from the 10 min baseline period was used to calculate the baseline activity. To calculate the R^2 value in this experiment, we analyzed the relationship between the mean z-score in each trial and the trial number using simple linear regression. The z-scored

change of activity was averaged across the last trial (10th) to generate a mean z-score value (Figure 3.15e).

For 10 min food access experiments, ingestive and post-ingestive responses were defined as the average z-scored change in activity during the 10 min access period and the 20 min period following ingestion, respectively. Post-ingestive activity was calculated as (post-ingestive response /ingestive response) x 100% (this was done to normalize for differences in photometry signal across individual mice). Food intake (kcal) was calculated as the mass of food consumed (g) multiplied by the caloric density (kcal/g).

Microendoscopy

Behavior: To habituate mice to the imaging setup, we head-fixed mice using a custom-built stage (ThorLabs) before applying additional restraint by placing the animal in a 50 mL conical tube (Fisher Scientific 14-432-22). A disposable fluff underpad (MSC281230) was used to reduce limb movement while ensuring that animals were comfortable under restraint. All mice were initially habituated to the imaging setup by receiving access to a bottle containing Ensure with the microendoscopic camera attached for two sessions (2 hours each) on two separate days.

Mice were food-deprived overnight before brief access experiments. On the day of the experiment, mice were head-fixed and restrained using the method described above and given 10 min for habituation, with the Inscopix camera turned on. After an additional 10 min baseline recording period, mice received brief 5 s access to a sipper containing the appropriate solution (Ensure, Intralipid, sucralose, water; same concentrations from photometry experiments) at 5 min intervals over 20 min.

For experiments involving CCK, mice were given brief 5 s access to sucralose at 5 min intervals over 15 min, before receiving a subcutaneous injection of CCK (30 μg/kg) near the

shoulder area. We continued the recording for an additional 15 min to measure the neural response to CCK.

Data collection and analysis: Data was collected using Inscopix nVista and nVoke microscopes. Videos were acquired at 20 Hz (20% LED power, 8.0 gain, 2x spatial downsampling) using Inscopix software (Data Acquisition Software v.151; https://support.inscopix.com/support/products/nvista-30-and-nvoke-20/data-acquisitionsoftware-v151). After acquisition, videos were first pre-processed, spatially (binning factor of 2) and temporally (binning factor of 5) downsampled, and motion-corrected using Inscopix software (v.1.7, http://support. inscopix.com/mosaic-workflow). Videos underwent additional motion correction with the Mosaic software (v.1.7, http://support.inscopix.com/mosaic-workflow), which produced estimates of the motion artifacts when mice were freely moving, head-fixed, or head-fixed and restrained (Figure 3.3). Activity traces for individual neurons were then extracted from these videos using the constrained non-negative matrix factorization (CNMF-E) pipeline in the Inscopix software. After initial CNMF-E segmentation, extracted neurons were manually refined to avoid potential confounding factors from uncorrected motion artifacts, region of interest duplication and over-segmentation of the same spatial components.

For each experiment, activity traces for individual neurons were extracted for each mouse and all responses were normalized using the function $z = (C_{raw} - \mu)/\sigma$, where C_{raw} is an output of the Inscopix software, μ is the mean C_{raw} during the 10 min baseline period before stimulus presentation and σ is the standard deviation of C_{raw} during the same baseline period.

To calculate the Tau time constant for Ensure lick bouts, we determined the earliest time point where 63.8% of the maximum z-score within a bout (averaged across all bouts and all neurons for each animal) is reached.

For analysis of single-cell responses during lick bouts, the 15 s prior to the start of each lick bout was used to calculate the baseline activity, which was used to calculate the z-score from 0-15 s. We defined a neuron as “activated” if the mean z-score was ≥ 1z. Neurons with a

mean z-score of < 1z was defined as “non-responsive”. To calculate the population-weighted z-score, we multiplied the fraction of neurons activated across all 4 bouts (+1z) by their z-scored activity change (averaged across all neurons). We calculated the z-score during each lick bout by averaging the z-scored change in activity of all activated neurons within that particular lick bout. To calculate the percentage of neurons activated during a particular number of bouts, we determined whether individual cells were activated (>1z) across all 4 bouts (“All bouts”), three bouts, two bouts, or only one bout.

To compare the z-score during sucralose consumption to the z-score after IP injection of CCK, we first measured the average z-scored change in activity across all 3 sucralose lick bouts (“z-score during licking”). Next, we calculated the average z-scored change in activity in the 15 min after IP injection of CCK (“z-score after injection”). Cells were classified as responsive to “Sucralose only” if the mean z-score during licking was >1z while the mean z-score after injection was ≤1z, “CCK only” if the mean z-score after injection was >1z while the mean z-score after during licking was ≤1z, “Both” if the mean z-score for both stimuli was >1z, and “None” if the mean z-score for both stimuli was ≤1z. We used the “fitlm” function in MATLAB to calculate the R^2 value between the z-score during licking and the z-score after injection.

Optogenetics

Laser parameters: For continuous stimulation, closed-loop stimulation, and pre-stimulation experiments, the laser was modulated at 20 Hz for a 2 s ON and 3 s OFF cycle with a 10 ms pulse width. For closed-loop stimulation or silencing experiments during ingestion, the laser was modulated for 2 s after each lick detected by the Graphic State software, which was synced with a contact lickometer. This closed-loop modulation was either at 20 Hz (stimulation) or continuous (inhibition). Closed-loop stimulation when the animal was not actively licking (Lick-OFF) was performed at 20 Hz for a 2 s ON and 3 s OFF cycle, and each new lick performed would turn off this modulation for 2 s. Photostimulation or photoinhibition was delivered by a

DPSS 473-nm laser (Shanghai Laser and Optics Century BL473-100FC) through a dual fiber optic patch cord (Doric, DFP_200/220/900-0.37_2m_DF0.8-2FC0) at a laser power of 10-15 mW (photostimulation) or 5-6 mW (photoinhibition), which was measured at the tip of the patch cable before each day's experiments.

Behavior: All experiments were fully counterbalanced for the order of stimulation and contained both within animal (+/- laser) and genotype (+/- opsin) controls. Genotype controls were typically littermates that lacked either the Cre or reporter allele. For all experiments, mice were placed in sound-isolated behavioral chambers (Coulbourn, Habitest Modular System; Med Associates, Davis Rig) without water or food access unless otherwise specified. Chambers were cleaned between experiments to remove olfactory cues from previous experiments. Mice were habituated for one night in the chambers before experiments. On a subsequent day, mice were attached to optogenetic patch cords and habituated to the chambers for a second session. On the day of experiments, mice were acclimated to the behavior chamber for 10 min prior to optogenetic manipulation and/or food access.

For open-loop stimulation experiments measuring chow consumption, animals were food-deprived overnight before the experiment was performed in the light phase. After habituation, animals received a pellet of standard chow (PicoLab 5053) for self-paced consumption over 15, 30, or 60 min, depending on the experiment. Animals also received open-loop stimulation (described above) during the entire session or no laser treatment.

For open-loop stimulation experiments measuring water consumption, animals were water-deprived overnight before the experiment was performed in the light phase. After habituation, animals were given access to a bottle containing water for 30 min alongside open-loop stimulation.

For experiments measuring single-bottle consumption of Ensure and Intralipid, animals were ad libitum fed and the experiments were performed in the dark phase (after 5 pm). After habituation, animals were given access to a bottle of Ensure or Intralipid for 1 h as they received

open-loop stimulation, closed-loop stimulation (during licking only or while not licking), or closed-loop silencing, depending on the experiment.

For two bottle preference experiments with Ensure, animals were ad libitum fed and the experiments were performed in the dark phase. On day 1, mice were given access to two identical bottles of Ensure on opposite ends of the behavioral chamber for 1 h of self-paced consumption. For closed-loop stimulation experiments, the more preferred bottle (more licks than the other bottle) was designated as bottle 1, while the less preferred bottle was designated a bottle 1 for closed-loop silencing experiments. On day 2 of the experiment (the following day), mice were again given access to two identical bottles of Ensure, where bottle 1 was paired with closed-loop stimulation or silencing. On the next day, mice once again received access to two bottles of Ensure, but bottle 2 is now paired with closed-loop stimulation of silencing. The location of bottle 1 and 2 was not changed during the experiment.

For two bottle preference experiments with water or sucralose, mice were ad libitum fed and experiments were performed in the dark phase. Mice received access to two bottles of the identical solution for 1 h, where one bottle was randomly paired with closed-loop silencing.

For pre-stimulation experiments with Ensure, ad libitum fed animals were habituated to the chambers in the dark phase, before receiving optogenetic stimulation for 1 h. After the pre-stimulation ended, mice were then given a bottle of Ensure for 1 h of self-paced consumption. For pre-stimulation experiments with chow, mice were food-deprived before receiving 15, 30, or 60 min of pre-stimulation in the light phase. Next, mice received a pellet of standard chow for 15 min of self-paced consumption.

Analysis: To measure chow consumption, the pellet was weighed before and after the experiment. For Ensure and Intralipid intake measurements, a bottle of Ensure (0.21g/mL) or Intralipid (20%) was weighed before and after consumption by individual mice. Excess spillage from the lickometer was collected and added to the bottle weight after consumption. Mass was converted to volume using the density of 21% Ensure (~1.07 g/mL) and Intralipid (~1 g/mL).

For licking bout analyses in optogenetic experiments, a licking bout was defined as any set of licks containing at least three licks, in which no inter-lick interval is greater than five seconds. Bout size was calculated as the average number of licks from all lick bouts in the 1 h dark phase session. Bout duration was calculated as the average length of all lick bouts in seconds. The bout number was the total number of bouts across the entire 1 h trial.

To measure the number of laser pulses received by individual mice, the bout duration (s) values from all lick bouts were summed to calculate the total time (seconds) each animal was consuming Ensure. To calculate the number of laser pulses in the Lick-ON test, the summed value was multiplied by 20, since the laser was modulated at 20 Hz. To calculate the number of laser pulses in the Lick-OFF test, the total time licking (seconds) for each animal was subtracted from the full trial (60 min or 3600 seconds) and then multiplied by 8, since the laser was modulated at 20 Hz for a 2 s ON 3 s OFF cycle (or 40 pulses over 5 seconds).

To measure the interlick interval (ILI) within a bout (Figure 3.13), we measured the time between each lick between 0 and 1 s. To calculate the Mu1 and Mu2 constants, we used the “fitgmdist“ function in MATLAB, with k = 2 components fitted to the data based on the two peaks observed in the probability mass function (Figure 3.14i,k).

Histology

Mice were anesthetized under isoflurane and then transcardially perfused with phosphate-buffered saline (PBS, 10 mL) followed by formalin (10%, 15 mL). Brains were dissected, post-fixed in 10% formalin overnight at 4 C, and switched to 30% sucrose the next day. All tissues were kept in 30% sucrose at 4 C for overnight cryo-protection and embedded in OCT before sectioning. Sections (50 μm) were prepared with a cryostat and collected in PBS or on Superfrost Plus slides. To visualize fluorescent labelling without staining, sections were mounted with DAPI Fluoromount-G (Southern Biotech) and then imaged by confocal microscopy (Zeiss, LSM 510).

For immunostaining, sections (50 μm) were washed 3 x 10 min with 0.1% PBST (0.1% Triton X-100 in PBS), blocked (5% NGS or NDS in 0.1% PBST) for 30 min at RT, and incubated with primary antibodies (1:1000 diluted in blocking solution) overnight at 4C. The next day, sections were washed 3x10 min with 0.1% PBST, incubated with secondary antibodies (1:500 diluted in blocking solution) for 2 h at RT, washed again 3 x 10 min with 0.1% PBST, and mounted with DAPI Fluoromount-G (Southern Biotech). Primary antibodies used were: chicken anti-GFP (Abcam, ab13970, 1:1000) and rabbit anti-TH (Millipore, AB152).

Statistics

All values are reported as mean ± sem (error bars or shaded areas). Sample size is the number of animal subjects per group. In figures, asterisks denote statistical significance: *p < 0.05, **p < 0.01, ***p < 0.001, ****p < 0.0001. In figures with simple linear regressions, dashed lines represent the 95% confidence interval for the line of best fit. Except for linear regressions or two-way analysis of variance (ANOVA), non-parametric tests were uniformly used. P values for paired or unpaired comparisons were calculated using the Wilcoxon Signed Rank test or Mann-Whitney U test and corrected for multiple comparisons using the Holm-Šidák multiple comparisons test. P values for comparisons across multiple groups were calculated using the Kruskal-Wallis test or two-way ANOVA and corrected for multiple comparisons using Dunn's multiple comparisons test and Šidák's or Dunnett's multiple comparisons test, respectively. Fisher's exact test was used to assess if overlapping neural responses were due to chance. To compare between groups, data from each animal were averaged for biological replicates. See Supplementary Table 1 and 2 for a complete summary of all statistics. No statistical method was used to predetermine sample size. Randomization and blinding were not used.
We analyzed fiber photometry data, behavior data, and microendoscopic imaging data with custom MATLAB (v.R2017a, http://www.Mathworks.com/products/matlab) scripts.

REFERENCES

1. Berthoud, H.-R. The Caudal Brainstem and the Control of Food Intake and Energy Balance. in *Neurobiology of Food and Fluid Intake* (eds. Stricker, E. M. & Woods, S. C.) 195–240 (Springer US, 2004). doi:10.1007/0-306-48643-1_9.
2. Chambers, A. P., Sandoval, D. A. & Seeley, R. J. Integration of satiety signals by the central nervous system. *Curr. Biol. CB* **23**, R379-388 (2013).
3. Cheng, W. *et al.* Hindbrain circuits in the control of eating behaviour and energy balance. *Nat. Metab.* **4**, 826–835 (2022).
4. Alcantara, I. C., Tapia, A. P. M., Aponte, Y. & Krashes, M. J. Acts of appetite: neural circuits governing the appetitive, consummatory, and terminating phases of feeding. *Nat. Metab.* **4**, 836–847 (2022).
5. Vrang, N., Phifer, C. B., Corkern, M. M. & Berthoud, H.-R. Gastric distension induces c-Fos in medullary GLP-1/2-containing neurons. *Am. J. Physiol. Regul. Integr. Comp. Physiol.* **285**, R470-478 (2003).
6. Williams, E. K. *et al.* Sensory Neurons that Detect Stretch and Nutrients in the Digestive System. *Cell* **166**, 209–221 (2016).
7. Ran, C., Boettcher, J. C., Kaye, J. A., Gallori, C. E. & Liberles, S. D. A brainstem map for visceral sensations. *Nature* **609**, 320–326 (2022).
8. Zittel, T. T., De Giorgio, R., Sternini, C. & Raybould, H. E. Fos protein expression in the nucleus of the solitary tract in response to intestinal nutrients in awake rats. *Brain Res.* **663**, 266–270 (1994).
9. Schwartz, G. J. & Moran, T. H. CCK elicits and modulates vagal afferent activity arising from gastric and duodenal sites. *Ann. N. Y. Acad. Sci.* **713**, 121–128 (1994).

10. Holt, M. K. *et al.* Preproglucagon Neurons in the Nucleus of the Solitary Tract Are the Main Source of Brain GLP-1, Mediate Stress-Induced Hypophagia, and Limit Unusually Large Intakes of Food. *Diabetes* **68**, 21–33 (2019).

11. Brierley, D. I. *et al.* Central and peripheral GLP-1 systems independently suppress eating. *Nat. Metab.* **3**, 258–273 (2021).

12. D'Agostino, G. *et al.* Appetite controlled by a cholecystokinin nucleus of the solitary tract to hypothalamus neurocircuit. *eLife* **5**, e12225 (2016).

13. Cheng, W. *et al.* Leptin receptor-expressing nucleus tractus solitarius neurons suppress food intake independently of GLP1 in mice. *JCI Insight* **5**, 134359 (2020).

14. Cheng, W. *et al.* Calcitonin Receptor Neurons in the Mouse Nucleus Tractus Solitarius Control Energy Balance via the Non-aversive Suppression of Feeding. *Cell Metab.* **31**, 301-312.e5 (2020).

15. Cheng, W. *et al.* NTS Prlh overcomes orexigenic stimuli and ameliorates dietary and genetic forms of obesity. *Nat. Commun.* **12**, 5175 (2021).

16. Liu, J. *et al.* Enhanced AMPA Receptor Trafficking Mediates the Anorexigenic Effect of Endogenous Glucagon-like Peptide-1 in the Paraventricular Hypothalamus. *Neuron* **96**, 897-909.e5 (2017).

17. Roman, C. W., Derkach, V. A. & Palmiter, R. D. Genetically and functionally defined NTS to PBN brain circuits mediating anorexia. *Nat. Commun.* **7**, 11905 (2016).

18. Schwartz, G. J. & Moran, T. H. Leptin and neuropeptide y have opposing modulatory effects on nucleus of the solitary tract neurophysiological responses to gastric loads: implications for the control of food intake. *Endocrinology* **143**, 3779–3784 (2002).

19. Li, M. *et al.* Gut-Brain Circuits for Fat Preference. *Nature* (2022) doi:10.1038/s41586-022-05266-z.

20. Appleyard, S. M. *et al.* Visceral afferents directly activate catecholamine neurons in the solitary tract nucleus. *J. Neurosci. Off. J. Soc. Neurosci.* **27**, 13292–13302 (2007).

21. Ludwig, M. Q. *et al.* A genetic map of the mouse dorsal vagal complex and its role in obesity. *Nat. Metab.* **3**, 530–545 (2021).

22. Kato, H. K., Chu, M. W., Isaacson, J. S. & Komiyama, T. Dynamic sensory representations in the olfactory bulb: modulation by wakefulness and experience. *Neuron* **76**, 962–975 (2012).

23. Kreisler, A. D., Davis, E. A. & Rinaman, L. Differential activation of chemically identified neurons in the caudal nucleus of the solitary tract in non-entrained rats after intake of satiating vs. non-satiating meals. *Physiol. Behav.* **136**, 47–54 (2014).

24. Tolhurst, G., Reimann, F. & Gribble, F. M. Intestinal sensing of nutrients. *Handb. Exp. Pharmacol.* 309–335 (2012) doi:10.1007/978-3-642-24716-3_14.

25. Tolhurst, G., Reimann, F. & Gribble, F. M. Intestinal sensing of nutrients. *Handb. Exp. Pharmacol.* 309–335 (2012) doi:10.1007/978-3-642-24716-3_14.

26. Beutler, L. R. *et al.* Dynamics of Gut-Brain Communication Underlying Hunger. *Neuron* **96**, 461-475.e5 (2017).

27. Bai, L. *et al.* Enteroendocrine cell types that drive food reward and aversion. *eLife* **11**, e74964 (2022).

28. Lawrence, C. B., Ellacott, K. L. J. & Luckman, S. M. PRL-releasing peptide reduces food intake and may mediate satiety signaling. *Endocrinology* **143**, 360–367 (2002).

29. Takayanagi, Y. *et al.* Endogenous prolactin-releasing peptide regulates food intake in rodents. *J. Clin. Invest.* **118**, 4014–4024 (2008).

30. Chang, R. S. & Lotti, V. J. Biochemical and pharmacological characterization of an extremely potent and selective nonpeptide cholecystokinin antagonist. *Proc. Natl. Acad. Sci. U. S. A.* **83**, 4923–4926 (1986).

31. Laugerette, F. *et al.* CD36 involvement in orosensory detection of dietary lipids, spontaneous fat preference, and digestive secretions. *J. Clin. Invest.* **115**, 3177–3184 (2005).

32. Berridge, K. C. & Robinson, T. E. Liking, Wanting and the Incentive-Sensitization Theory of Addiction. *Am. Psychol.* **71**, 670–679 (2016).

33. Gaykema, R. P. *et al.* Activation of murine pre-proglucagon-producing neurons reduces food intake and body weight. *J. Clin. Invest.* **127**, 1031–1045 (2017).

34. Kreisler, A. D. & Rinaman, L. Hindbrain glucagon-like peptide-1 neurons track intake volume and contribute to injection stress-induced hypophagia in meal-entrained rats. *Am. J. Physiol. Regul. Integr. Comp. Physiol.* **310**, R906-916 (2016).

35. Bai, L. *et al.* Genetic Identification of Vagal Sensory Neurons That Control Feeding. *Cell* **179**, 1129-1143.e23 (2019).

36. Chen, Y., Lin, Y.-C., Zimmerman, C. A., Essner, R. A. & Knight, Z. A. Hunger neurons drive feeding through a sustained, positive reinforcement signal. *eLife* **5**, e18640 (2016).

37. Chen, Y. *et al.* Sustained NPY signaling enables AgRP neurons to drive feeding. *eLife* **8**, e46348 (2019).

38. Dumping Syndrome - NIDDK. *National Institute of Diabetes and Digestive and Kidney Diseases* https://www.niddk.nih.gov/health-information/digestive-diseases/dumping-syndrome.

39. Wilding, J. P. H. *et al.* Once-Weekly Semaglutide in Adults with Overweight or Obesity. *N. Engl. J. Med.* **384**, 989–1002 (2021).

40. Hayashi, Y. *et al.* Mice deficient for glucagon gene-derived peptides display normoglycemia and hyperplasia of islet {alpha}-cells but not of intestinal L-cells. *Mol. Endocrinol. Baltim. Md* **23**, 1990–1999 (2009).

41. Ekstrand, M. I. *et al.* Molecular Profiling of Neurons Based on Connectivity. *Cell* **157**, 1230–1242 (2014).

42. Smith, G. P. Sham feeding in rats with chronic, reversible gastric fistulas. *Curr. Protoc. Neurosci.* **Chapter 8**, Unit 8.6D (2001).

43. Davis, J. D. & Campbell, C. S. Peripheral control of meal size in the rat. Effect of sham feeding on meal size and drinking rate. *J. Comp. Physiol. Psychol.* **83**, 379–387 (1973).

Publishing Agreement

It is the policy of the University to encourage open access and broad distribution of all theses, dissertations, and manuscripts. The Graduate Division will facilitate the distribution of UCSF theses, dissertations, and manuscripts to the UCSF Library for open access and distribution. UCSF will make such theses, dissertations, and manuscripts accessible to the public and will take reasonable steps to preserve these works in perpetuity.

I hereby grant the non-exclusive, perpetual right to The Regents of the University of California to reproduce, publicly display, distribute, preserve, and publish copies of my thesis, dissertation, or manuscript in any form or media, now existing or later derived, including access online for teaching, research, and public service purposes.

DocuSigned by:
Truong Ly
3AD2A3FCDE854C5...
Author Signature

7/16/2025
Date